

Is Turning Down the Sun a Good Proxy for Stratospheric Sulfate Geoengineering?

Daniele Vioni¹, Douglas G. MacMartin¹, Ben Kravitz^{2,3}

¹Sibley School for Mechanical and Aerospace Engineering, Cornell University, Ithaca, NY

²Department of Earth and Atmospheric Sciences, Indiana University, Bloomington, IN

³Atmospheric Sciences and Global Change Division, Pacific Northwest National Laboratory, Richland,
WA, USA

Key Points:

- Reducing the incoming solar radiation is often used to emulate injecting SO₂ in the stratosphere, but produces different surface outcomes
- Solar reduction matched to the pattern produced by the aerosol optical depth results in better surface climate matching between the two methods
- Including the stratospheric heating produced by the aerosols produces further improvements and highlights key physical mechanisms at play

Corresponding author: Daniele Vioni, daniele.vioni@cornell.edu

Abstract

Deliberately blocking out a small portion of the incoming solar radiation would cool the climate. One such approach would be injecting SO_2 into the stratosphere, which would produce sulfate aerosols that would remain in the atmosphere for 1–3 years, reflecting part of the incoming shortwave radiation. This would not affect the climate the same way as increased greenhouse gas (GHG) concentrations, leading to residual differences when a GHG increase is offset by stratospheric sulfate geoengineering. Many climate model simulations of geoengineering have used a uniform reduction of the incoming solar radiation as a proxy for stratospheric aerosols, both because many models are not designed to adequately capture relevant stratospheric aerosol processes, and because a solar reduction has often been assumed to capture the most important differences between how stratospheric aerosols and GHG would affect the climate. Here we show that dimming the sun does not produce the same surface climate effects as simulating aerosols in the stratosphere. By more closely matching the spatial pattern of solar reduction to that of the aerosols, some improvements in this idealized representation are possible, with further improvements if the stratospheric heating produced by the aerosols is included. This is relevant both for our understanding of the physical mechanisms driving the changes observed in stratospheric-sulfate geoengineering simulations, and in terms of the relevance of impact assessments that use a uniform solar dimming.

Plain Language Summary

Injecting SO_2 in the stratosphere has been proposed as a method to temporarily cool the planet by partially reflecting the incoming solar radiation. To assess the eventual side-effects of this method, some climate model simulations have simply reduced the solar constant in the model rather than simulating the actual aerosols that would be produced. We show here what the limits of simulating stratospheric sulfate injection this way are, and what are the physical causes behind the differences from simulations where stratospheric aerosols are represented.

1 Introduction

The possibility of injecting SO_2 in the stratosphere to mitigate some of the negative effects of anthropogenic global warming has been discussed for decades, starting with Budyko (1978) and notably by Crutzen (2006). Despite model simulations showing that it would be effective at offsetting many aspects of climate change (e.g. Kravitz et al., 2017; P. J. Irvine & Keith, 2020), deploying stratospheric sulfate (SS) injections would come with drawbacks of its own, and many studies have explored the possible side effects of this method, both in the stratosphere (Tilmes et al., 2008; Pitari et al., 2014) and at the surface (Jones et al., 2018; Jiang et al., 2019). One of the most important reasons for why a climate with high CO_2 levels but cooled by aerosols would be unavoidably different from one less warm due to lower CO_2 levels lies in the different ways in which CO_2 and aerosols affect the climate: while the aerosols partially reduce solar radiation (shortwave; SW) at the surface, the increasing CO_2 concentrations trap more outgoing longwave radiation (LW) emitted by the planet. Moreover, the spatial and seasonal dependence of the two forcings are also different (Govindasamy et al., 2003; Ban-Weiss & Caldeira, 2010; Jiang et al., 2019), since CO_2 is a well mixed gas with relatively uniform radiative effect in both space and season, while the insolation varies strongly with latitude and season, and the spatial distribution of stratospheric aerosols also varies due to the stratospheric circulation and injection location (Tilmes et al., 2017). The net results of these effects on the surface are that while the global mean temperature could be successfully reduced through stratospheric sulfate injections, the combination of stratospheric aerosol and increased CO_2 forcing would lead to residual differences such as regional changes to the hydrological cycle (Jones et al., 2018; I. Simpson et al., 2019; Cheng

et al., 2019). These changes, however, would very likely be smaller in magnitude than those produced by climate change itself (MacMartin et al., 2019; P. J. Irvine & Keith, 2020). Another important difference is to be found in the stratosphere, where the sulfate aerosols would absorb some near-infrared radiation and heat the air locally, resulting in changes to stratospheric dynamics (Aquila et al., 2014; Niemeier & Schmidt, 2017; Richter et al., 2017; Niemeier et al., 2020; Vioni, MacMartin, Kravitz, Lee, et al., 2020), chemistry (Vioni, Pitari, Aquila, Tilmes, et al., 2017; Tilmes, Richter, Mills, et al., 2018), and upper tropospheric clouds (Kuebbeler et al., 2012; Vioni, Pitari, Di Genova, et al., 2018). Furthermore, dynamical changes in the circulation in response to the stratospheric heating also affect the surface climate due, for instance, to shifts in the atmospheric circulation (I. Simpson et al., 2019).

Generally, the differential impact of longwave and shortwave radiative effects has been considered to be the main reason for the surface climate differences, and so reducing the solar constant rather than actually simulating the aerosols has been a widely used simulation technique (Kravitz, Caldeira, et al., 2013). While this simplification clearly would not capture impacts such as changes in ozone (Tilmes et al., 2008) or different ratio of direct/diffuse light (Kravitz et al., 2012), it does capture the simultaneous reduction of SW radiation and increase in LW radiation. Due to the uncertainties in our understanding of stratospheric sulfate microphysics and interaction with radiation, and to the lack, in some models, of a proper representation of stratospheric circulation, this simplification has also allowed more climate models to perform similar simulations (Kravitz, Caldeira, et al., 2013). Many studies have thus used a uniform reduction of the solar constant (solar dimming, SD) as a proxy to simulate the effects of stratospheric sulfate geo-engineering (SS), looking at its consequences on surface processes, for instance on the hydrological cycle (Smyth et al., 2017; Russotto & Ackerman, 2018a, 2018b; Guo et al., 2018; Ji et al., 2018; P. Irvine et al., 2019) and vegetation (Glienke et al., 2015; Dagon & Schrag, 2019). Some recent studies aiming to generally evaluate Solar Radiation Management (SRM) techniques in the framework of Integrated Assessment Modeling have also used SD climate simulations as a proxy for any SRM method (Tavoni et al., 2017; Oeschles et al., 2017; Low & Schfer, 2019; Harding et al., 2020).

However, reducing solar irradiance instead of simulating the stratospheric aerosols would only be a good proxy if the differential SW and LW effects dominate the surface climate impacts, as this approximation does not include stratospheric warming caused by the absorption of LW radiation by the sulfate aerosols (Richter et al., 2017; Niemeier & Schmidt, 2017; Kleinschmitt et al., 2018), nor does it capture differences in the spatio-temporal distribution of the aerosols (Dai et al., 2018; Vioni et al., 2019). Furthermore, there would be differences in the downwelling radiation at the surface, due to the different ratio of direct and scattered solar radiation that would affect ecosystems impact assessments. Previous studies have already compared the two methods and highlighted some of the differences in the surface response (Niemeier et al., 2013; Ferraro et al., 2015; Kalidindi et al., 2015; Xia et al., 2017), finding generally lower changes in the hydrological cycle when performing SD simulations compared to SS ones. However, these previous comparisons have always equated SD with a global decrease in the solar constant and SS with equatorial injections aimed at managing globally averaged quantities, either temperature or radiative forcing. Furthermore, earlier models oftentimes used either non-fully interactive or prescribed aerosols (Kalidindi et al., 2015; Xia et al., 2017) to simulate SS.

In recent years it has been shown that by combining injections at different latitudes it is possible to devise SS strategies capable of managing more than just global surface temperature (Kravitz et al., 2017). The ability of SS to be tailored to more precisely modify the distribution of the radiative forcing in order to minimize side effects (MacMartin et al., 2017; Dai et al., 2018; Lee et al., 2020) is therefore another important difference compared to SD.

Table 1. Summary of the simulations analyzed in this paper, with a general description of the method used to maintain surface temperatures at 2010-2030 levels.

Sim. name	Description
1×1 SD	Uniform solar dimming to maintain global mean temperature
1×1 SS	Stratospheric sulfate aerosols injected at the equator to maintain global mean temperature
3×3 SD	Solar dimming in three independently adjusted patterns (globally uniform, linear with sine of latitude, and quadratic with sine of latitude) to maintain global mean temperature, the interhemispheric temperature gradient, and the equator-to-pole temperature gradient
3×3 SS	Stratospheric sulfate aerosol injection at four independent locations (30°S , 15°S , 15°N , and 30°N) to maintain global mean temperature, the interhemispheric temperature gradient, and the equator-to-pole temperature gradient
3×3 SDH	As in 3×3 SD but with the stratospheric heating patterns from 3×3 SS superimposed

In light of this, we reconsider in this work the simulated physical differences between SS and SD simulations. Together with simulations more similar to those analyzed in the past (equatorial injections and spatially uniform reduction in the solar constant) we consider here also a set of SS simulations designed to maintain, through multiple injection locations, the global surface temperature together with the inter-hemispheric and equator-to-pole gradients of temperature (Tilmes, Richter, Kravitz, et al., 2018). We also consider a new set of SD simulations designed to achieve similar objectives through a non-spatially-uniform reduction in the solar constant (similar to Kravitz et al., 2016). Finally, we also include one more set including a 3×3 SD reduction while superimposing the stratospheric heating that would be produced by the aerosols in the analogous SS simulations. A similar experiment has been performed in I. Simpson et al. (2019), with heating rates from stratospheric aerosols imposed for 20 years in the period 2010-2030. In our case, the simultaneous presence of the stratospheric heating and of the non-uniform solar dimming allows for a more direct comparison between the sets of experiments, given the ability to maintain similar temperature gradients compared to the SS simulations. By cross-comparing these five sets (Table 1), we aim to better separate the differences produced by the various factors mentioned above, in particular those driven by differences in the obtained temperature gradients (caused by latitudinal differences in the amount of solar radiation reflected or attenuated) and those driven by the presence of the aerosols themselves, for instance by further isolating the role of the stratospheric heating in the changes observed in the SS simulations.

This paper is structured as follows: in Section 2 we explain how the 5 sets of simulations were built, and we expand on how the cross-comparisons can clarify single aspects of the climatic response. In Section 3.1 we compare the simulated results in terms of surface temperature and precipitation and try to understand the physical mechanisms behind them, then try to quantify how well the SD simulations represent the SS ones for some of those quantities in section 3.2. We then discuss other quantities for which the response is highly different in Section 3.3 for the surface and in Section 3.4 for stratospheric quantities. Finally, we discuss our results in Section 4.

2 Methods

We analyze here 5 sets of simulations performed with the Community Earth System Model (CESM), with the Whole Atmosphere Community Climate Model (WACCM)

as its atmospheric component (Mills et al., 2016, 2017), all with underlying greenhouse gas (GHGs) emissions under the RCP8.5 scenario, and with either solar dimming (SD) or stratospheric SO₂ injections (SS) to offset the warming relative to 2020 (calculated as the average over 2010–2030 from a 20-member ensemble of RCP8.5 simulations). The sets termed 1 × 1 aim to keep the global yearly surface temperature at the 2010–2030 average, either by means of a uniform reduction of the solar constant (1 × 1 SD) or by SO₂ injections at the equator at 25 km of altitude (1 × 1 SS) (Kravitz et al., 2019). The other sets, termed 3 × 3, aim to keep three temperature targets: keeping global yearly surface temperatures and inter-hemispheric and equator-to-pole temperature gradients at the 2010–2030 average, either by modifying the solar constant proportionally to constant, linear, and quadratic functions of the sine of latitude (projections of the first three Legendre polynomials onto area-weighted solar reduction) (3 × 3 SD) (see MacMartin et al., 2013; Kravitz et al., 2016) or by injecting SO₂ at 4 latitudes (30°S, 15°S, 15°N, and 30°N), 5 km above the tropopause and at the international date line, to achieve an aerosol optical depth (AOD) similar to the desired 3 × 3 solar reductions needed (3 × 3 SS) (Tilmes, Richter, Kravitz, et al., 2018). Decisions on the amount of solar reduction or on the amount of SO₂ to inject at each location are taken at the end of each year of simulation by a feedback loop (Kravitz et al., 2017) to ensure that the desired goals are met. Both SS sets have already been described and analyzed in Tilmes, Richter, Kravitz, et al. (2018) and Kravitz et al. (2019).

A final ensemble of simulations uses the the same method as the 3 × 3 SD ones to maintain the three surface temperature goals, but imposes in the stratosphere the same stratospheric heating rates that would result from the stratospheric aerosols in the 3 × 3 SS simulation in the same period, with a methodology similar to that described by I. Simpson et al. (2019) (monthly-varying 3D-heating rates above 100 hPa derived from a double call to the radiation scheme with and without the aerosols). While I. Simpson et al. (2019) imposed heating that was the same for the entire period, derived from the 2075–2095 period of aerosol injections, in our case the overall magnitude of the heating evolves year-by-year in the same way as the stratospheric heating in the 3 × 3 SS simulations. This is done in order to have both a more “uniform” perturbation year after year, but still realistically evolving in magnitude as if the aerosol burden was increased every year. A comparison of the different physical processes at play in each of the simulations is described in Fig. 1.

All analyses in this manuscript are for the period 2070–2089, as that 20-year time period has the greatest forcing of all periods simulated and thus the highest signal-to-noise ratio (MacMartin et al., 2019). The SS simulations are started in 2020. The SD simulations are branched off the SS simulations in 2060, substituting the injection of SO₂ for solar reduction (as in Visionsi, MacMartin, Kravitz, Richter, et al. (2020)). The first 10 years are left out of the analyses to give the system time to relax to the new state, even though all stratospheric aerosols are already removed after the first 2 years without injection. All simulations are compared against the period 2010–2030 (using the entire 20-member ensemble), termed Control in this work.

3 Results

All model simulations restore global surface temperature to within 0.17 K of the average in the Control period. In the period 2070–2089 considered in our analyses, that equates to an average cooling of 3.9K (Tilmes, Richter, Kravitz, et al., 2018) in order to maintain the same temperature as the period 2010–2030. The obtained AOD and solar dimming required to achieve the temperature goals are shown in Fig 2. There are clear differences in the solar dimming patterns that preview some of the observed changes that will be discussed later on. The uniform dimming in the 1 × 1 SD case implies an overcooling of the tropics and an undercooling at high latitudes (Govindasamy et al., 2003; Kravitz, Caldeira, et al., 2013), resulting in a reduction, for instance, in September sea

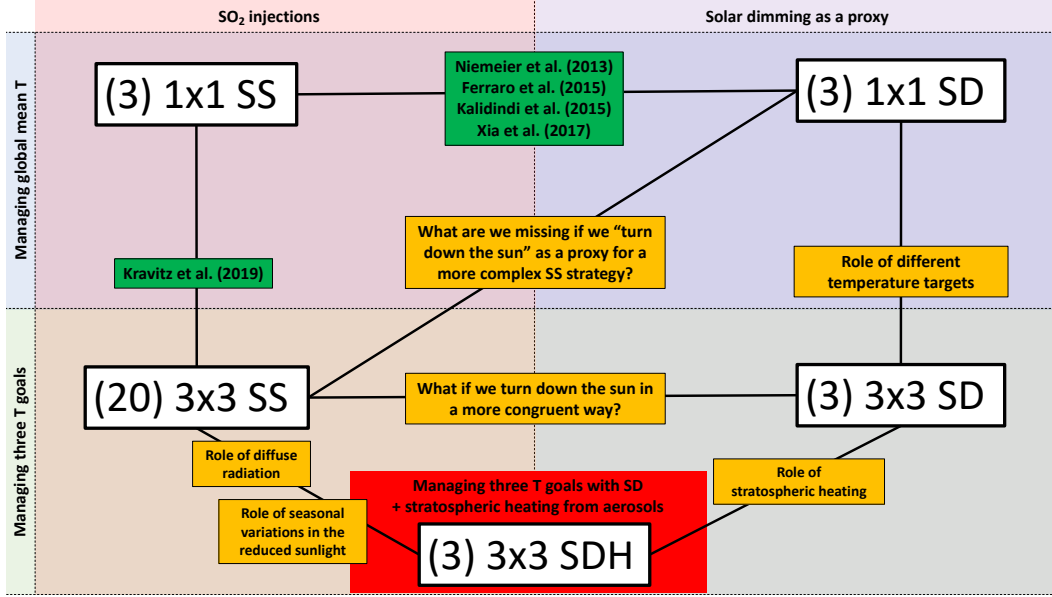


Figure 1. Summary of the simulations employed in this work, divided depending on the method used to maintain the climate goals (columns) and by the climate goals that we try to achieve (rows). In the green boxes, we list some of the comparisons between sets of simulations already available in the scientific literature. In the yellow boxes, we list new questions that we address with the simulations described in this paper. The white boxes give the name of these simulations as referred to in this paper and the size of the ensemble, in brackets.

Table 2. Summary of the main results of the five simulations, compared to the 2010-2030 period in Control: T_0 , T_1 and T_2 represent the projections of surface temperatures in the first three Legendre polynomial in K; Precipitation (P) and Precipitation-Evapotranspiration over land ($\Delta P-E_{land}$) in mm/day. Arctic September Sea ice (SSI) in $10^6 \times \text{km}^2$.

Simulation	ΔT_0	ΔT_1	ΔT_2	ΔP	$\Delta P-E_{land}$	ΔSSI
1×1 SD	-0.04	0.29	0.18	-0.09	-0.035	-1.1
1×1 SS	0.17	0.07	0.23	-0.14	-0.044	0.7
3×3 SD	-0.03	0.02	-0.02	-0.07	-0.041	2.7
3×3 SS	0.06	0.04	0.09	-0.12	-0.038	1.5
3×3 SDH	-0.10	0.02	-0.02	-0.10	-0.050	2.9

ice in the Arctic (Table 2) even when global surface temperatures are restored. There are also evident differences with the 1×1 SS case, where the AOD produced by equatorial injections is not latitudinally uniform due to the tropical confinement of the aerosols (Visioni, Pitari, Tuccella, & Curci, 2018), amplifying even more the tropical overcooling. The increasing fractional solar reduction at higher latitudes compensates for this in the 3×3 cases, either by directly reducing sunlight or by injecting outside the tropics. Over 60° of latitude, however, the 3×3 SS differs further from the SD case due to the dynamical transport barrier there (Visioni, MacMartin, Kravitz, Lee, et al., 2020). Roughly, an AOD of 0.1 equates to a reduction of 1% in incoming solar irradiance (e.g. Hansen et al., 2005). In the 3×3 cases, SDH requires more solar reduction compared to SD. This is due to an increase in stratospheric water vapor resulting from tropopause warming (Visioni, Pitari, & Aquila, 2017; Tilmes, Richter, Mills, et al., 2018) as we show in Fig. S1, that in turn warms the surface (Hansen et al., 2005; I. Simpson et al., 2019).

3.1 Comparison of simulated surface temperatures and precipitation

In Fig. 3 we show the annually averaged surface temperature response in all cases relative to Control. Despite global mean temperature being within 0.16 K of the objective, local differences of up to 1–2 K are present; however, these differences are much smaller than those due to RCP 8.5 alone. The comparison of the 1×1 SD with both SS simulations highlights that, aside from a few features, simply turning down the sun is not a good analogue for how regional temperatures would respond to the stratospheric aerosols. Exceptions include the sign of the tropical overcooling and high-latitude under-cooling and the warming over the northern Atlantic Ocean (due to over-compensating the GHG-driven slowing down of the Atlantic Meridional Overturning Circulation (AMOC) in this model, (Fasullo et al., 2018)).

These differences are due to various factors. For the 1×1 cases, as shown in Table 2, the magnitude of T1 and T2 in the SS case are not captured correctly by the SD case due to the peak in AOD in the tropics that does not resemble the uniform dimming in solar radiation (Fig. 2a). (Equatorial injection in this model results in slightly higher AOD in the northern hemisphere than the southern, roughly compensating T1 even though that was not an objective of the 1×1 SS simulation.) For the 3×3 cases this effect is less pronounced, since the injection locations are chosen so as to have a similar profile to the one actually achieved by the solar dimming (MacMartin et al., 2017). At very high latitudes, however, some differences are present mostly due to the polar transport barriers (Visioni, MacMartin, Kravitz, Lee, et al., 2020) that reduce the high-latitude AOD. It is likely that a more uniform AOD distribution using more latitudes of injection (see for instance Dai et al., 2018) could produce results more closely resembling those from 1×1 SD: however, some differences would still remain due to the considerable variation across different months of the AOD (Fig. 2) compared to the constant dimming produced by the SD cases: as shown by Visioni, MacMartin, Kravitz, Richter, et al. (2020), seasonal variations in AOD can result in notably different surface climates.

Lastly, the other difference between the simulation is the lack of stratospheric heating in the SD simulations. Previous papers point to the substantial warming in the winter (relative to baseline) over the continental northern high latitudes (Europe and Asia), (I. Simpson et al., 2019; Jiang et al., 2019), and consistent with what has been postulated in the past literature on the Pinatubo 1991 eruption (Robock & Mao, 1995; Robock, 2000), link this at least in part to the stratospheric heating produced by the aerosols. A recent paper by Polvani et al. (2019) has however cast doubts on the physical causal link relating the two, showing that in large ensembles of simulations (one of them performed with WACCM4, a model similar to that used for the simulations in this study) the winter warming does not appear to be a consistent result, being limited to only some members of the ensemble.

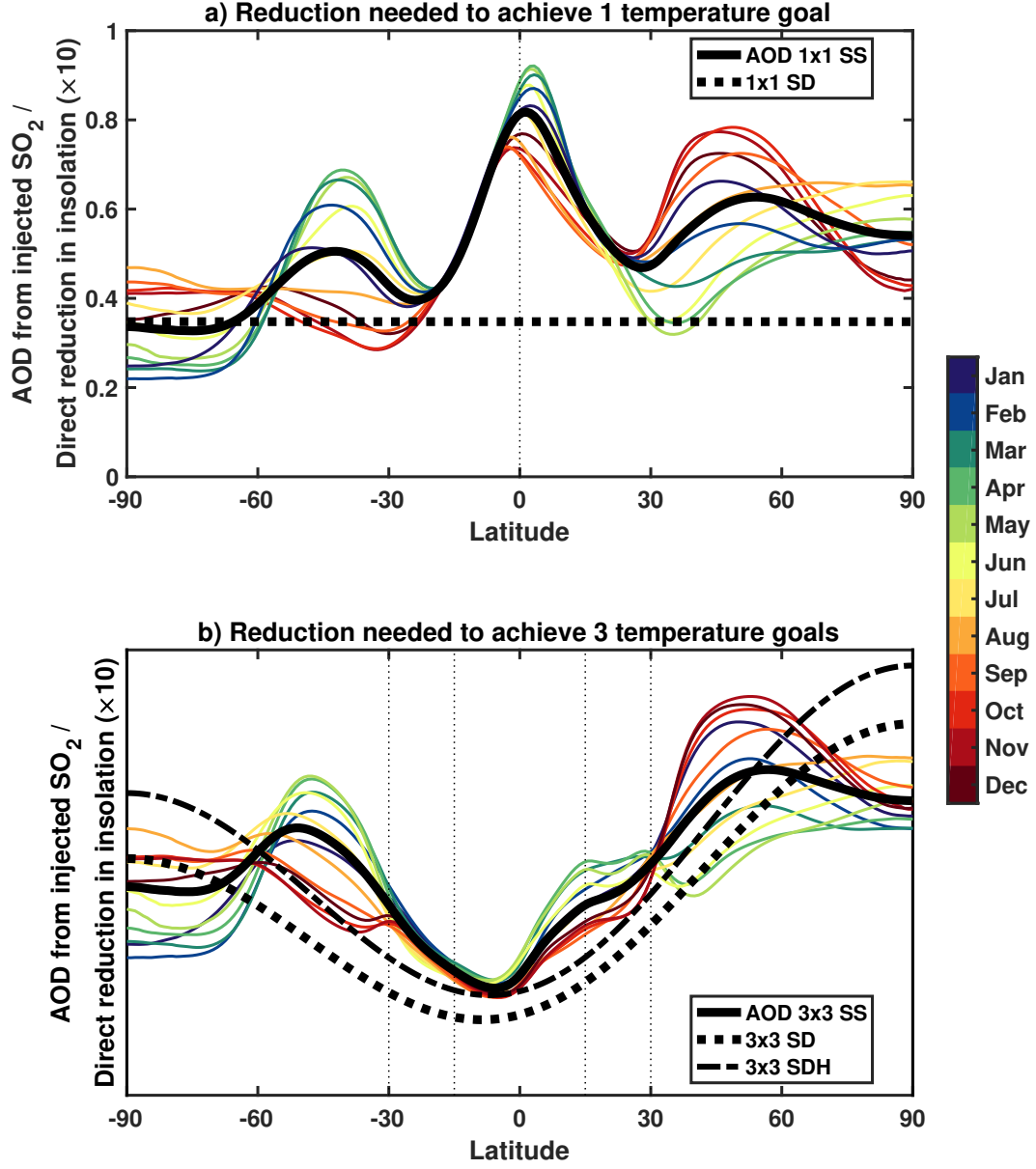


Figure 2. Comparison of stratospheric sulfate AOD obtained through SO_2 injections (SS) or solar dimming (SD) for the five simulations, both averaged over 2070-2089. In panel a), cases maintaining global mean temperature are shown. In panel b), cases maintaining global mean temperature, inter-hemispheric temperature gradient, and equator-to-pole temperature gradient are shown. The annual AOD average is shown with a black thick line, while the solar dimming (expressed in terms of fraction of incoming solar radiation reduced $\times 10$) is shown with a black thick dashed line. The AOD for each month is shown with the thin colored lines described in the colorbar. In panel b), the dash-dotted line shows the solar dimming necessary for the SDH simulations. The injection locations of SO_2 are indicated by the vertical thin black dashed line.

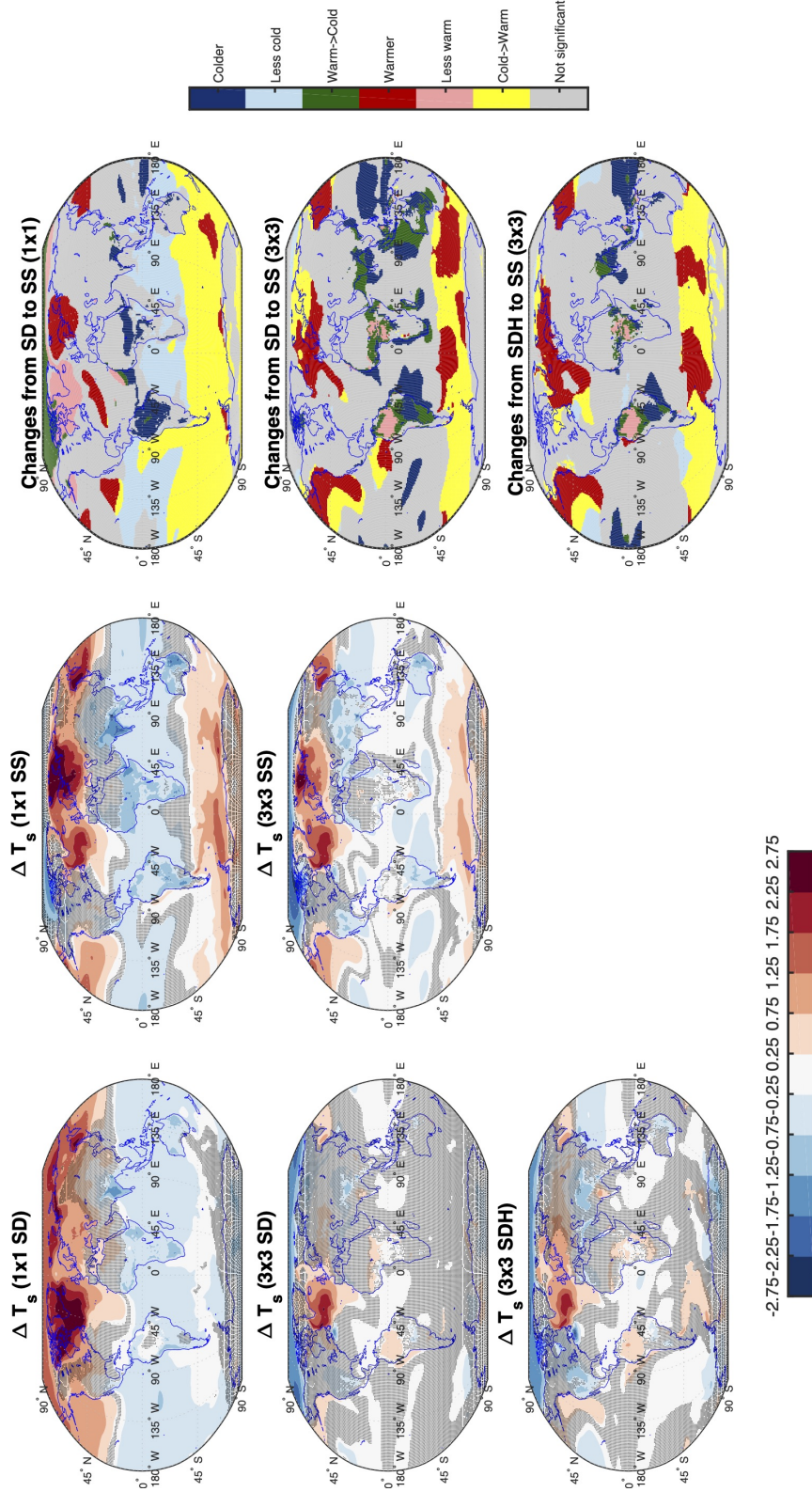


Figure 3. Surface temperature changes for all simulations for 2070-2089 relative to 2010-2030. In the third column, areas are highlighted where surface temperature shows statistically significant (using a two-sided t-test with $p < 0.05$) changes between the simulations with SD and SS. Grey areas indicate regions in all maps where the differences are not statistically different from zero.

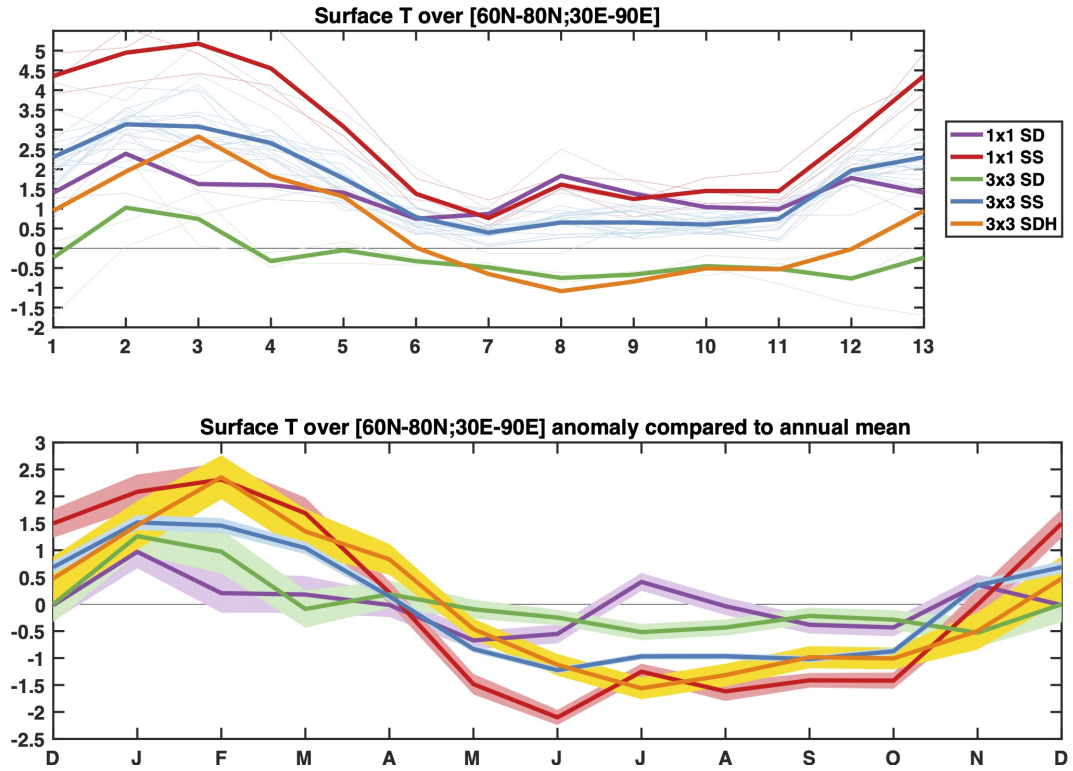


Figure 4. a) Seasonal cycle of surface temperatures over high northern latitudes for each ensemble (thick lines, see legend) and single ensemble members (thin lines of the same color). b) Same as a), but showing the anomaly compared to the annual mean and the shaded curves representing the ensemble variability as ± 1 standard error.

Jiang et al. (2019) suggest that shifts in the high-latitude seasonal cycle are partly due to the dynamic effects from the stratospheric heating and partly due to there being more sunlight to reflect in summer than winter, but were unable to quantify the breakdown of the relative importance of these. There they used, however, simulations with a stratospheric heating imposed on top of a 2010-2030 climate, and compared against a geoengineered climate at the end of the century. Here we have the opportunity to expand on previous analyses since we can directly compare simulations with similar temperature gradients and CO₂ concentrations, but different stratospheric responses. In Fig. 4a, we show the monthly temperatures over the selected area for all simulations: in this case, however, the locally enhanced warming over Eurasia is mixed with the different equator-to-pole temperature gradients (T2): for the 1×1 cases, the warming over high latitudes is primarily due to only keeping global mean temperature constant, which tends to overcool the tropics and undercool high latitudes (Ban-Weiss & Caldeira, 2010; Kravitz et al., 2019). This is further exacerbated in the case of SS since the AOD is mostly concentrated at tropical latitudes. As shown in Russotto and Ackerman (2018b) and Merlis and Henry (2018), the differences in energy transport due to differences in T2 also lead to a residual polar warming in simulations with uniform solar dimming. Therefore, isolating the contribution of residual warming in winter in particular to this high latitude annual-mean pattern requires looking at seasonal differences from the annual mean (Fig. 4b) as in Jiang et al. (2019).

Thus we can see that the SD cases both have a moderate warming over DJF relative to the annual mean (0.75 K) whereas the others have a stronger winter warming (1.22K for 3 × 3 SS, 1.43K for 3 × 3 SDH, and 1.97K for 1 × 1 SS). The 1 × 1 SS and 3 × 3 SDH cases seem to have similar warming, and both have different warming than the 3 × 3 SS case. The differences between the 3 × 3 SS and SDH cases may be explained by looking at the seasonal differences in AOD: as discussed by Visioni, MacMartin, Kravitz, Lee, et al. (2020), for the 3 × 3 SS case, the high latitude AOD reaches a relative peak compared to the annual average exactly in the months where the winter warming is expected, while for the 1 × 1 SS case, the AOD results are much more uniform seasonally. From the comparison of the SD and SDH cases, we can conclude that the winter warming observed over Eurasia in these simulations can only be partially explained by the stratospheric heating. Over half of the high latitude winter warming compared to the annual mean results from differences between SW and LW forcing which, as Govindasamy et al. (2003); Jiang et al. (2019) point out, is especially prominent at high latitudes, and that can't be avoided even if a more careful spatial distribution of the counteracting forcing is applied, as also suggested by Henry and Merlis (2020), where they decomposed the vertical structure of the forcing in a single column model and found that inhomogeneities in the two forcings always result in some residual warming at high latitudes.

In Fig. 5 we show the same comparison as in Fig. 3 but for total precipitation. Results for P-E (precipitation minus evapotranspiration) are reported in the supplementary material (Fig. S2). Generally, it is clear that even given the same temperature targets, there are substantial differences in the projected precipitation changes. In particular, both SD cases show reduced changes compared to the SS cases. Unlike for temperature, however, in this case the SDH case shows further similarities with 3 × 3 SS.

On a decadal scale, precipitation changes can be described by changes in total column energy, which can be broken up into column-integrated diabatic cooling and dry static energy flux divergence (Muller & O’Gorman, 2011). Kravitz, Rasch, et al. (2013) used this framework to explain a simulation analogous to 1 × 1 SD, and we adapt that method for the present study to explain the changes in Fig. 5, with the caveat that our period of analyses is not in a perfect steady state. Following the analyses in Kravitz, Rasch, et al. (2013), the differences in the column-integrated diabatic cooling (excluding latent heating), can be calculated as

$$\Delta Q = \Delta RF_{sf} - \Delta RF_{TOA} - \Delta SH \quad (1)$$

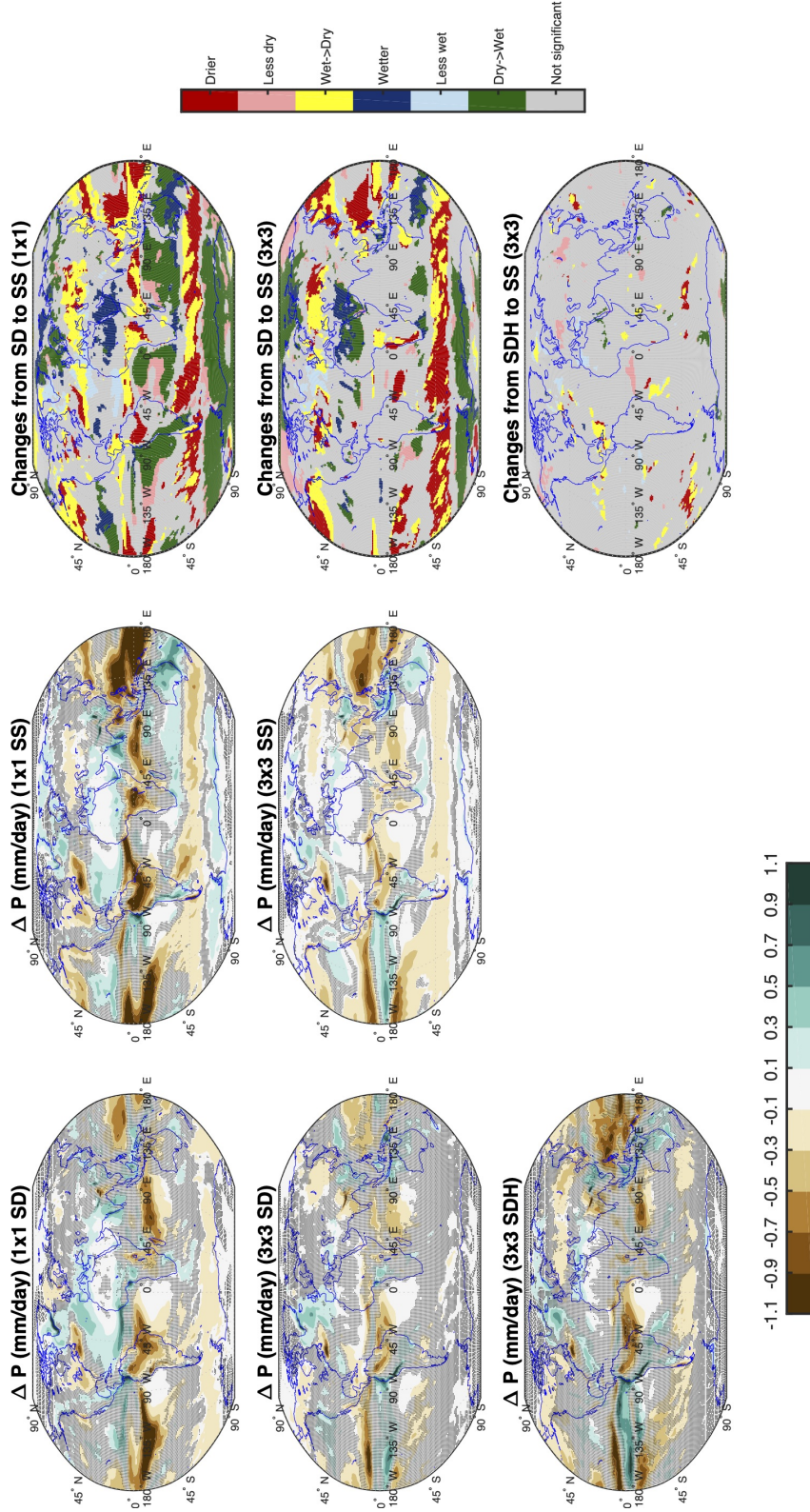


Figure 5. Precipitation changes for all simulations for 2070-2089 relative to 2010-2030. In the third column, areas are highlighted where surface precipitation shows statistically significant changes between the simulations with SD and SS. Grey areas indicate regions in all maps where the differences are not statistically different from zero.

where ΔRF_{sf_c} is the net radiative flux at the surface (SW + LW; positive downward), ΔRF_{TOA} is the net radiative flux at the top-of-atmosphere (positive downward), and ΔSH is the change in sensible heat flux (positive upward, as is customary for turbulent fluxes).

Changes in precipitation can then be calculated as

$$L_c \Delta P = \Delta Q + \Delta H \quad (2)$$

where L_c is the latent heat of condensation, ΔQ is the column integrated diabatic cooling, and ΔH is the dry static energy flux divergence (calculated as a residual). In Fig. 6a-c we show that the SD and 3×3 SS experiments have very different column energy budgets that can help explain some of the differences in surface precipitation shown in Fig. 5. The comparison between panels 6a and 6b indicates that a part of the changes in ΔQ are co-located with differences in temperature between the 1×1 and 3×3 cases, especially in the tropical regions, where a uniform solar reduction (or equatorial stratospheric aerosol injections) tends to overcool the tropics and shifts the inter-tropical convergence zone location. Comparing the results with those for the SDH simulation indicates that part of the precipitation differences between SD and SS simulations can be reduced if the stratospheric heating term is included in the model simulations, due to a more correct partition of energy in the column. Not all differences can be reduced this way: in Fig. 6d we show that differences in the energy flux divergence term are quite similar between the SD and SDH simulations, implying that some of the observed local changes are due to other processes. For instance, the seasonal dependence of AOD has been shown to affect precipitation in particular seasons in some locations (Visioni, MacMartin, Kravitz, Richter, et al., 2020). This can be observed in Fig. S3 and S4, where we show the precipitation changes in two of the seasons (DJF and JJA). As an example, over India the magnitude of precipitation changes in JJA is larger in the 3×3 SS simulations than in other seasons, compared to SD and SDH: in this case, differences in cooling over the Tibetan plateau, driven by the seasonal variation of the AOD, would affect the monsoonal circulation, combined with energetic changes in the column produced by the stratospheric heating (I. R. Simpson et al., 2018; Visioni, MacMartin, Kravitz, Richter, et al., 2020).

3.2 Solar dimming as a modeling analogue for sulfate injections

In this section we discuss our results in light of our initial question: is solar dimming a good proxy for stratospheric sulfate geoengineering? From our analyses, it is clear that generally the outcomes of SD simulations and SS simulations are different: in this section, we try to better quantify these differences. As a baseline for comparison, we use our 20 (members) × 20 (years) 3×3 SS simulations as our best estimate of the forced response (in this model) of an SS strategy that aims to minimize changes in surface climate, and we compare this with the other four simulations (3 members × 20 years for 1×1SD, 1×1SS, 3×3SD and 3×3DH). The metrics we use are surface temperature, precipitation, precipitation minus evapotranspiration, monthly maximum temperatures and monthly maximum precipitation, which have been used previously to define the impacts of geoengineering (P. Irvine et al., 2019), plotted on Taylor diagrams (Fig 7, Taylor, 2001). These kind of diagrams are generally used to evaluate multiple model performances compared to observations on three metrics: the Pearson correlation coefficient, plotted as the azimuthal angle, measures the pattern similarities; the root mean squared error (RMSE), proportional to the distance from the point on the x-axis defined as our benchmark, measures the overall difference between that benchmark and the other simulations; and the standard deviation σ , on the y-axis, that measures the amplitude of the variations in both simulated and the benchmark values (that lie on the dashed line). The similarity is then evaluated as the distance between the single value for each simulation and the benchmark value that lies on the x-axis. In Fig 7 we also include gray shading that serves as a measure of the differences induced by the natural variability. To construct this metric, we consider the general difference between any random pick

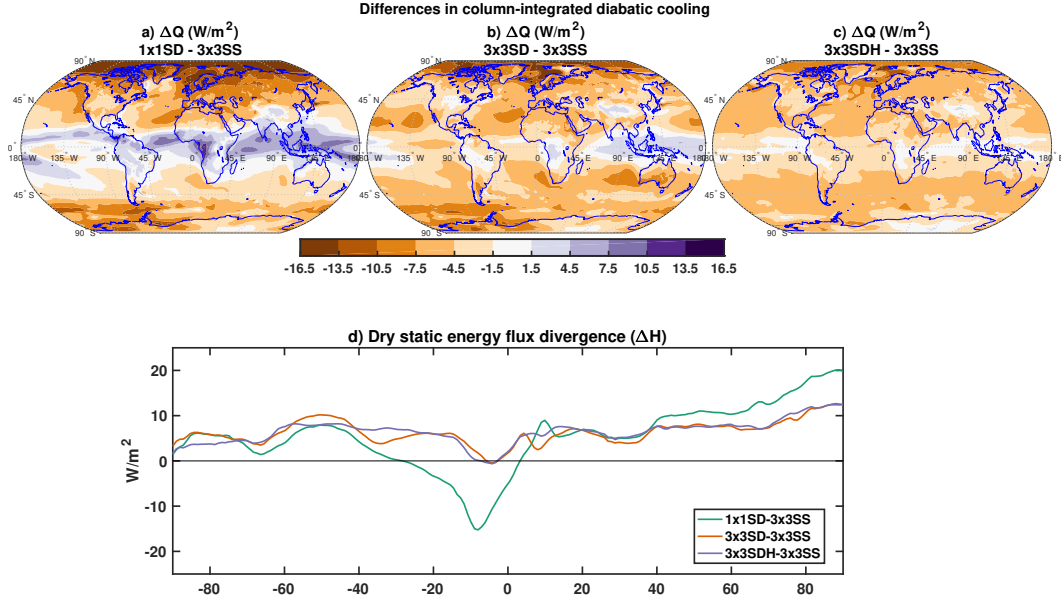


Figure 6. Differences in the column-integrated diabatic cooling (ΔQ , W/m^2) between the 3×3 SS case and the three SD experiments (panels a, b and c, 2070-2089 average). d) Zonal and annual mean differences in the dry static energy flux divergence (ΔH , W/m^2) between the 3×3 SS case and the three SD experiments. See Fig.S5 for a comparison of zonal mean precipitation (in W/m^2) and ΔQ .

of 3 ensemble members of 3×3 SS simulations (overall, $\binom{20}{3} = 1140$) and plot each of the resulting sub-sets against the full 20-members ensemble (the operation performed to obtain this is shown in Fig.S6). The grey shading can therefore be considered as the effect of sampling a smaller ensemble size: if one of the other simulations approaches this area, we cannot tell whether the residual difference is due to natural variability or physical differences between the simulations. From the results in Fig. 7, we conclude that simply turning down the sun produces regional climate results that are highly uncorrelated from those obtained in 3×3 SS simulations. The 3×3 SDH simulation is most similar to the baseline indicating the importance of (1) tailoring the pattern of solar dimming so that the net effect matches the radiative forcing of the aerosols, and (2) including stratospheric heating that would result from the aerosols. This result especially holds for hydrological quantities, indicating that the stratospheric changes produced as a response to stratospheric heating are an especially important component of the climate response to stratospheric sulfate aerosols. For temperature, the differences between 3×3 SD and 3×3 SDH are more marginal, indicating that differences from baseline are predominantly due to the pattern of forcing (see Fig. 2).

3.3 Simulation of other surface variables

Taylor diagrams are most effective for quantities that present at least some patterns of similarity to the baseline. There are other quantities where this does not hold, for example incoming solar radiation at the surface, where previous studies looking at ecologically-relevant metrics (Dagon & Schrag, 2019) have used solar dimming simulations to predict vegetation changes under geoengineering. In Fig. 8 we show some of the differences between SD and SS in 14 locations around the globe (the specific locations are shown in Fig. S7). We have chosen these locations as some of the largest biomass regions in the world: large forest (Song et al., 2018) in all continents save Antarctica, and the US Corn-belt (Green et al., 2018). We first consider the overall amount of incom-

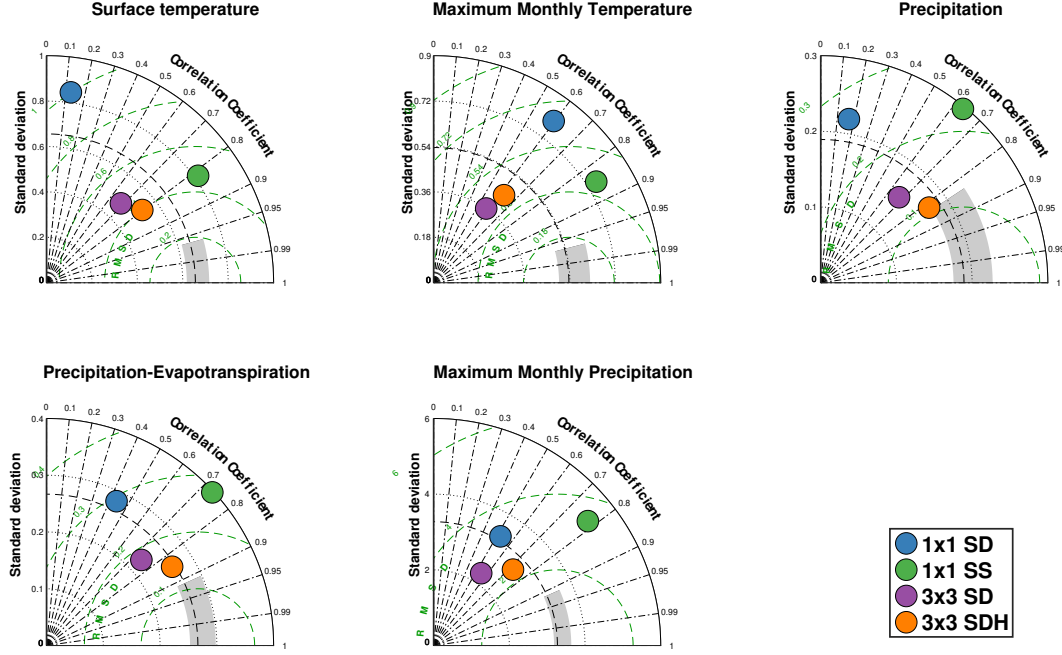


Figure 7. Taylor diagrams for various simulated quantities as compared to the 3×3 SS case. Gray shaded area represents the natural variability in the full 20 members 3×3 SS ensemble, compared to any random pick of three ensemble members from the same set. Therefore, if one of the other sets falls in the shaded area, its differences would be indistinguishable from those produced by natural variability. See text and Fig. S6 for further description.

ing solar radiation at the surface in these zones, and find that differences attributable to both the objectives (1×1 and 3×3) and strategies (SD and SS). In some places, counter-intuitively, the overall amount of incoming solar radiation even goes up compared to the control period, mainly due to local changes in cloud coverage (Fig. 9). Differences between SD and SS simulations in this case are associated with very high clouds, and results would be rather different if we consider low-, medium- or high-altitude clouds (see Figs. S8-S10), suggesting different mechanisms by which geoengineering, in these simulations, affects cloud coverage. In particular, while low-altitude clouds show very similar changes between SS and SD simulations, medium-altitude clouds present differences that are resolved (at mid and low latitudes) by including the stratospheric heating term, suggesting their modification is driven mostly by dynamical changes produced by the temperature anomalies in the lower stratosphere and not by climate-change driven factors (e.g. Norris et al., 2016). High-altitude ice clouds, that have a strong radiative effect on outgoing longwave radiation at mid-latitudes (Fusina et al., 2007), show the highest differences. Contrary to previous research (Kuebbeler et al., 2012; Visoni, Pitari, Di Genova, et al., 2018) with different models that showed how these changes are also driven by the vertical temperature gradient, here the main cause of the changes seems to be the aerosols themselves. While it has already been suggested that this might be due to incorrect parametrizations in CESM1(WACCM) (Schmidt et al., 2018), further investigation is warranted.

Similarly, large differences are present when considering the changes in direct and diffuse radiation, that might be very important when considering effects on vegetation (Proctor et al., 2018): in this case large differences are not only present between SS and SD cases, but even among different strategies for similar methods (e.g., differences between 1×1 SS and 3×3 SS). Therefore, when assessing possible side effects on vege-

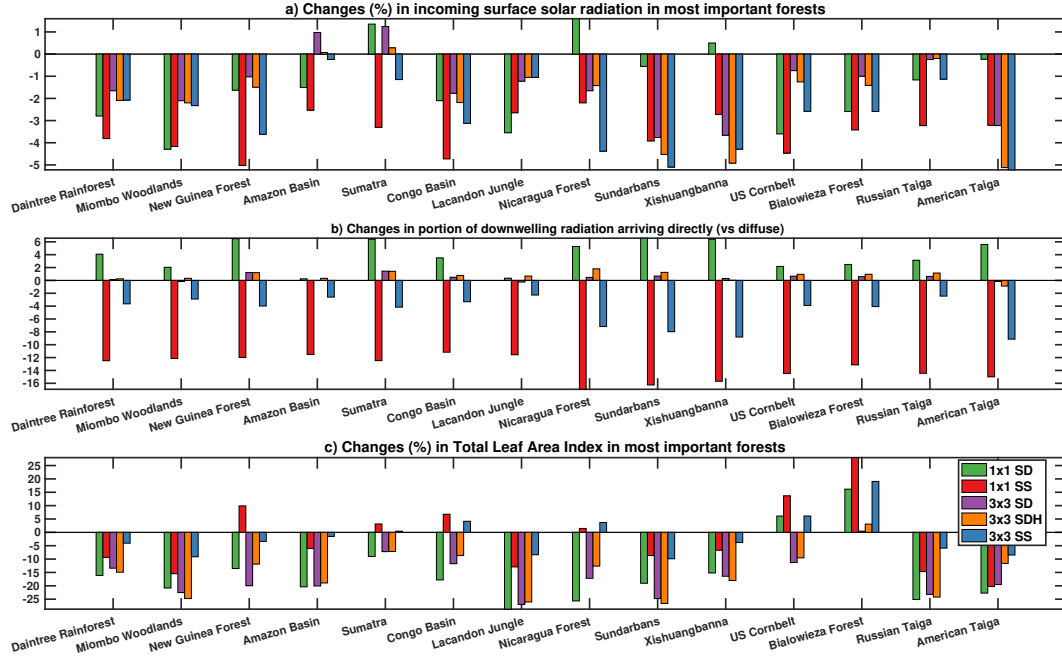


Figure 8. a) Changes in incoming solar radiation in 14 locations with some of the largest forests (see Fig. S7 and text) for all five experiments. b) Changes in the portion of incoming solar radiation arriving directly, compared to the portion arriving as diffuse. c) Simulated changed in Total Leaf Area Index in those locations.

tation or agriculture, studies should take great care to use simulations where the aerosols are present in a realistic distribution.

A correct representation of the changes in cloudiness would be important not just for the radiation effects on ecosystems: the importance of clouds in the surface radiative budget of continental ice sheets (McIlhatten et al., 2017; van Kampenhout et al., 2020) indicates that, in order to assess the ability of SG to limit sea level rise (P. J. Irvine et al., 2018) and restore continental glaciers extent, SD simulations as a proxy might produce incorrect results by incorrectly reproducing cloud changes and, partially, high-latitude warming produced by the stratospheric heating.

3.4 Simulation of the stratospheric response

As we've shown in the previous sections, the stratospheric response is an important component in correctly capturing the climate response to sulfate injections. In the case of surface variables, this mainly happens due to dynamical changes in the circulation (Fig. S11). Previous works have shown that stratospheric chemistry would also be impacted by the sulfate aerosols (Visioni, Pitari, Aquila, Tilmes, et al., 2017; Tilmes, Richter, Mills, et al., 2018; Vattioni et al., 2019) but in most cases, these changes (such as in the concentration of N_2O and CH_4) are also due to modifications of stratospheric dynamics. The effects of SS on stratospheric ozone may however vary due to different causes other than dynamical changes (Tilmes et al., 2008; Pitari et al., 2014; Tilmes, Richter, Mills, et al., 2018), for instance by the direct increase in Surface Area Density (SAD) resulting in changes in heterogeneous chemistry (Richter et al., 2017), both in the tropics and at higher altitudes. These changes might be important to project changes in surface UV (Madronich et al., 2018), with consequent human impacts (Eastham et al., 2018).

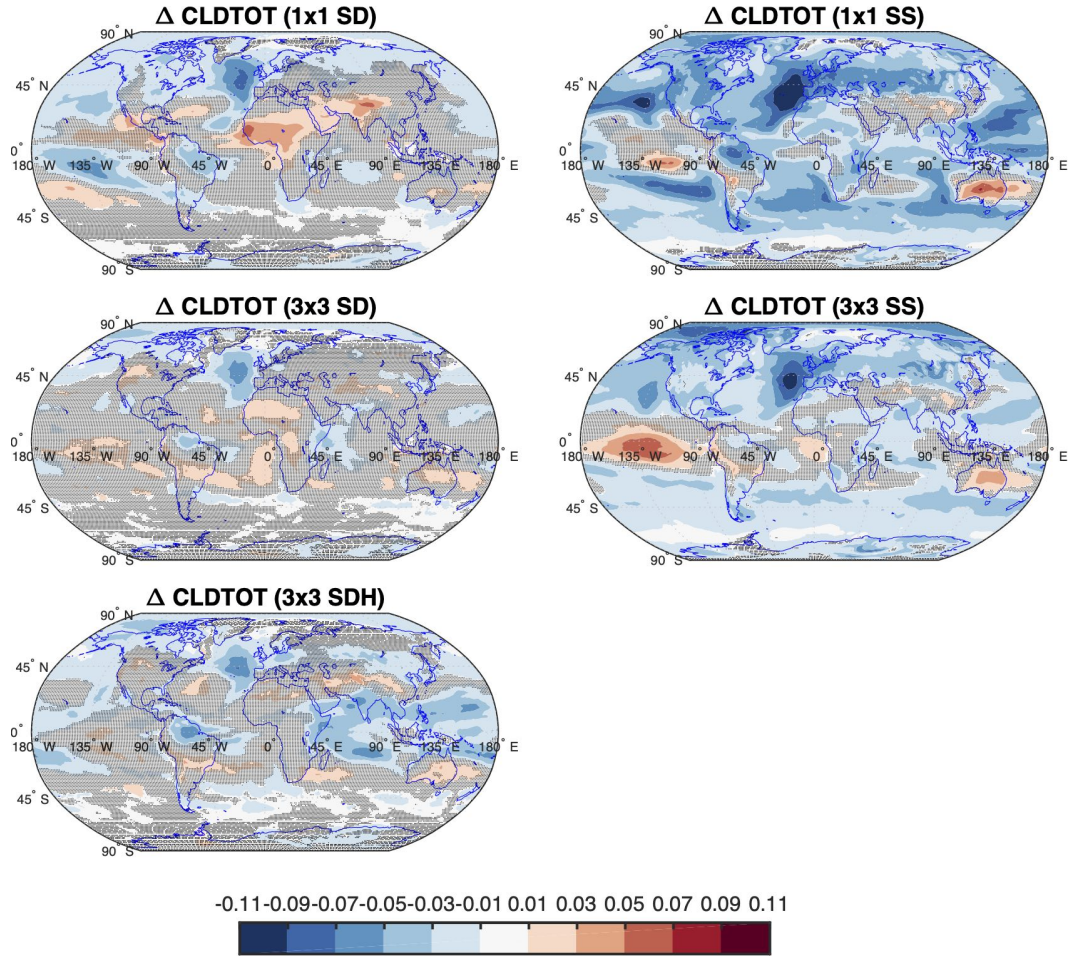


Figure 9. Changes in simulated total cloud fraction in the 5 geoengineering experiments compared to the Control 2010-2030 period.

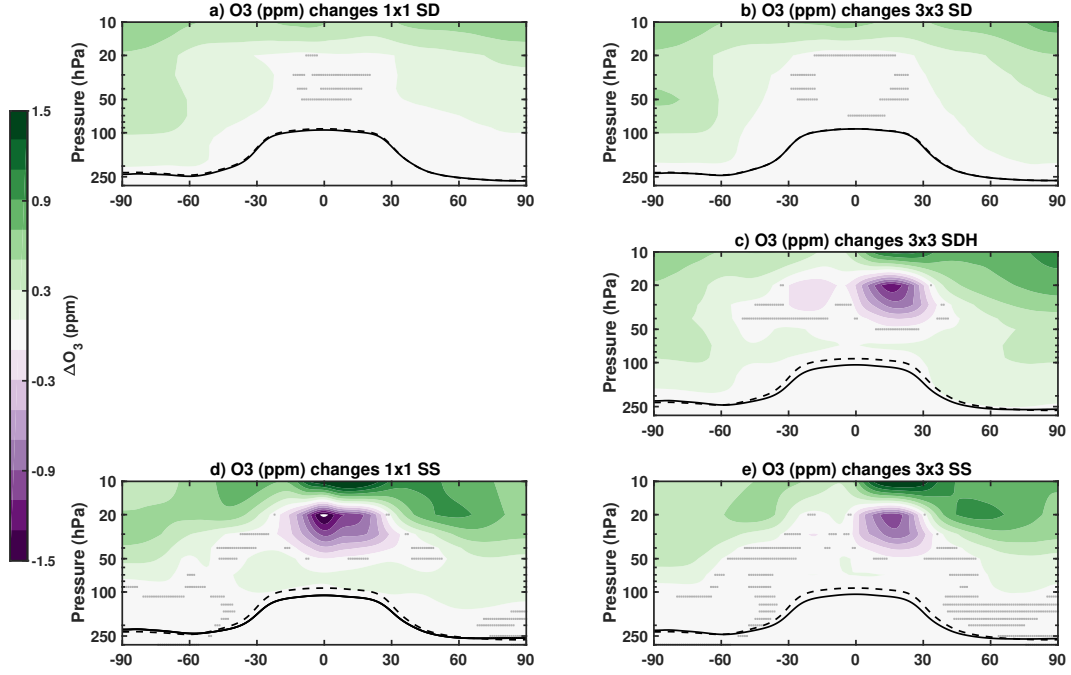


Figure 10. Changes in stratospheric ozone concentrations (ppm) compared to Control. Average tropopause height for Control (continuous black line) and the simulations shown in the panels (dashed black line) are also shown.

Chemical ozone destruction due to increased SAD, especially in the polar regions, is mostly tied to changes in ozone-depleting substances (Morgenstern et al., 2018) that are projected to strongly decrease in the following decades (Dhomse et al., 2018). Therefore, the relative contributions of chemical versus dynamical ozone destruction depend on the decade of analyses. In our analyses towards the end of the century, the predominant effect in the tropical regions is driven by dynamical circulation changes, as can be observed in the comparison between Fig. 10c and 10e, whereas at higher latitudes the SAD-induced changes result in a delay of the predicted recovery (Tilmes et al., 2008) that is not observed in the SDH case in Fig. 10e.

4 Conclusions

Simulations with climate models are our main instrument for understanding the possible changes to the Earth System that would be produced by using geoengineering to counteract the effects of increases in GHGs. Properly simulating the projected regional effects is crucial in order to inform policy-makers and the general population about the possible outcomes.

Even just for climate change, there are uncertainties in the projected local changes, although with improvements in climate models, these uncertainties are decreasing (Christensen et al., 2007; Matte et al., 2019). For solar geoengineering, our assessment of local changes would however depend on more factors than for climate change: aside from the uncertainty in specific physical processes (Kravitz & MacMartin, 2020), these factors include i) the desired level of cooling (P. Irvine et al., 2019; MacMartin et al., 2019; Tilmes et al., 2020); ii) the specific technique simulated (Niemeier et al., 2013), and iii) within the same technique, the specific strategy deployed (Kravitz et al., 2019; Visioni, MacMartin, Kravitz, Richter, et al., 2020). There is thus a compound of different kinds of uncertainties that result in challenges in clearly determining - and communicating - what effects geoengineering would have locally.

This is made even more challenging if the term “solar geoengineering” is used improperly to conflate different things, and in particular, stratospheric sulfate injections in all its forms and a global reduction in the incoming solar radiation (i.e. the G1 experiment described in Kravitz et al., 2011). On one hand, the use of the latter to simplify the former is understandable, considering the challenges in correctly simulating stratospheric dynamics and stratospheric sulfate interactions (Timmreck et al., 2018; Kravitz & MacMartin, 2020). But, as we show in this work, the outcomes in the two different cases are widely different in many aspects of the response of the climate system: we have shown here the differences on surface temperature, precipitation and incoming solar radiation. The reason for these differences comes from three different major causes:

1. the aerosols do not produce a uniform reduction in the incoming solar radiation (both latitudinally and during the year, Fig. 2). Especially if the deployed injection strategy has particular goals resulting in a particular aerosol distribution (e.g., the strategy described in Tilmes, Richter, Kravitz, et al., 2018), the comparison with a uniform solar dimming produces widely different results, both in regional temperatures and precipitations. This is mainly due to differences in the resulting temperature gradients, that produce shifts in the climate response (as discussed, for different SS strategies, in Kravitz et al. (2019)). Because of this, these discrepancies can be reduced if the solar constant is dimmed not uniformly, but in a way more closely resembling the actual distribution of the aerosols, in order to have the same temperature gradients that SS would strive to maintain.
2. the aerosols produce a stratospheric warming that results in various changes at the surface and in the upper atmosphere. Even if the same temperature gradients are maintained, quantities such as precipitation and P-E still show differences if the sun is dimmed compared to the presence of the aerosols. In our simulations, combining solar dimming to maintain temperature targets with stratospheric heating helps further reduce the differences with the 3×3 SS strategy.
3. the aerosols scatter part of the incoming sunlight, modifying the ratio of direct to diffuse radiation, possibly modifying the projected changes on vegetation and evapotranspiration. The aerosols also affect stratospheric chemistry (principally ozone), and also ultimately result in the deposition of sulfate at the surface that might have environmental effects (albeit those are usually small, see Kravitz et al., 2009; Visioni, Slessarev, et al., 2020). This can only be simulated if the aerosols are effectively in the stratosphere. These latter points are summarized in Fig. 11,

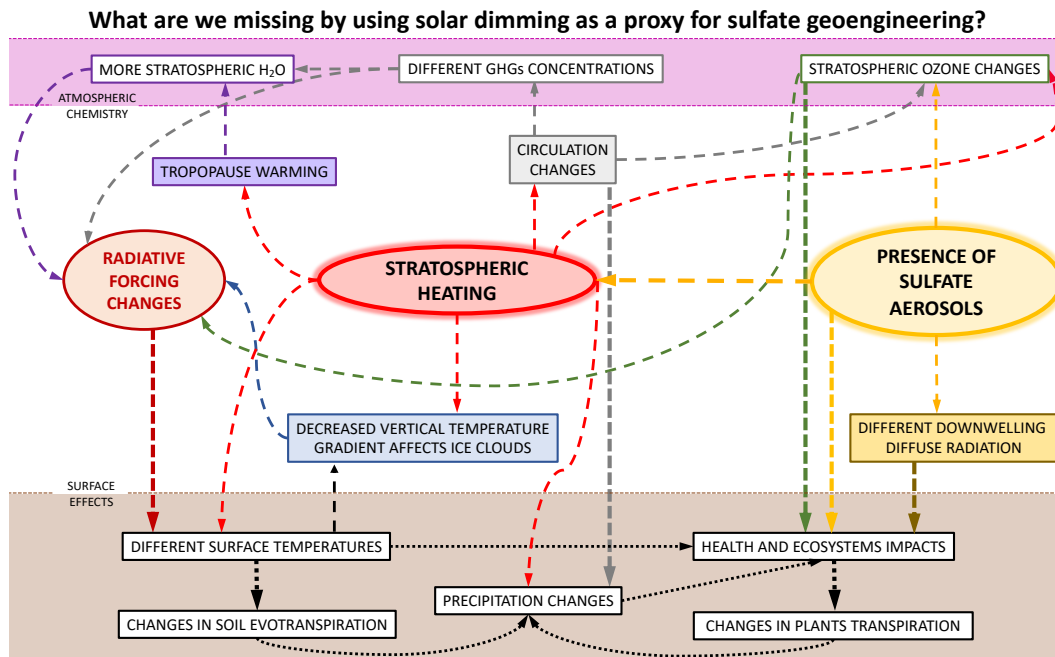


Figure 11. Summary of all physical effects on the climate system produced by the inclusion of the stratospheric aerosols.

highlighting the interconnections in the climate system that result, ultimately, in changes at the surface.

Are the changes in the surface climate that would be produced significant? This is a question that depends on the amount of cooling provided by the geoengineering and thus on the amount of injected SO_2 . In the simulations analyzed here, we use the RCP8.5 scenario, that has extremely high emissions throughout all the century and that result in around 4 degrees of warming in the period we consider. Ours can therefore be considered an ‘extreme’ scenario unlikely to happen, resulting in the need of very high injection amounts producing a considerable perturbation in stratospheric temperature. Considering a peak-shaving scenario where a limited deployment is aimed at remaining below an otherwise dangerous temperature threshold (MacMartin & Kravitz, 2019; Tilmes et al., 2020) would very likely result in some of these changes being indistinguishable from the normal climate variability (MacMartin et al., 2019).

In the last years, however, the topic of the impacts of climate engineering has gathered more and more interest not only from climate scientists but also from the broader scientific community, interested in impacts both on human activities (Tavoni et al., 2017) and on the environment and ecosystems (Proctor et al., 2018). Because of this, a proper, robust assessment of all possible side effects is becoming increasingly crucial. While this mainly requires tackling uncertainties in our physical knowledge and shortcomings in our climate simulations (Kravitz & MacMartin, 2020), the importance of recognizing the shortcomings of using solar dimming as a proxy for stratospheric sulfate geoengineering can’t be ignored.

Acknowledgments

The authors would like to thank I.R. Simpson for the numerous meaningful discussions and I.R. Simpson and S. Tilmes for their support with the CESM1(WACCM) simula-

tions. We would like to acknowledge high-performance computing support from Cheyenne (https://doi.org/10. 5065/D6RX99HX) provided by NCAR’s Computational and Information Systems Laboratory, sponsored by the National Science Foundation. Support for D. V. and D. G. M. was provided by the Atkinson Center for a Sustainable Future at Cornell University and by the National Science Foundation through agreement CBET-1818759. Support for B.K. was provided in part by the National Science Foundation through agreement CBET-1931641, the Indiana University Environmental Resilience Institute, and the *Prepared for Environmental Change* Grand Challenge initiative. The Pacific Northwest National Laboratory is operated for the US Department of Energy by Battelle Memorial Institute under contract DE-AC05-76RL01830.

References

- Aquila, V., Garfinkel, C., Newman, P., Oman, L., & Waugh, D. (2014). Modifications of the quasi-biennial oscillation by a geoengineering perturbation of the stratospheric aerosol layer. *Geophysical Research Letters*, 41(5), 1738–1744.
- Ban-Weiss, G. A., & Caldeira, K. (2010). Geoengineering as an optimization problem. *Environmental Research Letters*, 5(3). doi: 10.1088/1748-9326/5/3/034009
- Budyko, M. I. (1978). *The climate of the future*. American Geophysical Union. Retrieved from <http://dx.doi.org/10.1002/9781118665251.ch7> doi: 10.1002/9781118665251.ch7
- Cheng, W., MacMartin, D. G., Dagon, K., Kravitz, B., Tilmes, S., Richter, J. H., ... Simpson, I. R. (2019). Soil moisture and other hydrological changes in a stratospheric aerosol geoengineering large ensemble. *Journal of Geophysical Research: Atmospheres*, 124(23), 12773–12793. Retrieved from <https://agupubs.onlinelibrary.wiley.com/doi/abs/10.1029/2018JD030237> doi: 10.1029/2018JD030237
- Christensen, J. H., Hewitson, B., Busuioc, A., Chen, A., Gao, X., Held, R., ... others (2007). Regional climate projections. In *Climate Change, 2007: The Physical Science Basis. Contribution of Working group I to the Fourth Assessment Report of the Intergovernmental Panel on Climate Change*, University Press, Cambridge, Chapter 11 (pp. 847–940).
- Crutzen, P. J. (2006). Albedo enhancement by stratospheric sulfur injections: A contribution to resolve a policy dilemma? *Climatic Change*, 77(3), 211–220. Retrieved from <http://dx.doi.org/10.1007/s10584-006-9101-y> doi: 10.1007/s10584-006-9101-y
- Dagon, K., & Schrag, D. P. (2019). Quantifying the effects of solar geoengineering on vegetation. *Climatic Change*, 153(1), 235–251.
- Dai, Z., Weisenstein, D. K., & Keith, D. W. (2018). Tailoring Meridional and Seasonal Radiative Forcing by Sulfate Aerosol Solar Geoengineering. *Geophysical Research Letters*, 45(2), 1030–1039. doi: 10.1002/2017GL076472
- Dhomse, S. S., Kinnison, D., Chipperfield, M. P., Salawitch, R. J., Cionni, I., Hegglin, M. I., ... Zeng, G. (2018). Estimates of ozone return from Chemistry-Climate Model Initiative simulations. *Atmospheric Chemistry and Physics*, 18(11), 8409–8438. doi: 10.5194/acp-18-8409-2018
- Eastham, S. D., Weisenstein, D. K., Keith, D. W., & Barrett, S. R. (2018). Quantifying the impact of sulfate geoengineering on mortality from air quality and UV-B exposure. *Atmospheric Environment*, 187, 424 - 434. Retrieved from <http://www.sciencedirect.com/science/article/pii/S1352231018303510> doi: <https://doi.org/10.1016/j.atmosenv.2018.05.047>
- Fasullo, J. T., Simpson, I. R., Kravitz, B., Tilmes, S., Richter, J. H., MacMartin, D. G., & Mills, M. J. (2018). Persistent polar ocean warming in a strategically geoengineered climate. *Nature Geoscience*, 11(12), 910–914. Retrieved from <http://dx.doi.org/10.1038/s41561-018-0249-7> doi:

- 10.1038/s41561-018-0249-7
- Ferraro, A. J., Charlton-Perez, A. J., & Highwood, E. J. (2015). Stratospheric dynamics and midlatitude jets under geoengineering with space mirrors and sulfate and titania aerosols. *Journal of Geophysical Research: Atmospheres*, 120(2), 414-429. Retrieved from <https://agupubs.onlinelibrary.wiley.com/doi/abs/10.1002/2014JD022734> doi: 10.1002/2014JD022734
- Fusina, F., Spichtinger, P., & Lohmann, U. (2007). Impact of ice supersaturated regions and thin cirrus on radiation in the midlatitudes. *Journal of Geophysical Research: Atmospheres*, 112(D24), n/a–n/a. Retrieved from <http://dx.doi.org/10.1029/2007JD008449> (D24S14) doi: 10.1029/2007JD008449
- Glienke, S., Irvine, P. J., & Lawrence, M. G. (2015). The impact of geoengineering on vegetation in experiment G1 of the GeoMIP. *Journal of Geophysical Research: Atmospheres*, 120(19), 10,196-10,213. Retrieved from <https://agupubs.onlinelibrary.wiley.com/doi/abs/10.1002/2015JD024202> doi: 10.1002/2015JD024202
- Govindasamy, B., Caldeira, K., & Duffy, P. (2003). Geoengineering earth's radiation balance to mitigate climate change from a quadrupling of CO₂. *Global and Planetary Change*, 37(1), 157 - 168. Retrieved from <http://www.sciencedirect.com/science/article/pii/S0921818102001959> (Evaluation, Intercomparison and Application of Global Climate Models) doi: [https://doi.org/10.1016/S0921-8181\(02\)00195-9](https://doi.org/10.1016/S0921-8181(02)00195-9)
- Green, T. R., Kipka, H., David, O., & McMaster, G. S. (2018). Where is the USA Corn Belt, and how is it changing? *Science of The Total Environment*, 618, 1613 - 1618. Retrieved from <http://www.sciencedirect.com/science/article/pii/S0048969717326761> doi: <https://doi.org/10.1016/j.scitotenv.2017.09.325>
- Guo, A., Moore, J. C., & Ji, D. (2018). Tropical atmospheric circulation response to the G1 sunshade geoengineering radiative forcing experiment. *Atmospheric Chemistry and Physics*, 18(12), 8689–8706. Retrieved from <https://www.atmos-chem-phys.net/18/8689/2018/> doi: 10.5194/acp-18-8689-2018
- Hansen, J., Sato, M., Ruedy, R., Nazarenko, L., Lacis, A., Schmidt, G. A., ... Zhang, S. (2005). Efficacy of climate forcings. *Journal of Geophysical Research: Atmospheres*, 110(D18). Retrieved from <https://agupubs.onlinelibrary.wiley.com/doi/abs/10.1029/2005JD005776> doi: 10.1029/2005JD005776
- Harding, A. R., Ricke, K., Heyen, D., MacMartin, D. G., & Moreno-Cruz, J. (2020). Climate econometric models indicate solar geoengineering would reduce inter-country income inequality. *Nature Communications*, 11(1), 227. Retrieved from <https://doi.org/10.1038/s41467-019-13957-x> doi: 10.1038/s41467-019-13957-x
- Henry, M., & Merlis, T. M. (2020). Forcing dependence of atmospheric lapse rate changes dominates residual polar warming in solar radiation management climate scenarios. *Geophysical Research Letters*, 47(15), e2020GL087929. Retrieved from <https://agupubs.onlinelibrary.wiley.com/doi/abs/10.1029/2020GL087929> (e2020GL087929 10.1029/2020GL087929) doi: 10.1029/2020GL087929
- Irvine, P., Emanuel, K., He, J., Horowitz, L. W., Vecchi, G., & Keith, D. (2019). Halving warming with idealized solar geoengineering moderates key climate hazards. *Nature Climate Change*, 9(4), 295–299. Retrieved from <http://dx.doi.org/10.1038/s41558-019-0398-8> doi: 10.1038/s41558-019-0398-8
- Irvine, P. J., & Keith, D. W. (2020, mar). Halving warming with stratospheric aerosol geoengineering moderates policy-relevant climate hazards. *Environmental Research Letters*, 15(4), 044011. doi: 10.1088/1748-9326/ab76de
- Irvine, P. J., Keith, D. W., & Moore, J. (2018). Brief communication: Understanding solar geoengineering's potential to limit sea level rise requires attention from cryosphere experts. *The Cryosphere*, 12(7), 2501–2513. Re-

- trieved from <https://tc.copernicus.org/articles/12/2501/2018/> doi: 10.5194/tc-12-2501-2018
- Ji, D., Fang, S., Curry, C. L., Kashimura, H., Watanabe, S., Cole, J. N. S., ... Moore, J. C. (2018). Extreme temperature and precipitation response to solar dimming and stratospheric aerosol geoengineering. *Atmospheric Chemistry and Physics*, 18(14), 10133–10156. Retrieved from <https://www.atmos-chem-phys.net/18/10133/2018/> doi: 10.5194/acp-18-10133-2018
- Jiang, J., Cao, L., MacMartin, D. G., Simpson, I. R., Kravitz, B., Cheng, W., ... Mills, M. J. (2019). Stratospheric Sulfate Aerosol Geoengineering Could Alter the High-Latitude Seasonal Cycle. *Geophysical Research Letters*, 46(23), 14153–14163. doi: 10.1029/2019GL085758
- Jones, A. C., Hawcroft, M. K., Haywood, J. M., Jones, A., Guo, X., & Moore, J. C. (2018). Regional Climate Impacts of Stabilizing Global Warming at 1.5 K Using Solar Geoengineering. *Earth's Future*, 6(2), 230–251. doi: 10.1002/2017EF000720
- Kalidindi, S., Bala, G., Modak, A., & Caldeira, K. (2015). Modeling of solar radiation management: a comparison of simulations using reduced solar constant and stratospheric sulphate aerosols. *Climate Dynamics*, 44(9), 2909–2925. Retrieved from <https://doi.org/10.1007/s00382-014-2240-3> doi: 10.1007/s00382-014-2240-3
- Kleinschmitt, C., Boucher, O., & Platt, U. (2018). Sensitivity of the radiative forcing by stratospheric sulfur geoengineering to the amount and strategy of the so2 injection studied with the LMDZ-S3A model. *Atmospheric Chemistry and Physics*, 18(4), 2769–2786. Retrieved from <https://www.atmos-chem-phys.net/18/2769/2018/> doi: 10.5194/acp-18-2769-2018
- Kravitz, B., Caldeira, K., Boucher, O., Robock, A., Rasch, P. J., Alterskjær, K., ... Yoon, J.-H. (2013). Climate model response from the geoengineering model intercomparison project (geomip). *Journal of Geophysical Research: Atmospheres*, 118(15), 8320–8332. Retrieved from <https://agupubs.onlinelibrary.wiley.com/doi/abs/10.1002/jgrd.50646> doi: 10.1002/jgrd.50646
- Kravitz, B., Lamarque, J.-F., Tribbia, J. J., Tilmes, S., Vitt, F., Richter, J. H., ... Mills, M. J. (2017). First Simulations of Designing Stratospheric Sulfate Aerosol Geoengineering to Meet Multiple Simultaneous Climate Objectives. *Journal of Geophysical Research: Atmospheres*, 122(23), 12,616–12,634. doi: 10.1002/2017jd026874
- Kravitz, B., & MacMartin, D. G. (2020). Uncertainty and the basis for confidence in solar geoengineering research. *Nature Reviews Earth & Environment*, 1(1), 64–75. Retrieved from <http://dx.doi.org/10.1038/s43017-019-0004-7> doi: 10.1038/s43017-019-0004-7
- Kravitz, B., MacMartin, D. G., & Caldeira, K. (2012). Geoengineering: Whiter skies? *Geophysical Research Letters*, 39(11). Retrieved from <https://agupubs.onlinelibrary.wiley.com/doi/abs/10.1029/2012GL051652> doi: 10.1029/2012GL051652
- Kravitz, B., MacMartin, D. G., Tilmes, S., Richter, J. H., Mills, M. J., Cheng, W., ... Vitt, F. (2019). Comparing surface and stratospheric impacts of geoengineering with different SO2 injection strategies. *Journal of Geophysical Research: Atmospheres*, 124(14), 7900–7918. Retrieved from <https://agupubs.onlinelibrary.wiley.com/doi/abs/10.1029/2019JD030329> doi: 10.1029/2019JD030329
- Kravitz, B., MacMartin, D. G., Wang, H., & Rasch, P. J. (2016). Geoengineering as a design problem. *Earth System Dynamics*, 7(2), 469–497. doi: 10.5194/esd-7-469-2016
- Kravitz, B., Rasch, P. J., Forster, P. M., Andrews, T., Cole, J. N., Irvine, P. J., ...

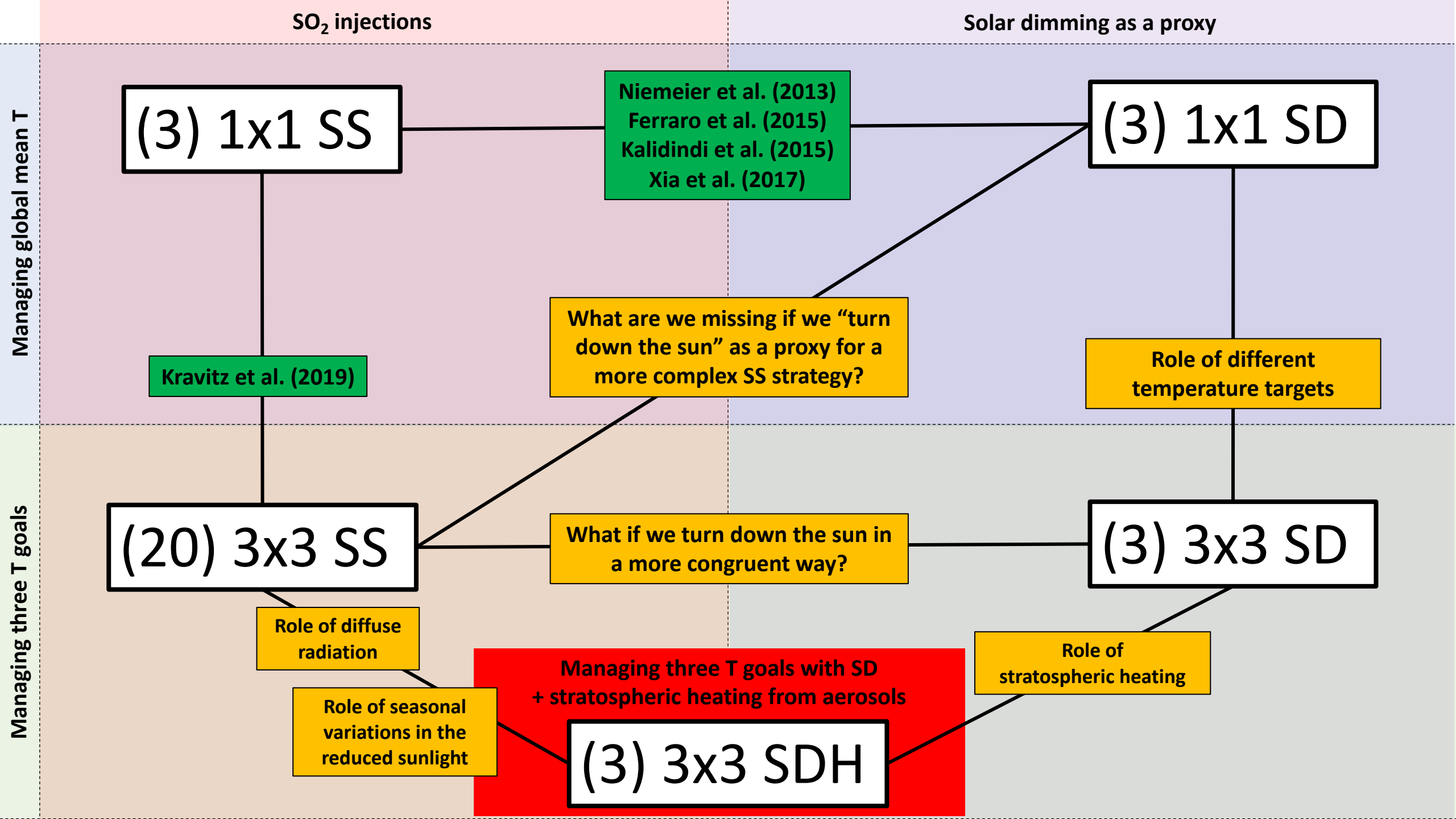
- Yoon, J. H. (2013). An energetic perspective on hydrological cycle changes in the Geoengineering Model Intercomparison Project. *Journal of Geophysical Research Atmospheres*, 118(23), 13,087–13,102. doi: 10.1002/2013JD020502
- Kravitz, B., Robock, A., Boucher, O., Schmidt, H., Taylor, K. E., Stenchikov, G., & Schulz, M. (2011). The Geoengineering Model Intercomparison Project (GeoMIP). *Atmospheric Science Letters*, 12(2), 162–167. Retrieved from <https://rmets.onlinelibrary.wiley.com/doi/abs/10.1002/asl.316> doi: 10.1002/asl.316
- Kravitz, B., Robock, A., Oman, L., Stenchikov, G., & Marquardt, A. B. (2009). Sulfuric acid deposition from stratospheric geoengineering with sulfate aerosols. *Journal of Geophysical Research Atmospheres*, 114(14), 1–7. doi: 10.1029/2009JD011918
- Kuebbeler, M., Lohmann, U., & Feichter, J. (2012). Effects of stratospheric sulfate aerosol geo-engineering on cirrus clouds. *Geophysical Research Letters*, 39(23). Retrieved from <http://dx.doi.org/10.1029/2012GL053797> (L23803) doi: 10.1029/2012GL053797
- Lee, W., MacMartin, D., Vioni, D., & Kravitz, B. (2020). Expanding the design space of stratospheric aerosol geoengineering to include precipitation-based objectives and explore trade-offs. *Earth System Dynamics Discussions*, 2020, 1–31. Retrieved from <https://esd.copernicus.org/preprints/esd-2020-58/> doi: 10.5194/esd-2020-58
- Low, S., & Schfer, S. (2019). Tools of the trade: practices and politics of researching the future in climate engineering. *Sustainability Science*, 14(4), 953–962. Retrieved from <https://doi.org/10.1007/s11625-019-00692-x> doi: 10.1007/s11625-019-00692-x
- MacMartin, D. G., Keith, D. W., Kravitz, B., & Caldeira, K. (2013). Management of trade-offs in geoengineering through optimal choice of non-uniform radiative forcing. *Nature Climate Change*, 3(4), 365–368. Retrieved from <https://doi.org/10.1038/nclimate1722> doi: 10.1038/nclimate1722
- MacMartin, D. G., & Kravitz, B. (2019). Mission-driven research for stratospheric aerosol geoengineering. *Proceedings of the National Academy of Sciences*, 116(4), 1089–1094. doi: 10.1073/pnas.1811022116
- MacMartin, D. G., Kravitz, B., Mills, M. J., Tribbia, J. J., Tilmes, S., Richter, J. H., ... Lamarque, J.-F. (2017). The Climate Response to Stratospheric Aerosol Geoengineering Can Be Tailored Using Multiple Injection Locations. *Journal of Geophysical Research: Atmospheres*, 122(23), 12,574–12,590. doi: 10.1002/2017jd026868
- MacMartin, D. G., Wang, W., Richter, J. H., Mills, M. J., Kravitz, B., & Tilmes, S. (2019). Timescale for Detecting the Climate Response to Stratospheric Aerosol Geoengineering. *Journal of Geophysical Research: Atmospheres*, 1233–1247. doi: 10.1029/2018jd028906
- Madronich, S., Tilmes, S., Kravitz, B., MacMartin, D. G., & Richter, J. H. (2018). Response of surface ultraviolet and visible radiation to stratospheric SO₂ injections. *Atmosphere*, 9(11). doi: 10.3390/atmos9110432
- Matte, D., Larsen, M. A. D., Christensen, O. B., & Christensen, J. H. (2019). Robustness and scalability of regional climate projections over Europe. *Frontiers in Environmental Science*, 6, 163. Retrieved from <https://www.frontiersin.org/article/10.3389/fenvs.2018.00163> doi: 10.3389/fenvs.2018.00163
- McIlhattan, E. A., Lacuyer, T. S., & Miller, N. B. (2017, 05). Observational Evidence Linking Arctic Supercooled Liquid Cloud Biases in CESM to Snowfall Processes. *Journal of Climate*, 30(12), 4477–4495. Retrieved from <https://doi.org/10.1175/JCLI-D-16-0666.1> doi: 10.1175/JCLI-D-16-0666.1
- Merlis, T. M., & Henry, M. (2018, 06). Simple Estimates of Polar Amplification in Moist Diffusive Energy Balance Models. *Journal of Climate*, 31(15), 5811–5824. Retrieved from <https://doi.org/10.1175/JCLI-D-17-0578.1> doi: 10

- .1175/JCLI-D-17-0578.1
- Mills, M. J., Richter, J. H., Tilmes, S., Kravitz, B., Macmartin, D. G., Glanville, A. A., ... Kinnison, D. E. (2017). Radiative and chemical response to interactive stratospheric sulfate aerosols in fully coupled CESM1(WACCM). *Journal of Geophysical Research: Atmospheres*, 122(23), 13,061–13,078. doi: 10.1002/2017JD027006
- Mills, M. J., Schmidt, A., Easter, R., Solomon, S., Kinnison, D. E., Ghan, S. J., ... Gettelman, A. (2016). Global volcanic aerosol properties derived from emissions, 1990–2014, using CESM1(WACCM). *Journal of Geophysical Research: Atmospheres*, 121(5), 2332–2348. Retrieved from <https://agupubs.onlinelibrary.wiley.com/doi/abs/10.1002/2015JD024290> doi: 10.1002/2015JD024290
- Morgenstern, O., Stone, K. A., Schofield, R., Akiyoshi, H., Yamashita, Y., Kinnison, D. E., ... Chipperfield, M. P. (2018). Ozone sensitivity to varying greenhouse gases and ozone-depleting substances in CCMI-1 simulations. *Atmospheric Chemistry and Physics*, 18(2), 1091–1114. Retrieved from <https://www.atmos-chem-phys.net/18/1091/2018/> doi: 10.5194/acp-18-1091-2018
- Muller, C. J., & O’Gorman, P. A. (2011). An energetic perspective on the regional response of precipitation to climate change. *Nature Climate Change*, 1(5), 266–271. Retrieved from <https://doi.org/10.1038/nclimate1169> doi: 10.1038/nclimate1169
- Niemeier, U., Richter, J. H., & Tilmes, S. (2020). Differing responses of the QBO to SO₂ injections in two global models. *Atmospheric Chemistry and Physics Discussions*, 2020, 1–21. Retrieved from <https://www.atmos-chem-phys-discuss.net/acp-2020-206/> doi: 10.5194/acp-2020-206
- Niemeier, U., & Schmidt, H. (2017). Changing transport processes in the stratosphere by radiative heating of sulfate aerosols. *Atmospheric Chemistry and Physics*, 17(24), 14871–14886. Retrieved from <https://www.atmos-chem-phys.net/17/14871/2017/> doi: 10.5194/acp-17-14871-2017
- Niemeier, U., Schmidt, H., Alterskjær, K., & Kristjánsson, J. E. (2013). Solar irradiance reduction via climate engineering: Impact of different techniques on the energy balance and the hydrological cycle. *Journal of Geophysical Research: Atmospheres*, 118(21), 11,905–11,917. Retrieved from <https://agupubs.onlinelibrary.wiley.com/doi/abs/10.1002/2013JD020445> doi: 10.1002/2013JD020445
- Norris, J. R., Allen, R. J., Evan, A. T., Zelinka, M. D., O’Dell, C. W., & Klein, S. A. (2016). Evidence for climate change in the satellite cloud record. *Nature*, 536(7614), 72–75. Retrieved from <https://doi.org/10.1038/nature18273> doi: 10.1038/nature18273
- Oschlies, A., Held, H., Keller, D., Keller, K., Mengis, N., Quaas, M., ... Schmidt, H. (2017). Indicators and metrics for the assessment of climate engineering. *Earth’s Future*, 5(1), 49–58. Retrieved from <https://agupubs.onlinelibrary.wiley.com/doi/abs/10.1002/2016EF000449> doi: 10.1002/2016EF000449
- Pitari, G., Aquila, V., Kravitz, B., Robock, A., Watanabe, S., Cionni, I., ... Tilmes, S. (2014). Stratospheric ozone response to sulfate geoengineering: Results from the geoengineering model intercomparison project (geomip). *Journal of Geophysical Research: Atmospheres*, 119(5), 2629–2653. Retrieved from <https://agupubs.onlinelibrary.wiley.com/doi/abs/10.1002/2013JD020566> doi: 10.1002/2013JD020566
- Polvani, L. M., Banerjee, A., & Schmidt, A. (2019). Northern hemisphere continental winter warming following the 1991 Mt. Pinatubo eruption: reconciling models and observations. *Atmospheric Chemistry and Physics*, 19(9), 6351–6366. Retrieved from <https://www.atmos-chem-phys.net/19/6351/2019/> doi: 10.5194/acp-19-6351-2019

- Proctor, J., Hsiang, S., Burney, J., Burke, M., & Schlenker, W. (2018). Estimating global agricultural effects of geoengineering using volcanic eruptions. *Nature*, 560(7719), 480–483. Retrieved from <https://doi.org/10.1038/s41586-018-0417-3> doi: 10.1038/s41586-018-0417-3
- Richter, J. H., Tilmes, S., Mills, M. J., Tribbia, J. J., Kravitz, B., Macmartin, D. G., ... Lamarque, J. F. (2017). Stratospheric dynamical response and ozone feedbacks in the presence of SO₂ injections. *Journal of Geophysical Research: Atmospheres*, 122(23), 12,557–12,573. doi: 10.1002/2017JD026912
- Robock, A. (2000). Volcanic eruptions and climate. *Reviews of Geophysics*, 38(2), 191–219. Retrieved from <https://agupubs.onlinelibrary.wiley.com/doi/abs/10.1029/1998RG000054> doi: 10.1029/1998RG000054
- Robock, A., & Mao, J. (1995). The volcanic signal in surface temperature observations. *Journal of Climate*, 8(5), 1086–1103. Retrieved from [https://doi.org/10.1175/1520-0442\(1995\)008<1086:TVSIST>2.0.CO;2](https://doi.org/10.1175/1520-0442(1995)008<1086:TVSIST>2.0.CO;2) doi: 10.1175/1520-0442(1995)008<1086:TVSIST>2.0.CO;2
- Russotto, R. D., & Ackerman, T. P. (2018a). Changes in clouds and thermodynamics under solar geoengineering and implications for required solar reduction. *Atmospheric Chemistry and Physics*, 18(16), 11905–11925. Retrieved from <https://www.atmos-chem-phys.net/18/11905/2018/> doi: 10.5194/acp-18-11905-2018
- Russotto, R. D., & Ackerman, T. P. (2018b). Energy transport, polar amplification, and ITCZ shifts in the GeoMIP G1 ensemble. *Atmospheric Chemistry and Physics*, 18(3), 2287–2305. Retrieved from <https://www.atmos-chem-phys.net/18/2287/2018/> doi: 10.5194/acp-18-2287-2018
- Schmidt, A., Mills, M. J., Ghan, S., Gregory, J. M., Allan, R. P., Andrews, T., ... Toon, O. B. (2018). Volcanic radiative forcing from 1979 to 2015. *Journal of Geophysical Research: Atmospheres*, 123(22), 12491–12508. Retrieved from <https://agupubs.onlinelibrary.wiley.com/doi/abs/10.1029/2018JD028776> doi: 10.1029/2018JD028776
- Simpson, I., Tilmes, S., Richter, J., Kravitz, B., MacMartin, D., Mills, M., ... Pendergrass, A. (2019). The regional hydroclimate response to stratospheric sulfate geoengineering and the role of stratospheric heating. *Journal of Geophysical Research: Atmospheres*, 2019JD031093. Retrieved from <https://onlinelibrary.wiley.com/doi/abs/10.1029/2019JD031093> doi: 10.1029/2019JD031093
- Simpson, I. R., Hitchcock, P., Seager, R., Wu, Y., & Callaghan, P. (2018). The downward influence of uncertainty in the northern hemisphere stratospheric polar vortex response to climate change. *Journal of Climate*, 31(16), 6371–6391. Retrieved from <https://doi.org/10.1175/JCLI-D-18-0041.1> doi: 10.1175/JCLI-D-18-0041.1
- Smyth, J. E., Russotto, R. D., & Storelvmo, T. (2017). Thermodynamic and dynamic responses of the hydrological cycle to solar dimming. *Atmospheric Chemistry and Physics*, 17(10), 6439–6453. Retrieved from <https://www.atmos-chem-phys.net/17/6439/2017/> doi: 10.5194/acp-17-6439-2017
- Song, X.-P., Hansen, M. C., Stehman, S. V., Potapov, P. V., Tyukavina, A., Vermote, E. F., & Townshend, J. R. (2018). Global land change from 1982 to 2016. *Nature*, 560(7720), 639–643. Retrieved from <https://doi.org/10.1038/s41586-018-0411-9> doi: 10.1038/s41586-018-0411-9
- Tavoni, M., Bosetti, V., Shayegh, S., Drouet, L., Emmerling, J., Fuss, S., ... Rickels, W. (2017). Challenges and opportunities for integrated modeling of climate engineering. *FEEM Working Paper*(38). doi: <http://dx.doi.org/10.2139/ssrn.3035166>
- Taylor, K. E. (2001). Summarizing multiple aspects of model performance in a single diagram. *Journal of Geophysical Research: Atmospheres*, 106(D7), 7183–7192. Retrieved from <https://agupubs.onlinelibrary.wiley.com/doi/abs/>

- 10.1029/2000JD900719 doi: 10.1029/2000JD900719
- Tilmes, S., MacMartin, D. G., Lenaerts, J. T. M., van Kampenhout, L., Muntjewerf, L., Xia, L., ... Robock, A. (2020). Reaching 1.5 and 2.0C global surface temperature targets using stratospheric aerosol geoengineering. *Earth System Dynamics*, 11(3), 579–601. Retrieved from <https://esd.copernicus.org/articles/11/579/2020/> doi: 10.5194/esd-11-579-2020
- Tilmes, S., Müller, R., & Salawitch, R. (2008). The sensitivity of polar ozone depletion to proposed geoengineering schemes. *Science*, 320(5880), 1201–1204. Retrieved from <https://science.sciencemag.org/content/320/5880/1201> doi: 10.1126/science.1153966
- Tilmes, S., Richter, J. H., Kravitz, B., Macmartin, D. G., Mills, M. J., Simpson, I. R., ... Ghosh, S. (2018). CESM1(WACCM) stratospheric aerosol geoengineering large ensemble project. *Bulletin of the American Meteorological Society*(11), 2361–2371. doi: 10.1175/BAMS-D-17-0267.1
- Tilmes, S., Richter, J. H., Mills, M. J., Kravitz, B., MacMartin, D. G., Garcia, R. R., ... Vitt, F. (2018). Effects of Different Stratospheric SO₂ Injection Altitudes on Stratospheric Chemistry and Dynamics. *Journal of Geophysical Research: Atmospheres*, 123(9), 4654–4673. doi: 10.1002/2017JD028146
- Tilmes, S., Richter, J. H., Mills, M. J., Kravitz, B., Macmartin, D. G., Vitt, F., ... Lamarque, J. F. (2017). Sensitivity of aerosol distribution and climate response to stratospheric SO₂ injection locations. *Journal of Geophysical Research: Atmospheres*, 122(23), 12,591–12,615. doi: 10.1002/2017JD026888
- Timmreck, C., Mann, G. W., Aquila, V., Hommel, R., Lee, L. A., Schmidt, A., ... Weisenstein, D. (2018). The interactive stratospheric aerosol model intercomparison project (ISA-MIP): motivation and experimental design. *Geoscientific Model Development*, 11(7), 2581–2608. Retrieved from <https://gmd.copernicus.org/articles/11/2581/2018/> doi: 10.5194/gmd-11-2581-2018
- van Kampenhout, L., Lenaerts, J. T. M., Lipscomb, W. H., Lhermitte, S., Noël, B., Vizcaíno, M., ... van den Broeke, M. R. (2020). Present-day greenland ice sheet climate and surface mass balance in CESM2. *Journal of Geophysical Research: Earth Surface*, 125(2), e2019JF005318. Retrieved from <https://agupubs.onlinelibrary.wiley.com/doi/abs/10.1029/2019JF005318> (e2019JF005318 10.1029/2019JF005318) doi: 10.1029/2019JF005318
- Vattioni, S., Weisenstein, D., Keith, D., Feinberg, A., Peter, T., & Stenke, A. (2019). Exploring accumulation-mode H₂SO₄ versus SO₂ stratospheric sulfate geoengineering in a sectional aerosol-chemistry-climate model. *Atmospheric Chemistry and Physics*, 19(7), 4877–4897. Retrieved from <https://www.atmos-chem-phys.net/19/4877/2019/> doi: 10.5194/acp-19-4877-2019
- Visioni, D., MacMartin, D. G., Kravitz, B., Lee, W., Simpson, I. R., & Richter, J. H. (2020). Reduced poleward transport due to stratospheric heating under stratospheric aerosols geoengineering. *Geophysical Research Letters*, n/a(n/a), e2020GL089470. Retrieved from <https://agupubs.onlinelibrary.wiley.com/doi/abs/10.1029/2020GL089470> (e2020GL089470 2020GL089470) doi: 10.1029/2020GL089470
- Visioni, D., MacMartin, D. G., Kravitz, B., Richter, J. H., Tilmes, S., & Mills, M. J. (2020). Seasonally modulated stratospheric aerosol geoengineering alters the climate outcomes. *Geophysical Research Letters*, n/a(n/a), e2020GL088337. Retrieved from <https://agupubs.onlinelibrary.wiley.com/doi/abs/10.1029/2020GL088337> (e2020GL088337 2020GL088337) doi: 10.1029/2020GL088337
- Visioni, D., MacMartin, D. G., Kravitz, B., Tilmes, S., Mills, M. J., Richter, J. H., & Boudreau, M. P. (2019). Seasonal injection strategies for stratospheric aerosol geoengineering. *Geophysical Research Letters*, 46(13), 7790–7799. Retrieved from <https://agupubs.onlinelibrary.wiley.com/doi/abs/>

- 10.1029/2019GL083680 doi: 10.1029/2019GL083680
- Visioni, D., Pitari, G., & Aquila, V. (2017). Sulfate geoengineering: A review of the factors controlling the needed injection of sulfur dioxide. *Atmospheric Chemistry and Physics*. doi: 10.5194/acp-17-3879-2017
- Visioni, D., Pitari, G., Aquila, V., Tilmes, S., Cionni, I., Di Genova, G., & Mancini, E. (2017). Sulfate geoengineering impact on methane transport and lifetime: results from the geoengineering model intercomparison project (GeoMIP). *Atmospheric Chemistry and Physics*, 17(18), 11209–11226. Retrieved from <https://www.atmos-chem-phys.net/17/11209/2017/> doi: 10.5194/acp-17-11209-2017
- Visioni, D., Pitari, G., Di Genova, G., Tilmes, S., & Cionni, I. (2018). Upper tropospheric ice sensitivity to sulfate geoengineering. *Atmospheric Chemistry and Physics*. doi: 10.5194/acp-18-14867-2018
- Visioni, D., Pitari, G., Tuccella, P., & Curci, G. (2018). Sulfur deposition changes under sulfate geoengineering conditions: Quasi-biennial oscillation effects on the transport and lifetime of stratospheric aerosols. *Atmospheric Chemistry and Physics*. doi: 10.5194/acp-18-2787-2018
- Visioni, D., Slessarev, E., MacMartin, D., Mahowald, N. M., Goodale, C. L., & Xia, L. (2020). What goes up must come down: impacts of deposition in a sulfate geoengineering scenario. *Environmental Research Letters*, 15(9). Retrieved from <http://iopscience.iop.org/10.1088/1748-9326/ab94eb>
- Xia, L., Nowack, P. J., Tilmes, S., & Robock, A. (2017). Impacts of stratospheric sulfate geoengineering on tropospheric ozone. *Atmospheric Chemistry and Physics*, 17(19), 11913–11928. Retrieved from <https://www.atmos-chem-phys.net/17/11913/2017/> doi: 10.5194/acp-17-11913-2017



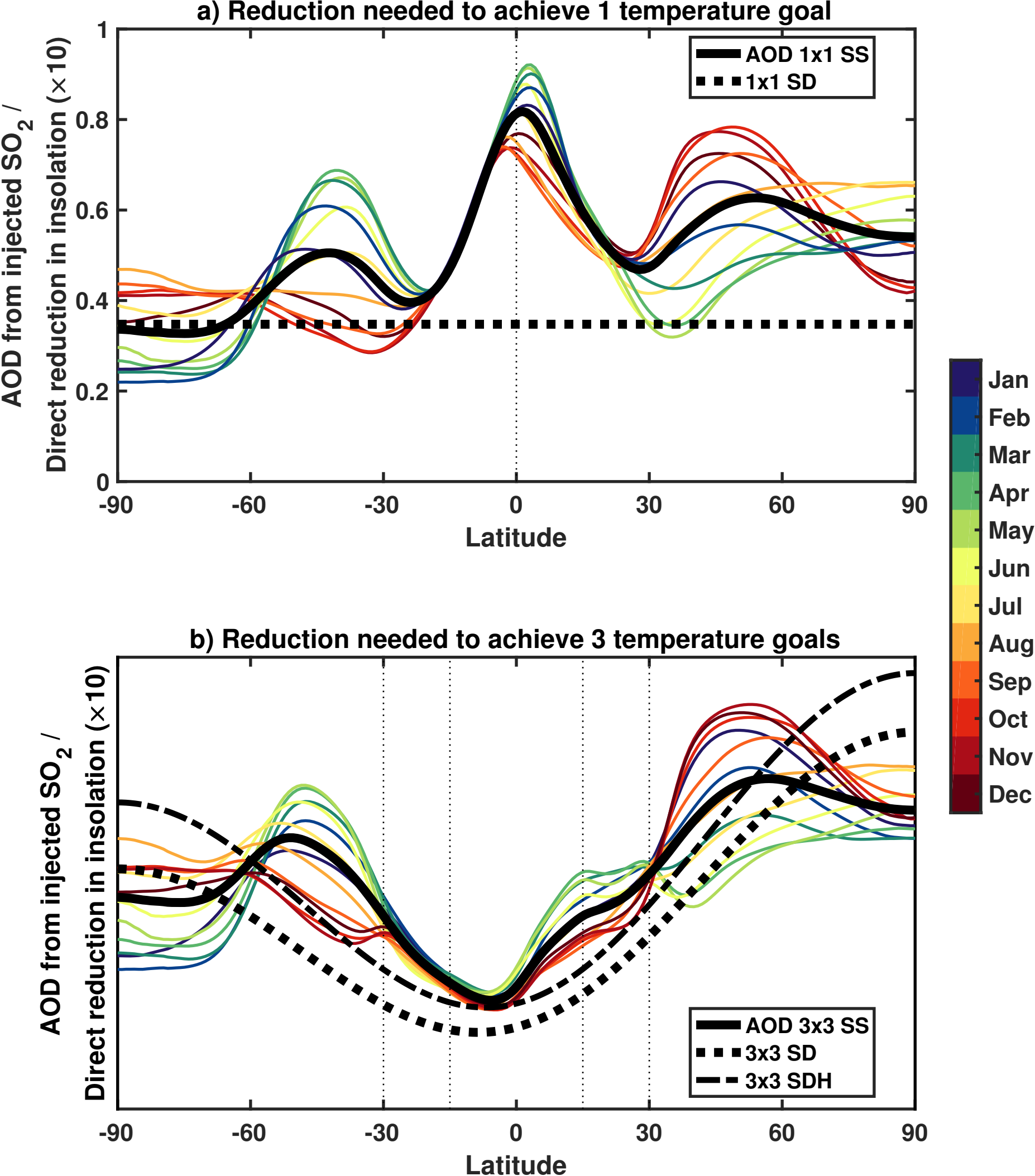
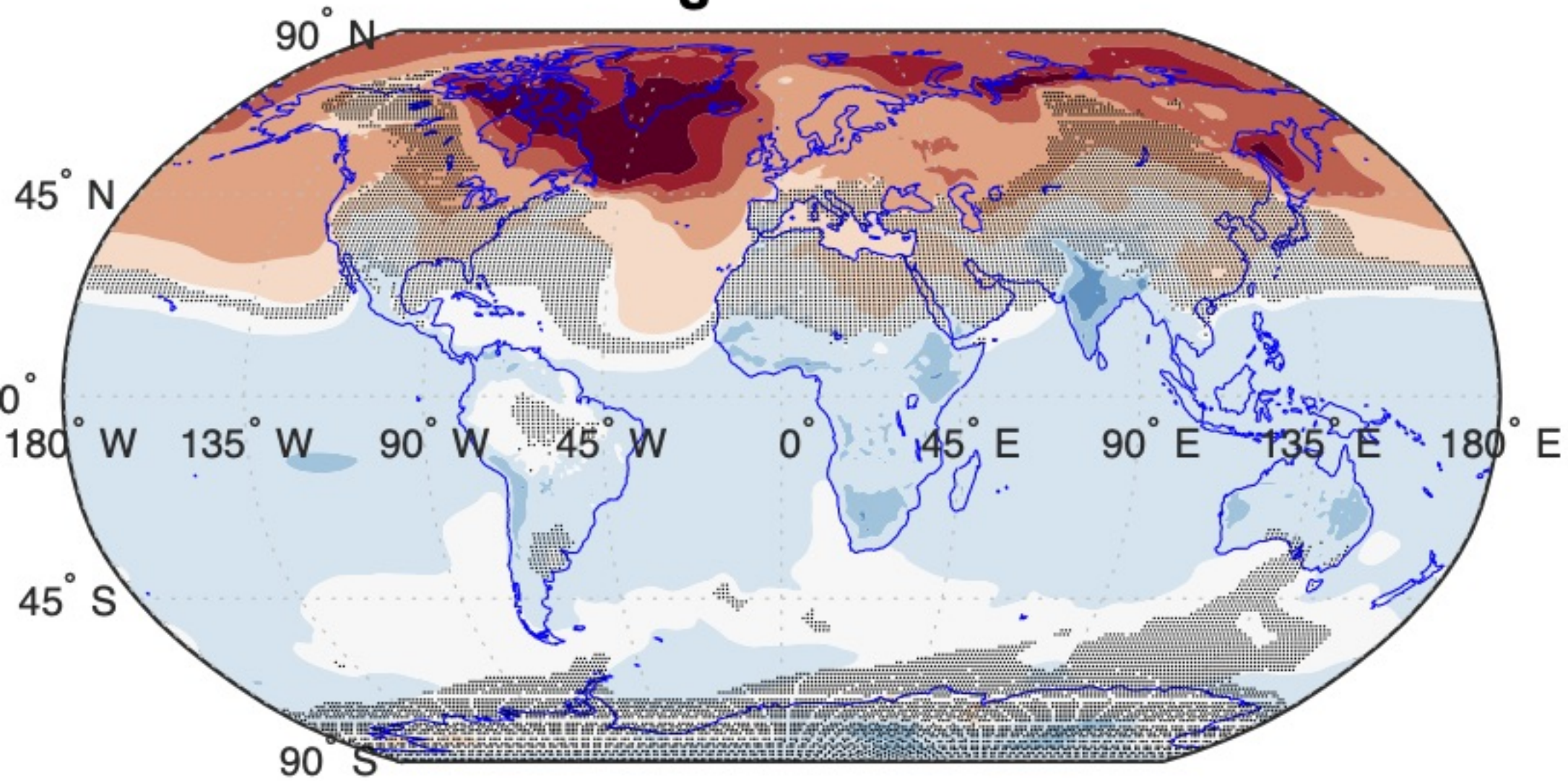
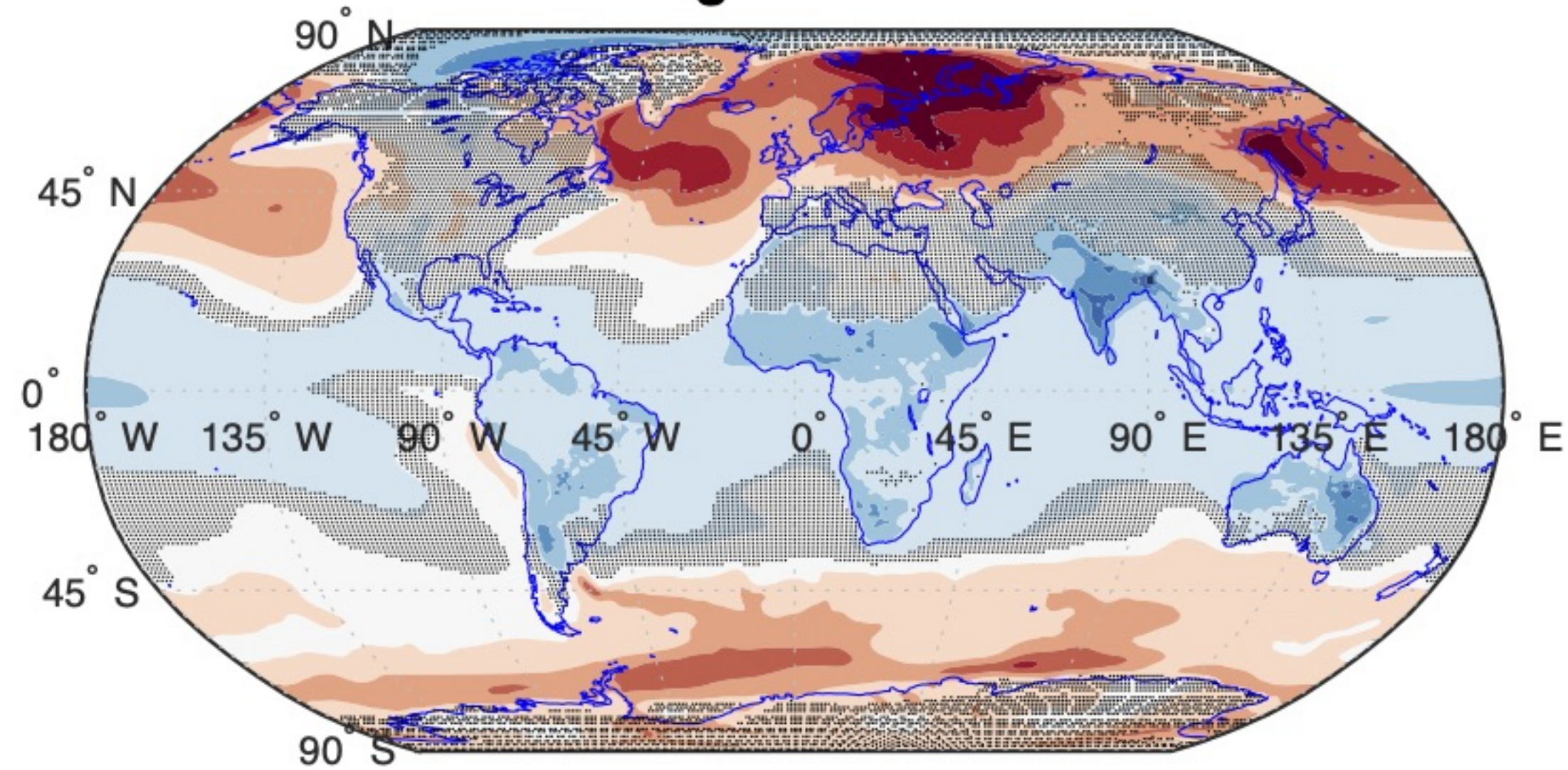


Fig_3.

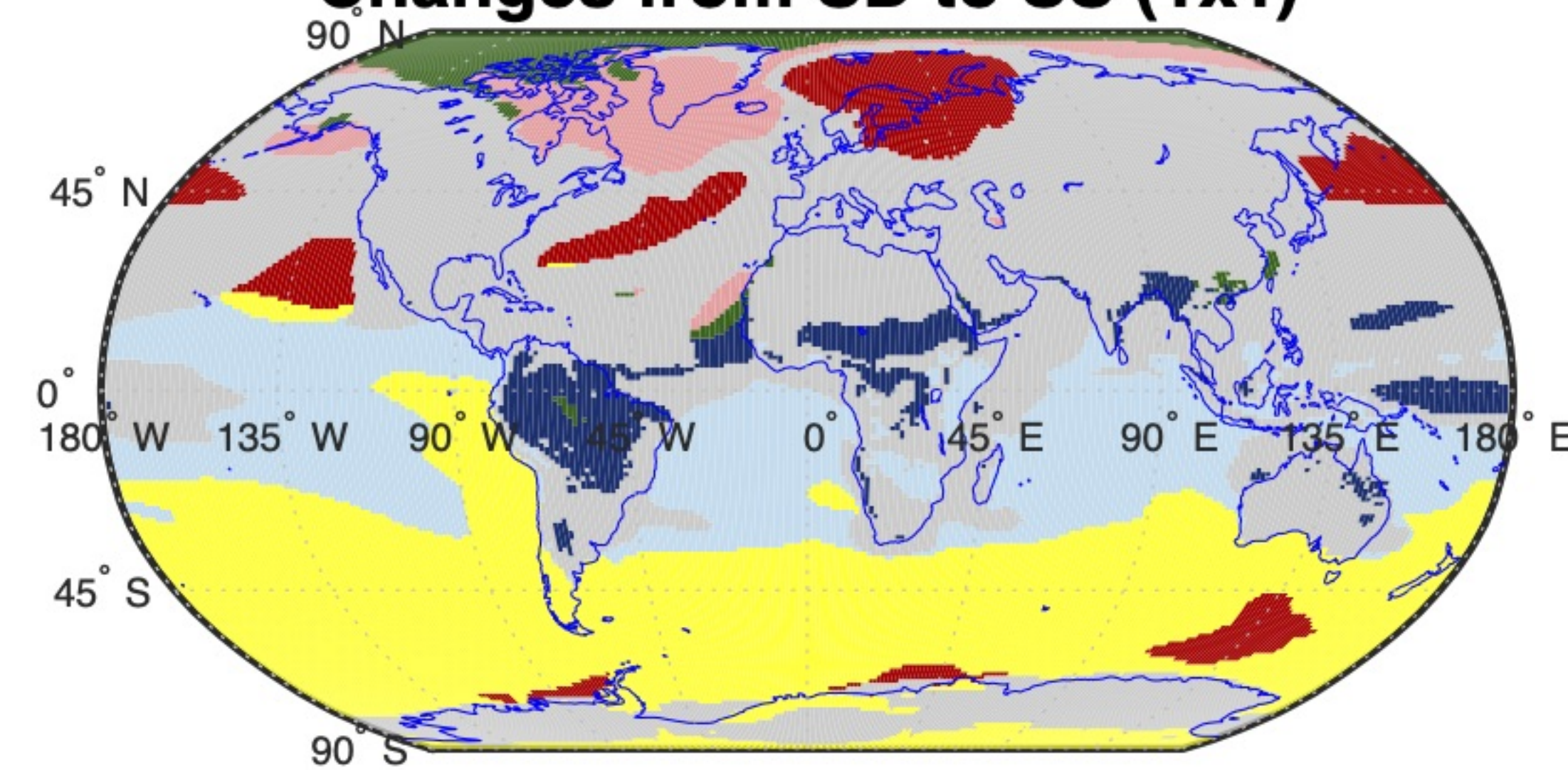
ΔT_s (1x1 SD)



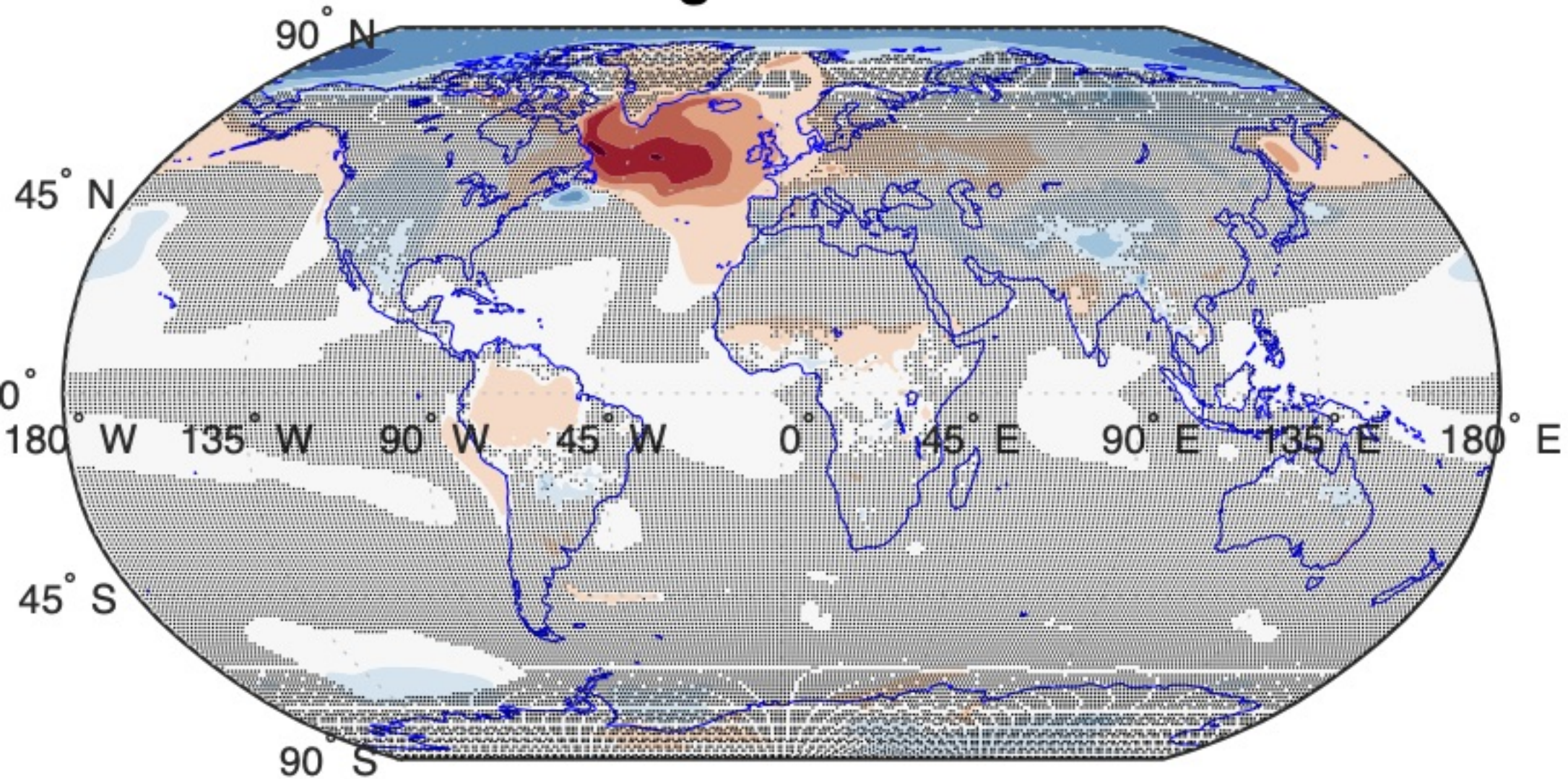
ΔT_s (1x1 SS)



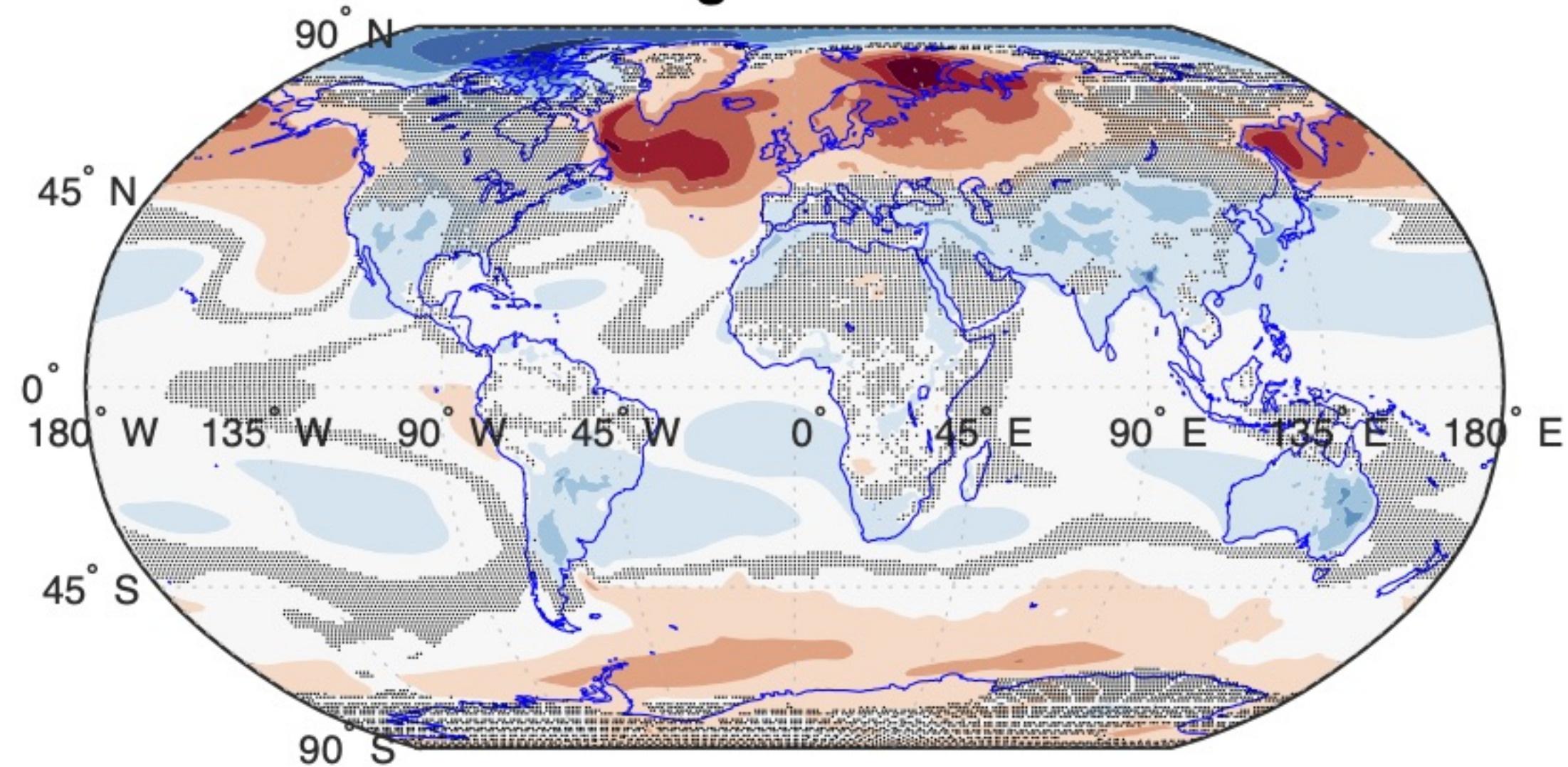
Changes from SD to SS (1x1)



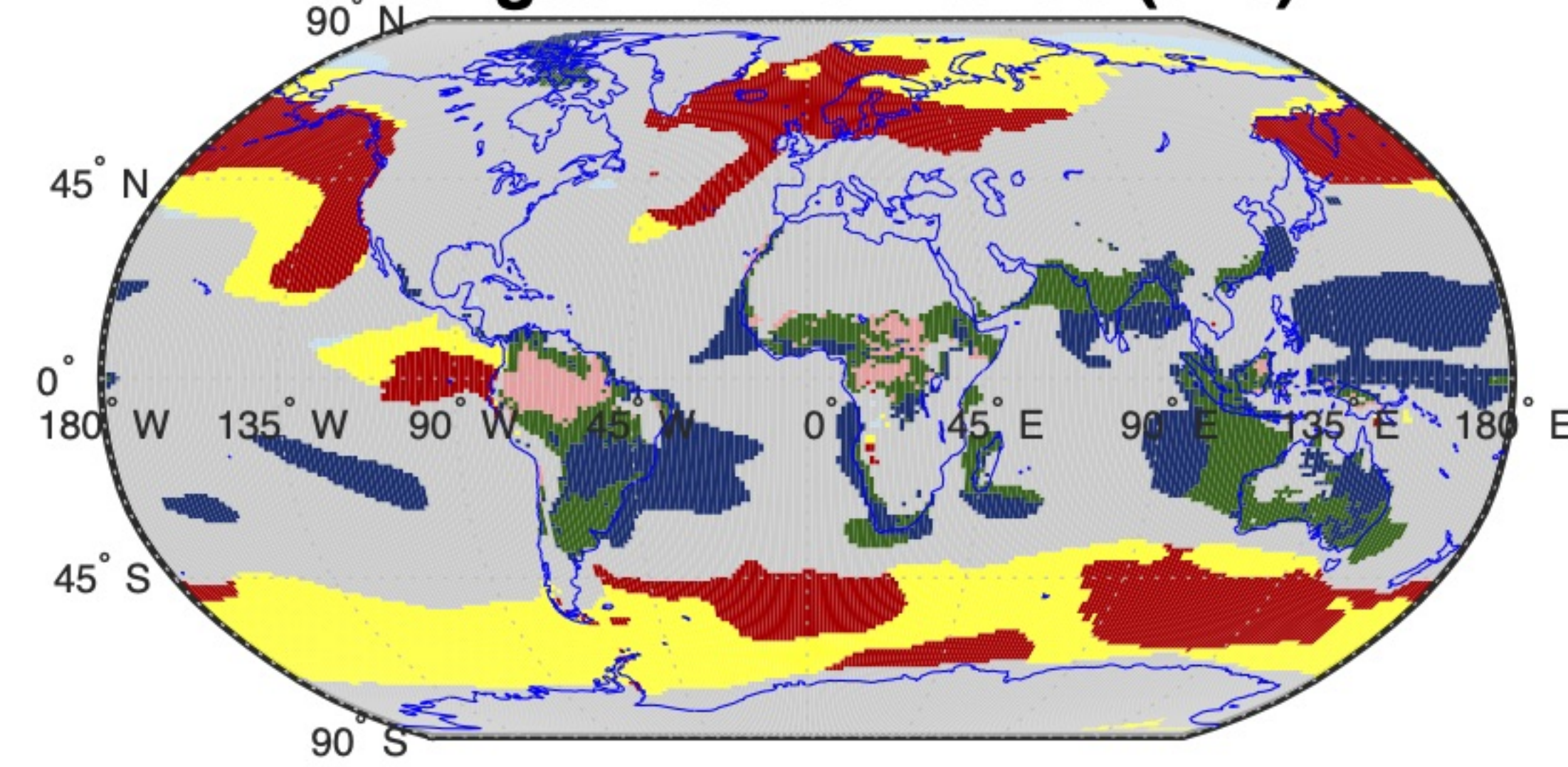
ΔT_s (3x3 SD)



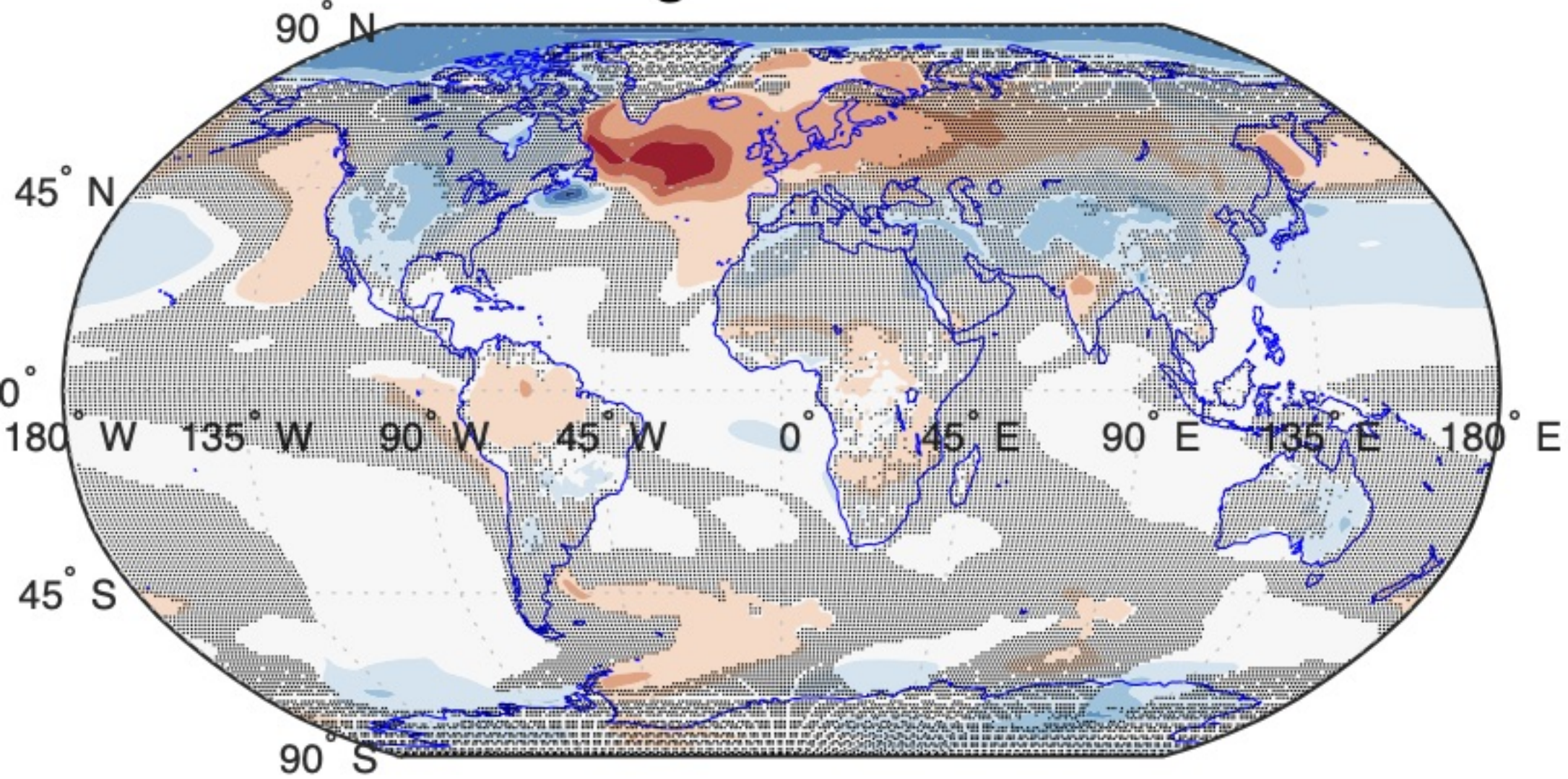
ΔT_s (3x3 SS)



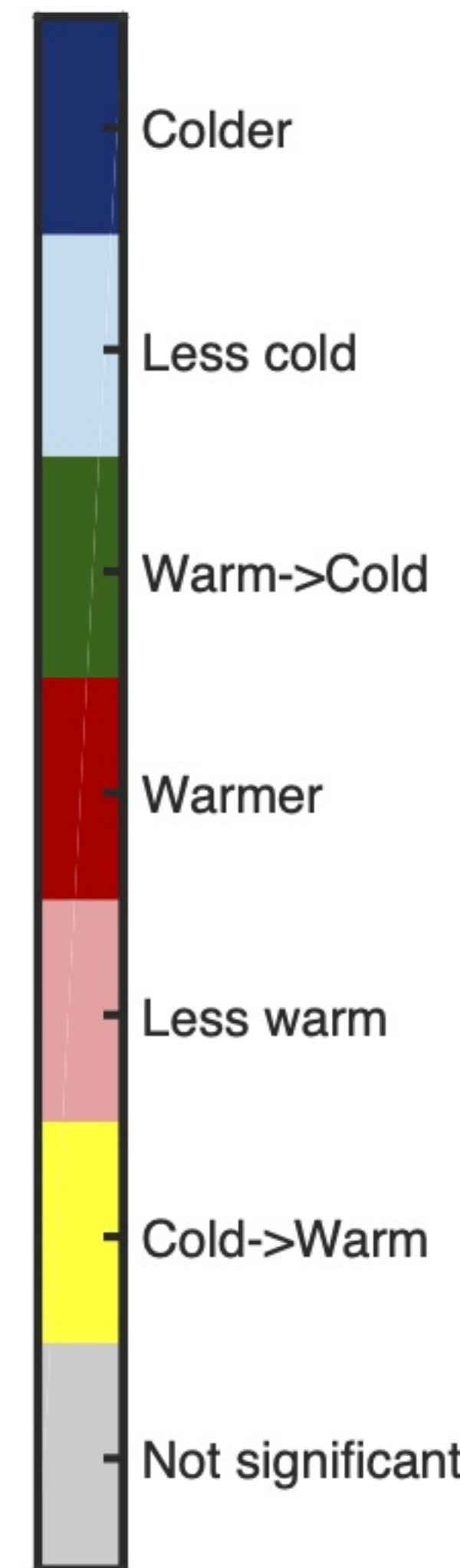
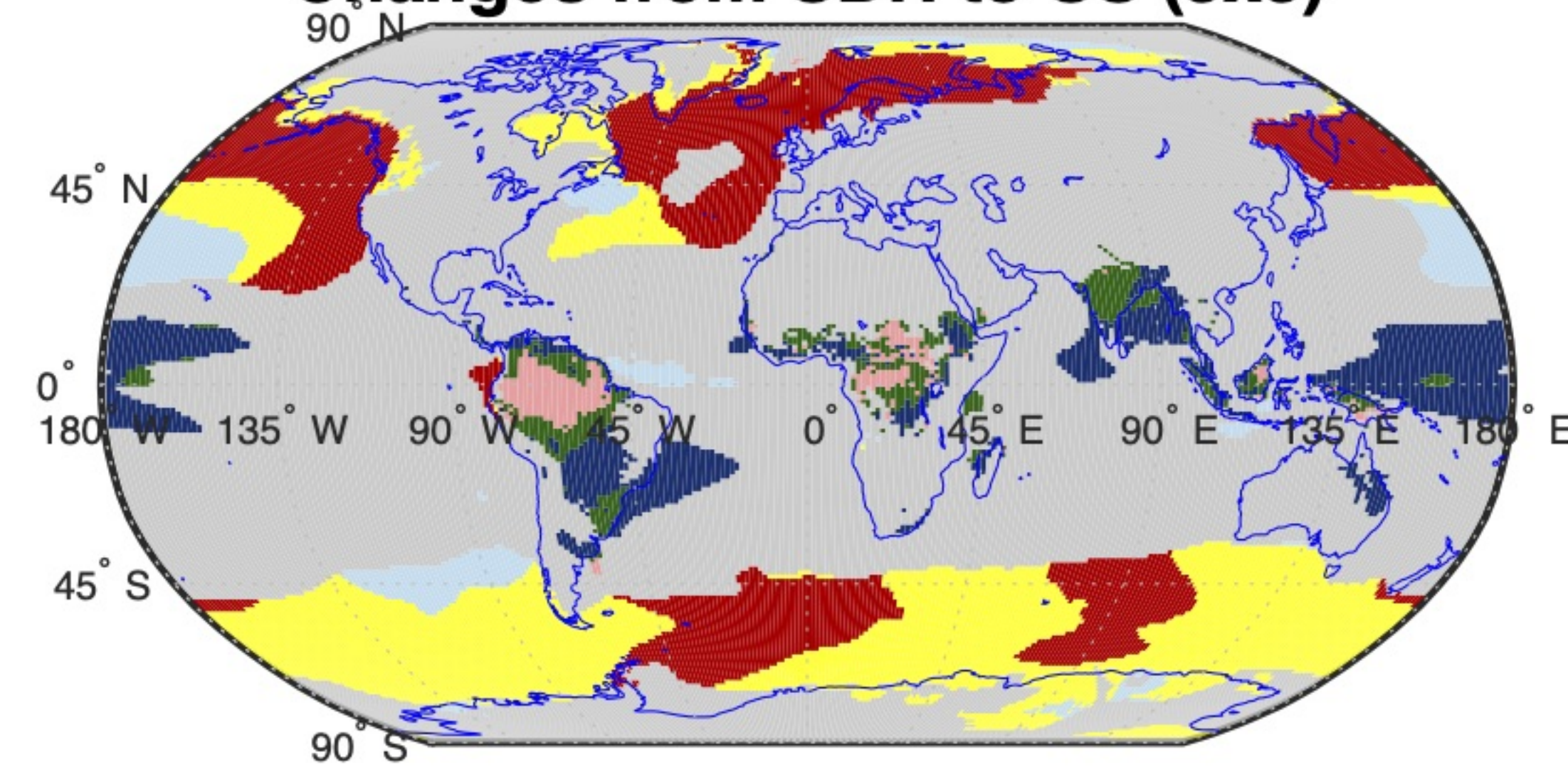
Changes from SD to SS (3x3)



ΔT_s (3x3 SDH)



Changes from SDH to SS (3x3)

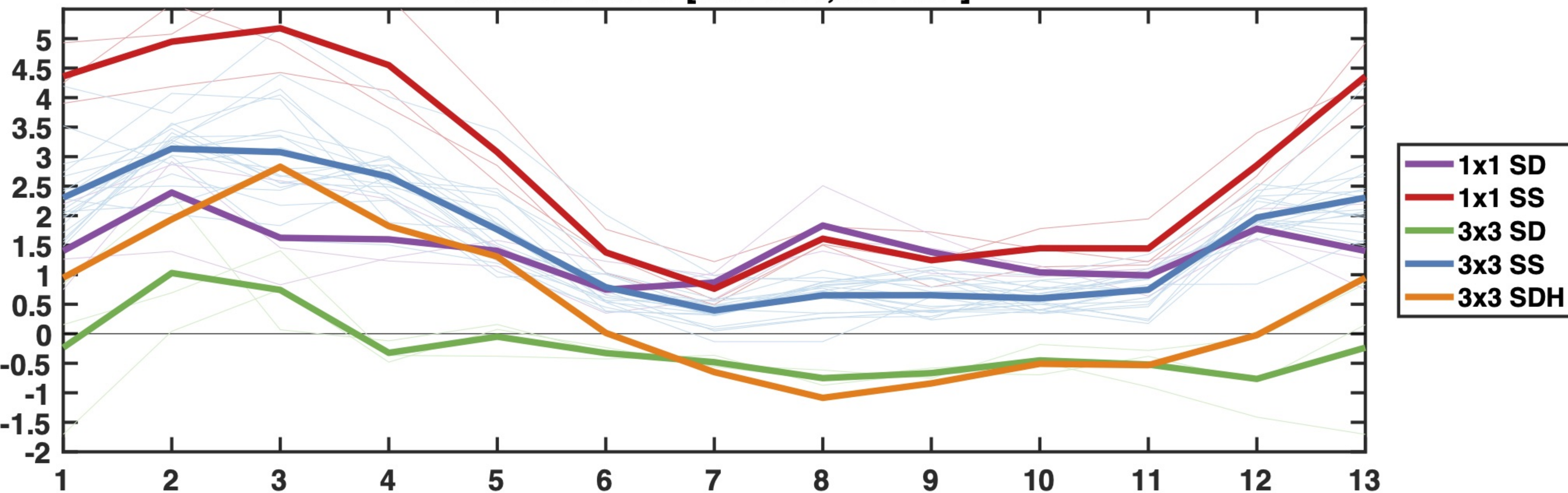


-2.75 -2.25 -1.75 -1.25 -0.75 -0.25 0.25 0.75 1.25 1.75 2.25 2.75



Fig_4.

Surface T over [60N-80N;30E-90E]



Surface T over [60N-80N;30E-90E] anomaly compared to annual mean

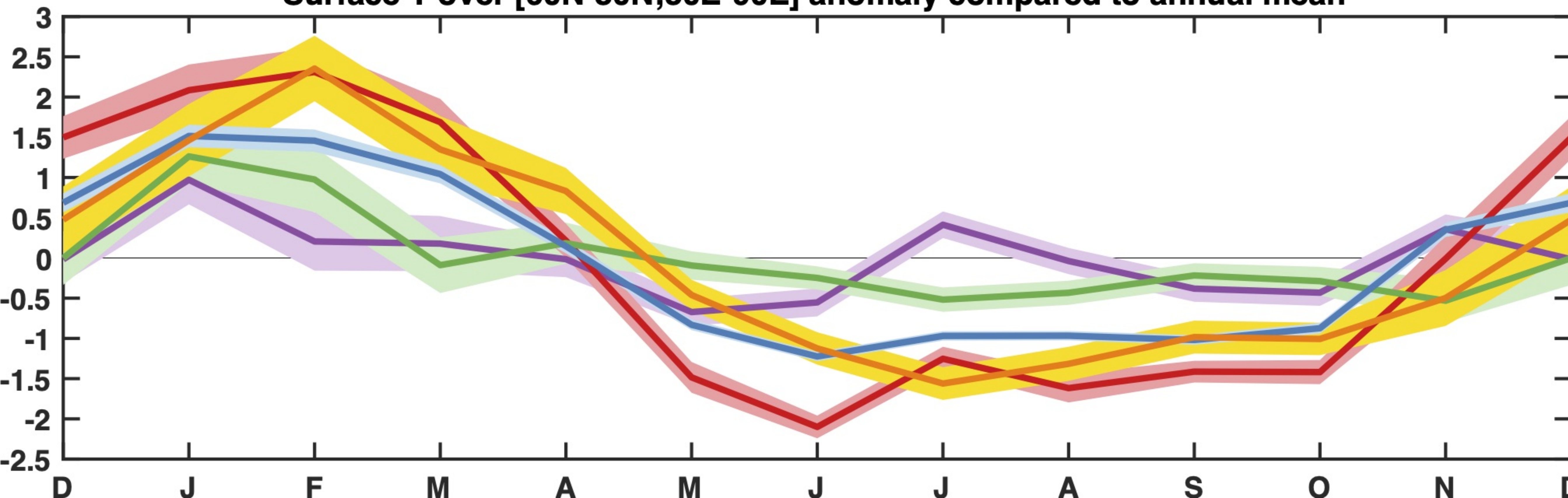
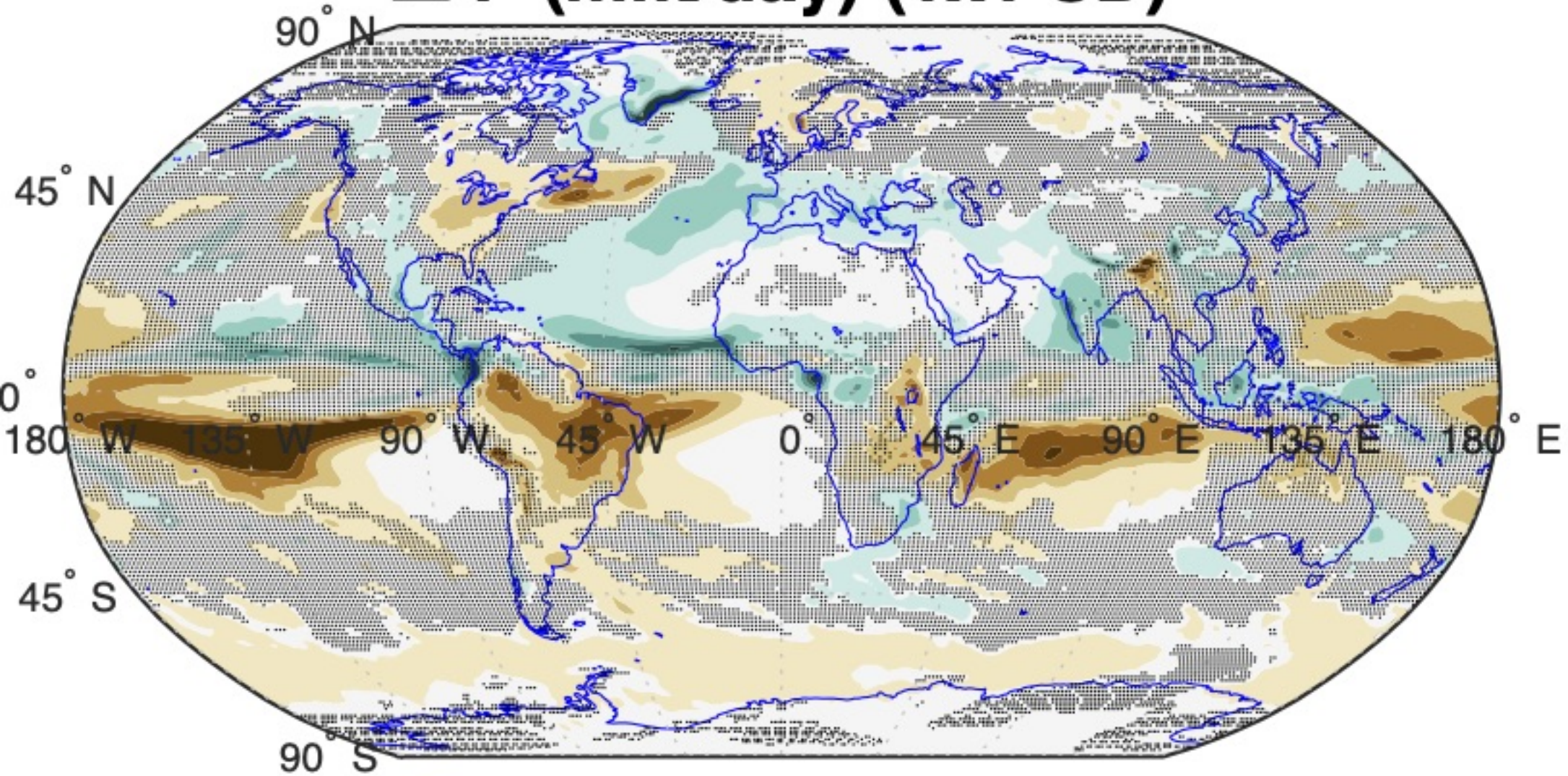
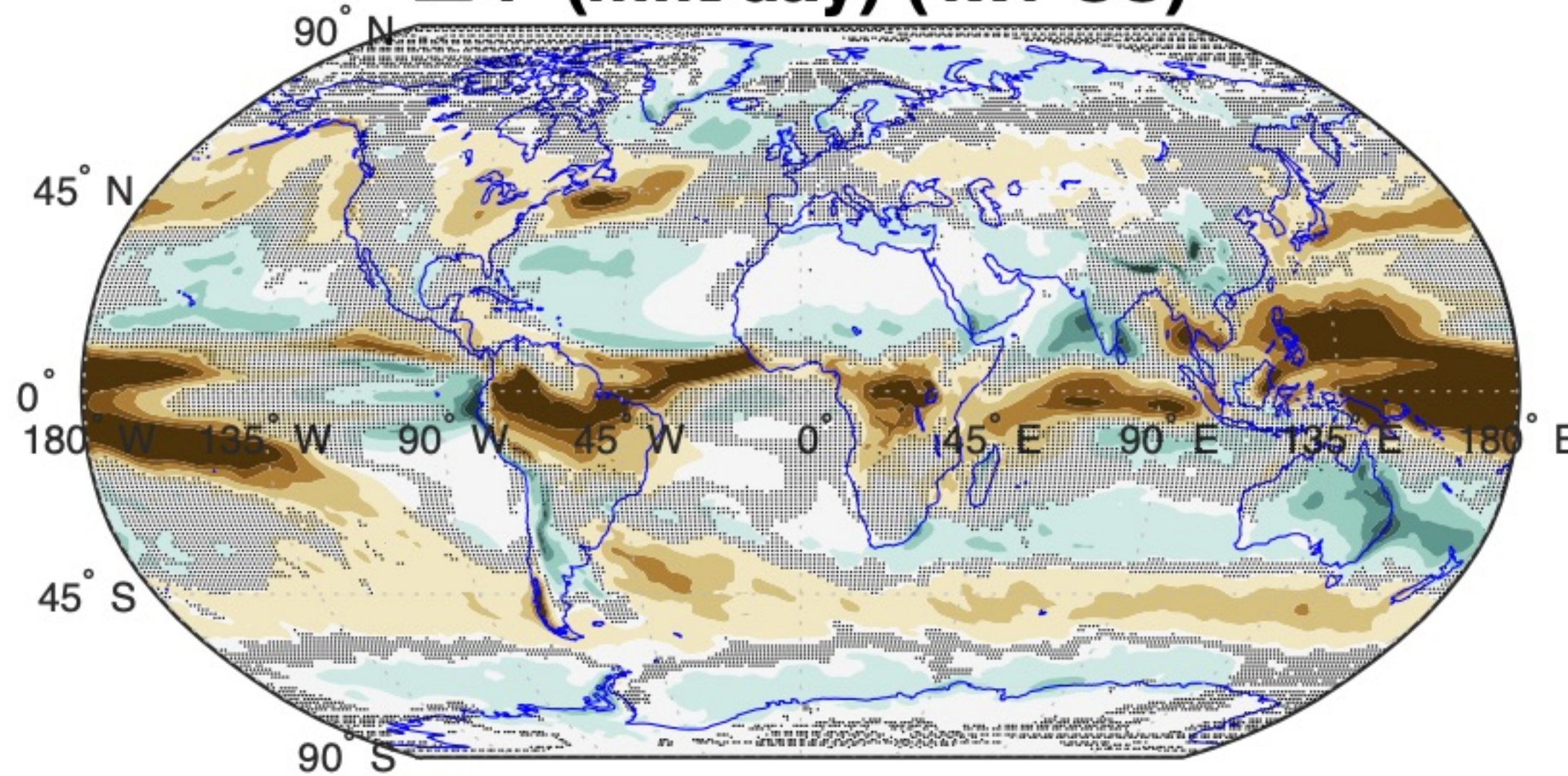


Fig_5.

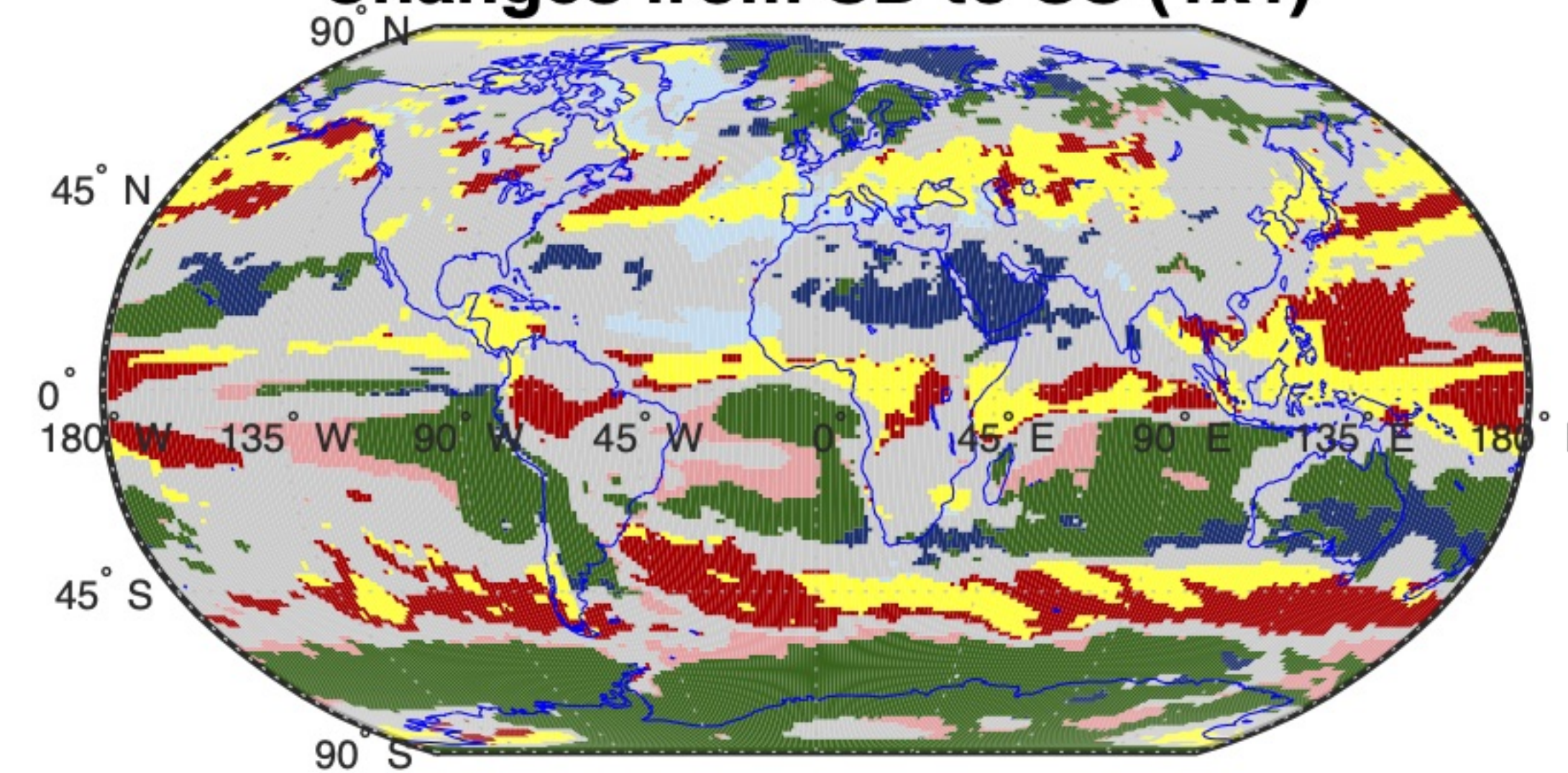
ΔP (mm/day) (1x1 SD)



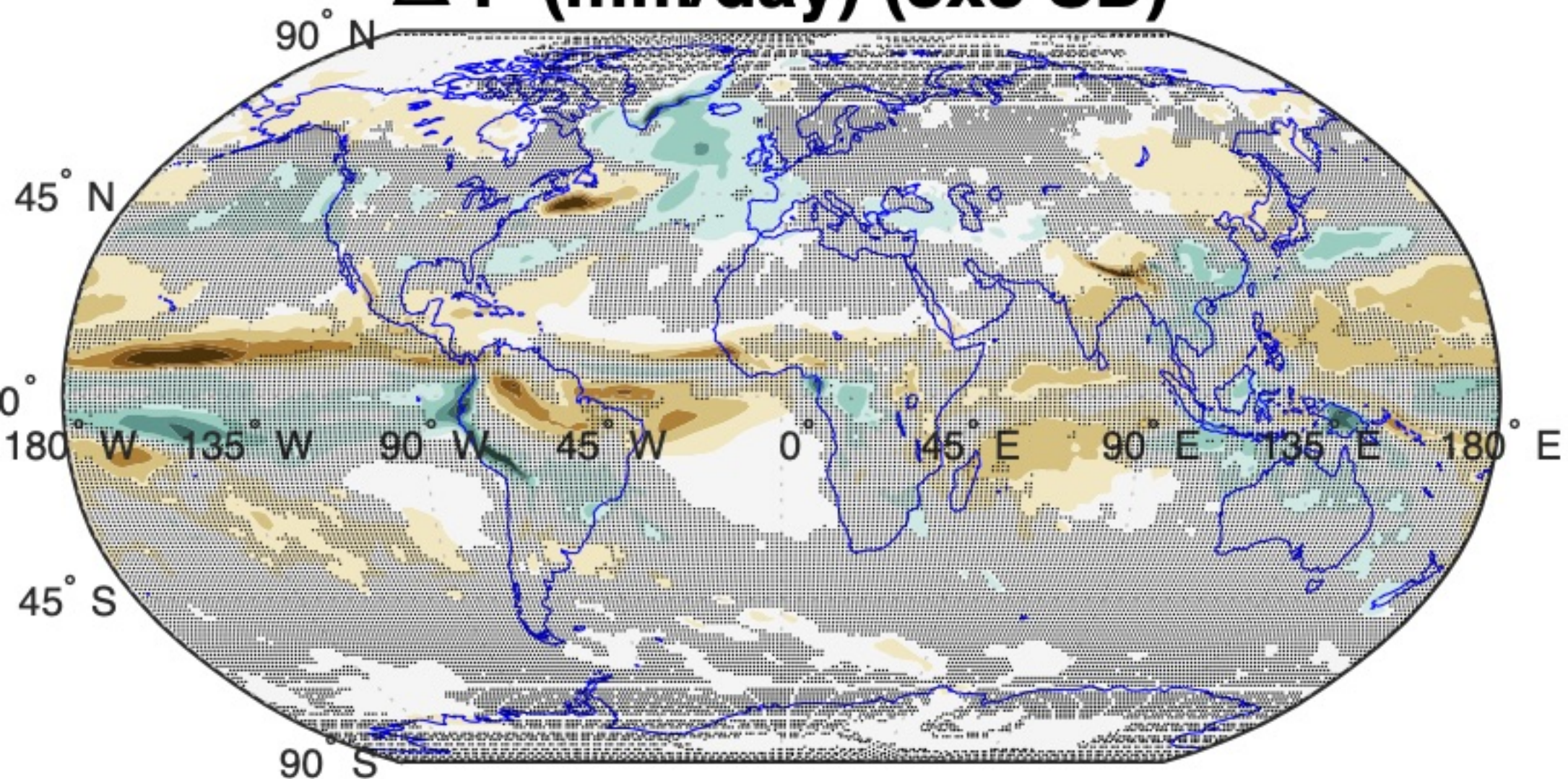
ΔP (mm/day) (1x1 SS)



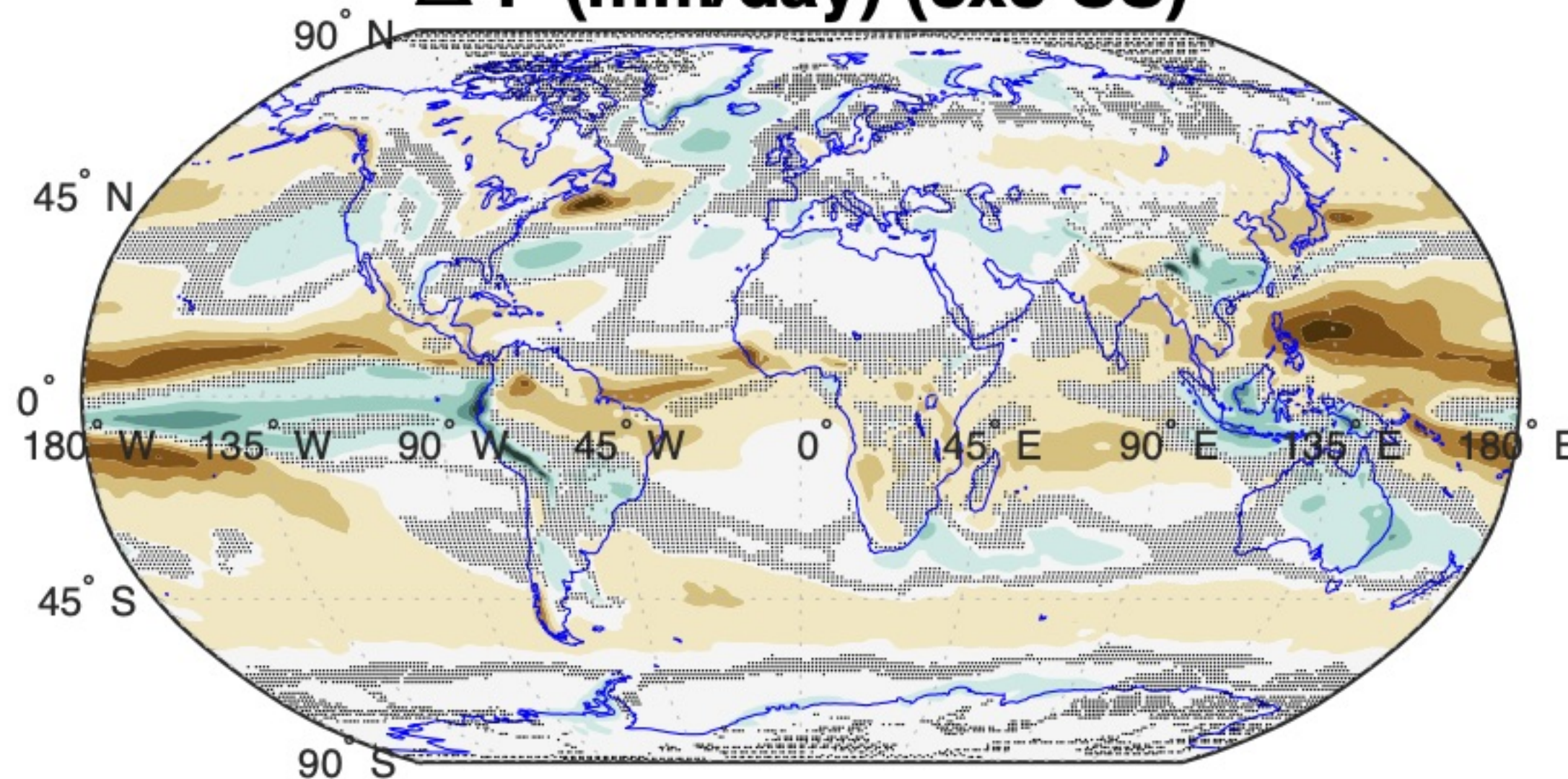
Changes from SD to SS (1x1)



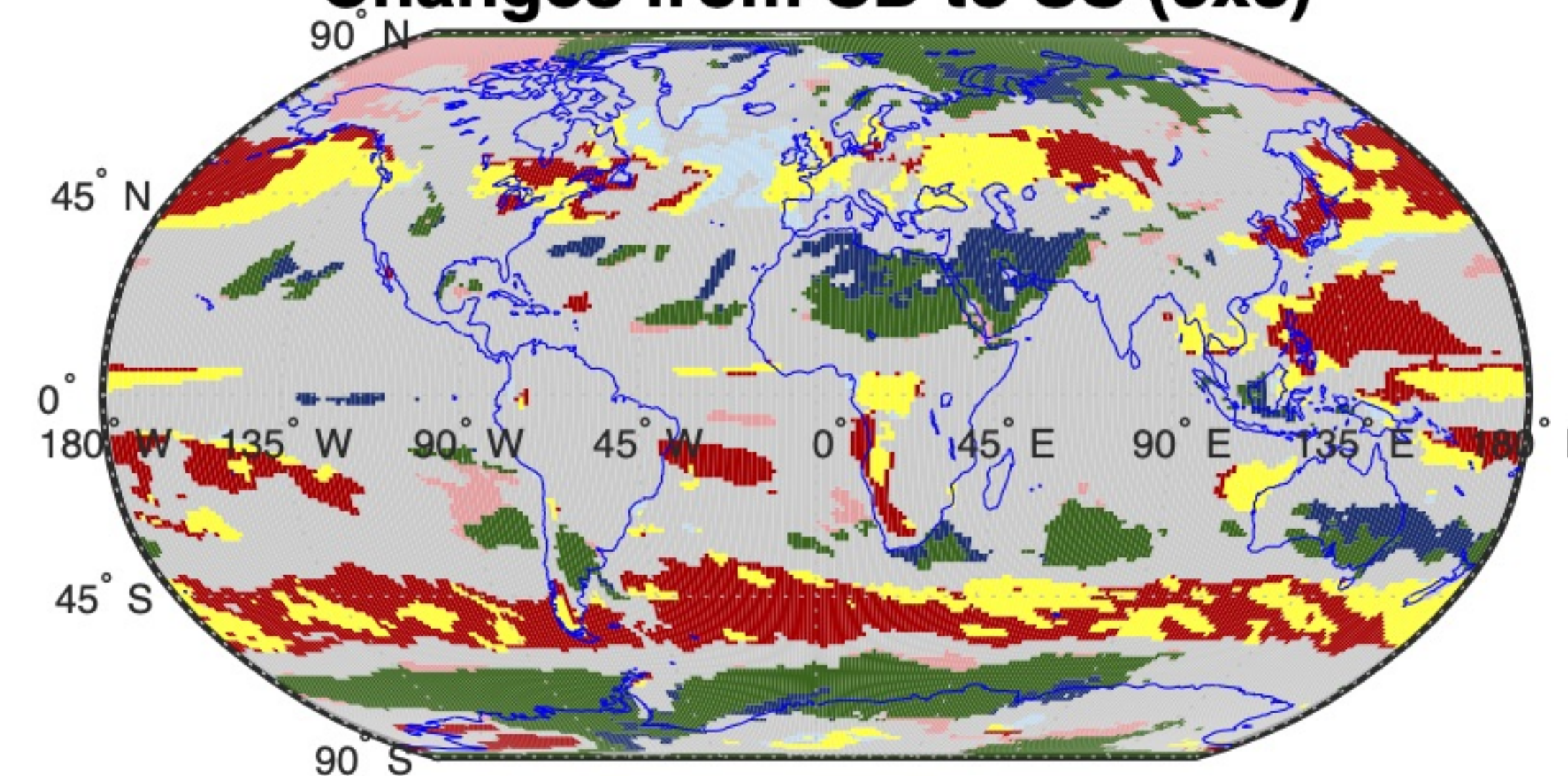
ΔP (mm/day) (3x3 SD)



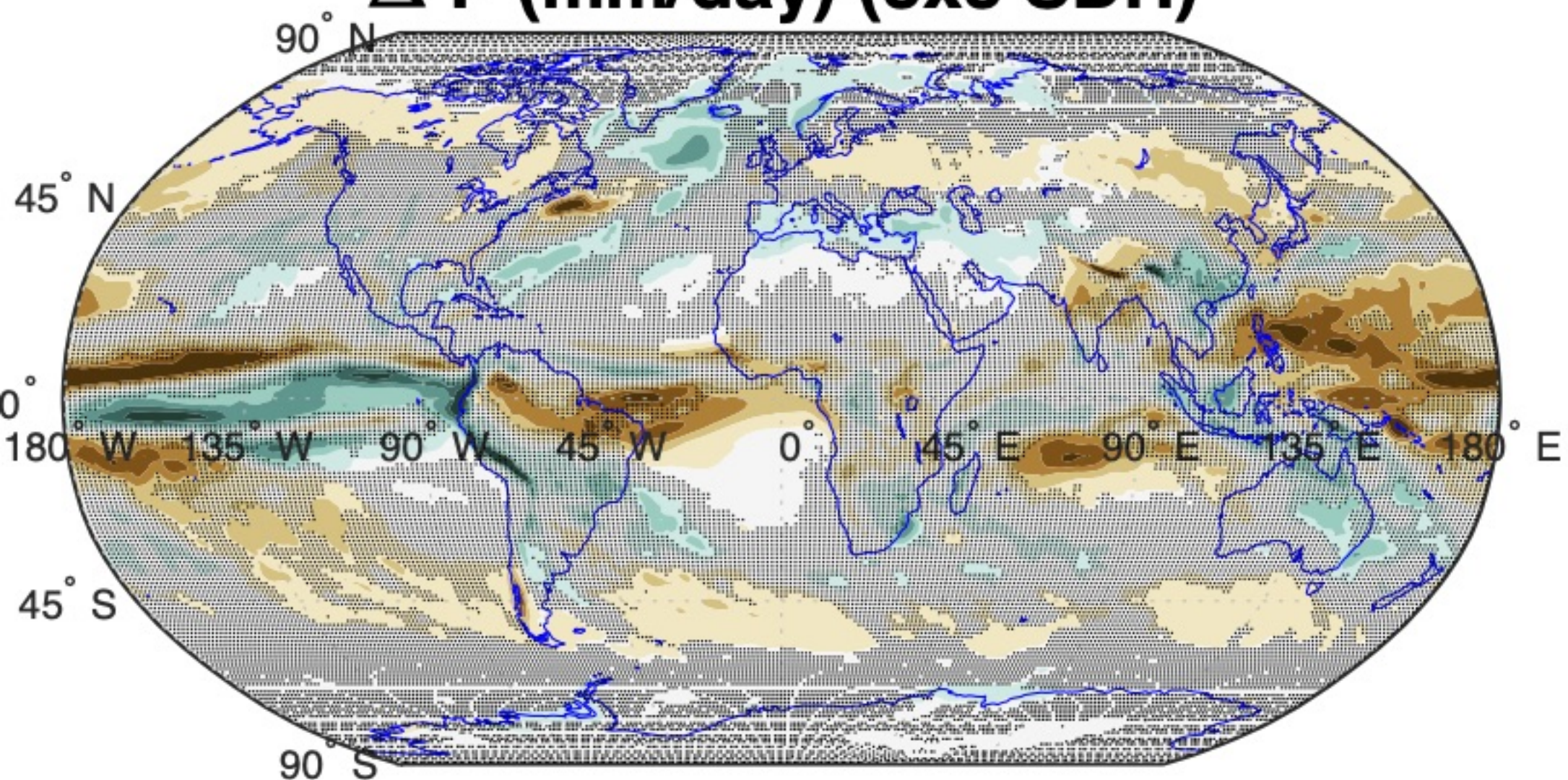
ΔP (mm/day) (3x3 SS)



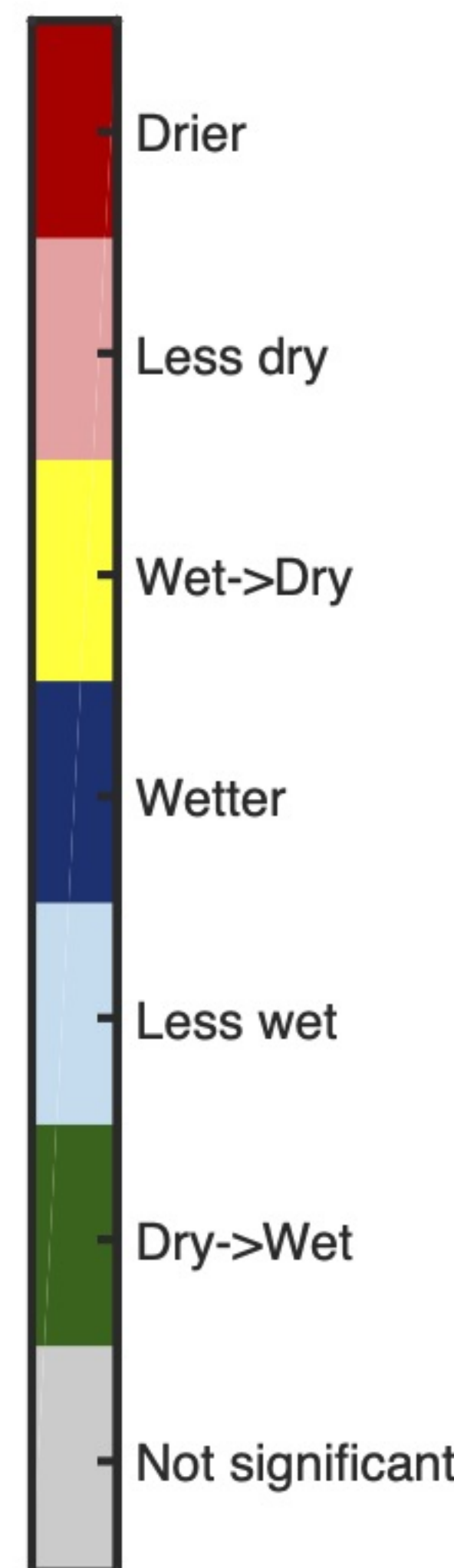
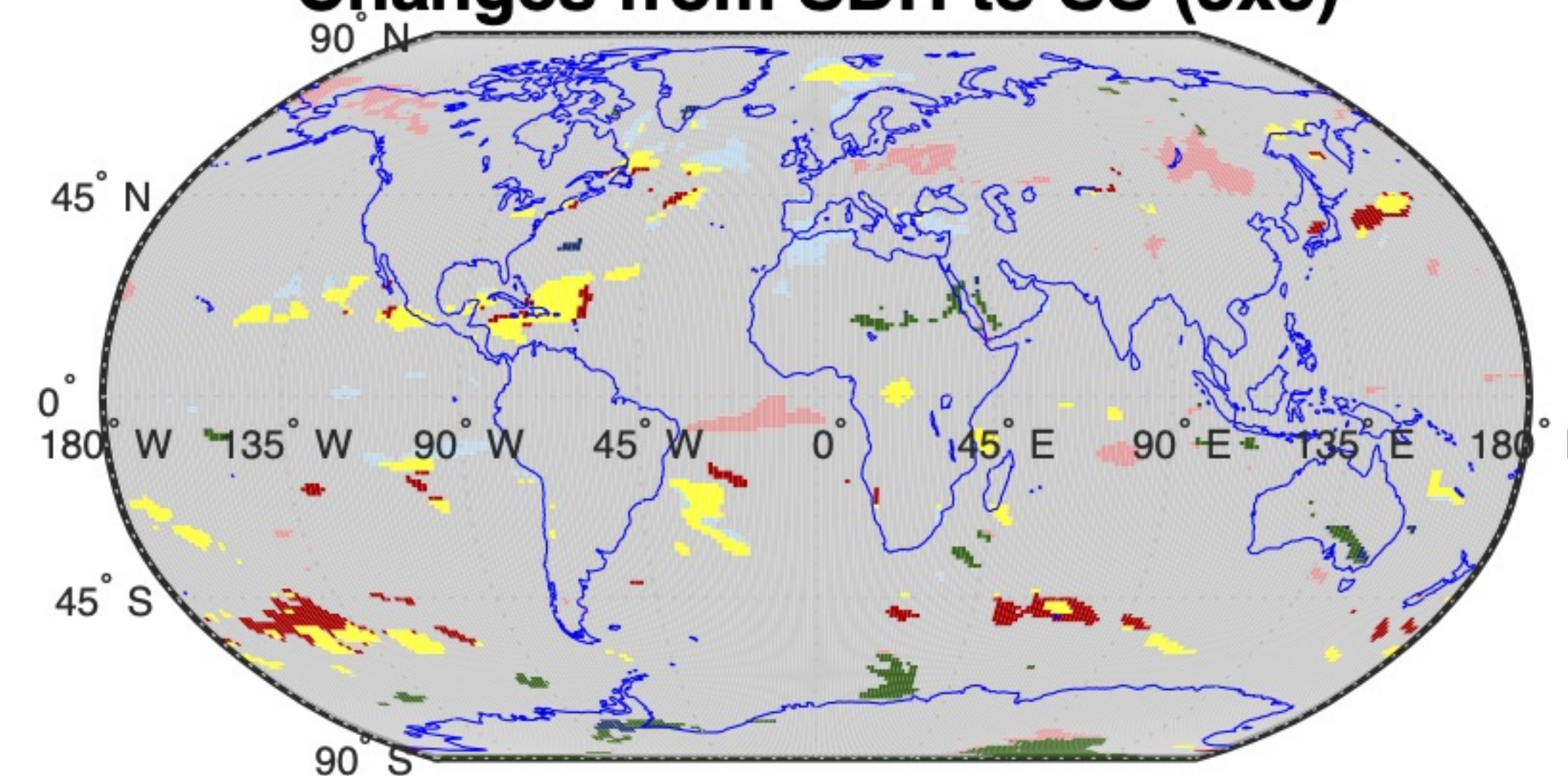
Changes from SD to SS (3x3)



ΔP (mm/day) (3x3 SDH)



Changes from SDH to SS (3x3)



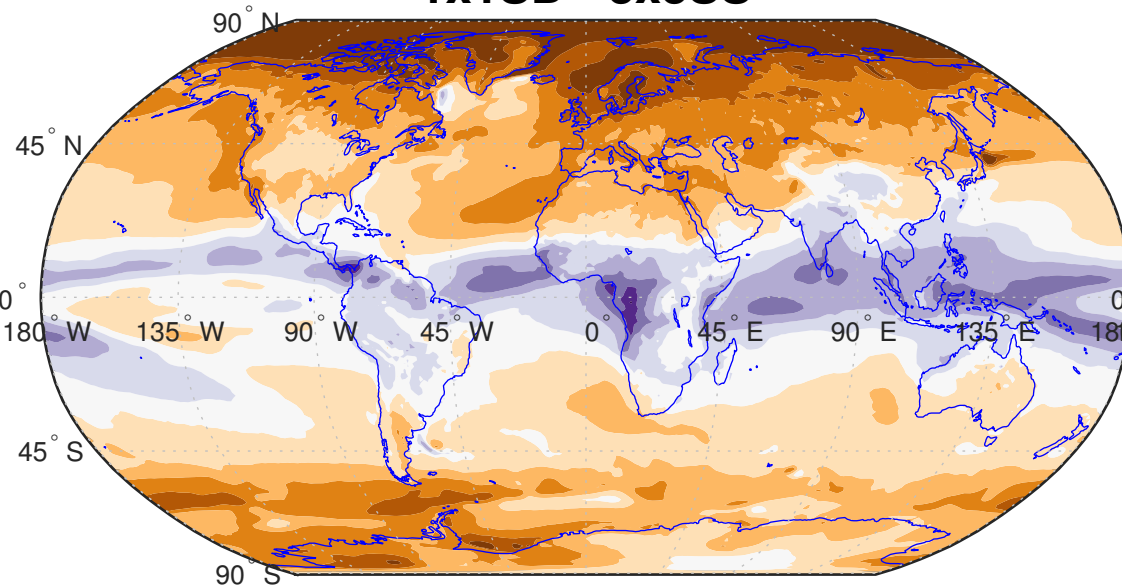
-1.1 -0.9 -0.7 -0.5 -0.3 -0.1 0.1 0.3 0.5 0.7 0.9 1.1



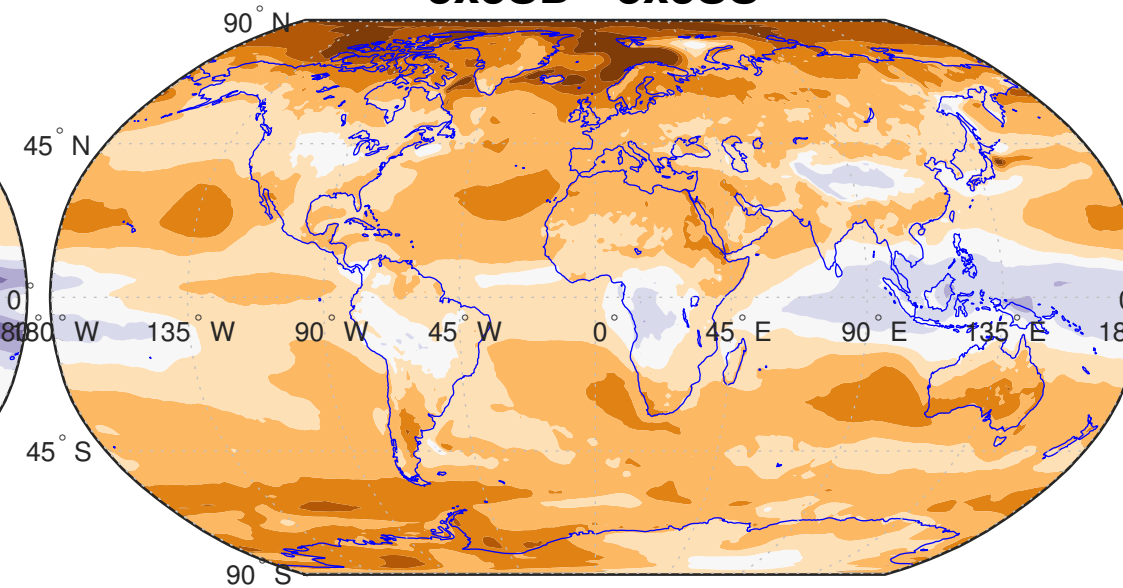
Fig_6.

Differences in column-integrated diabatic cooling

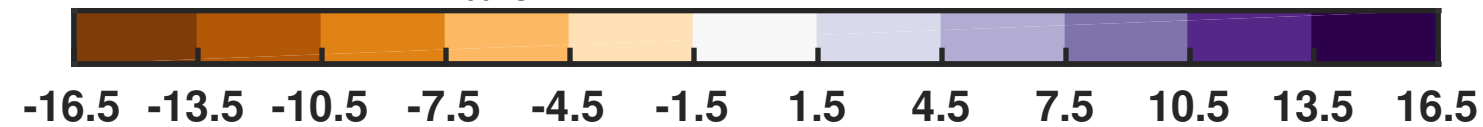
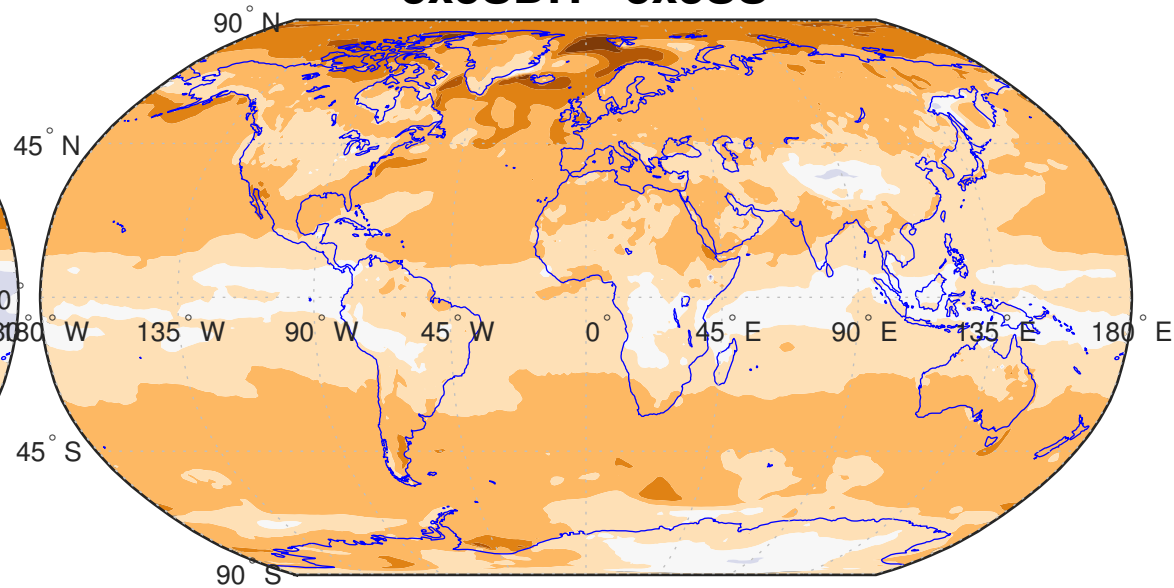
a) ΔQ (W/m^2)
1x1SD - 3x3SS



b) ΔQ (W/m^2)
3x3SD - 3x3SS



c) ΔQ (W/m^2)
3x3SDH - 3x3SS



d) Dry static energy flux divergence (ΔH)

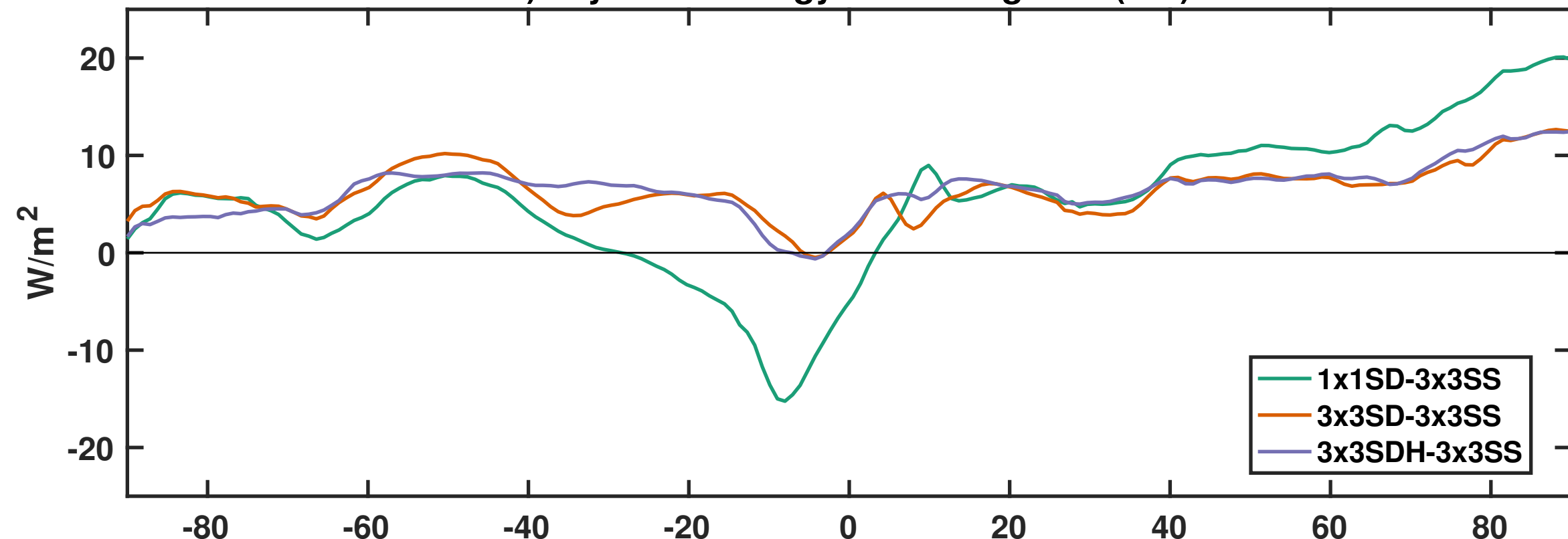
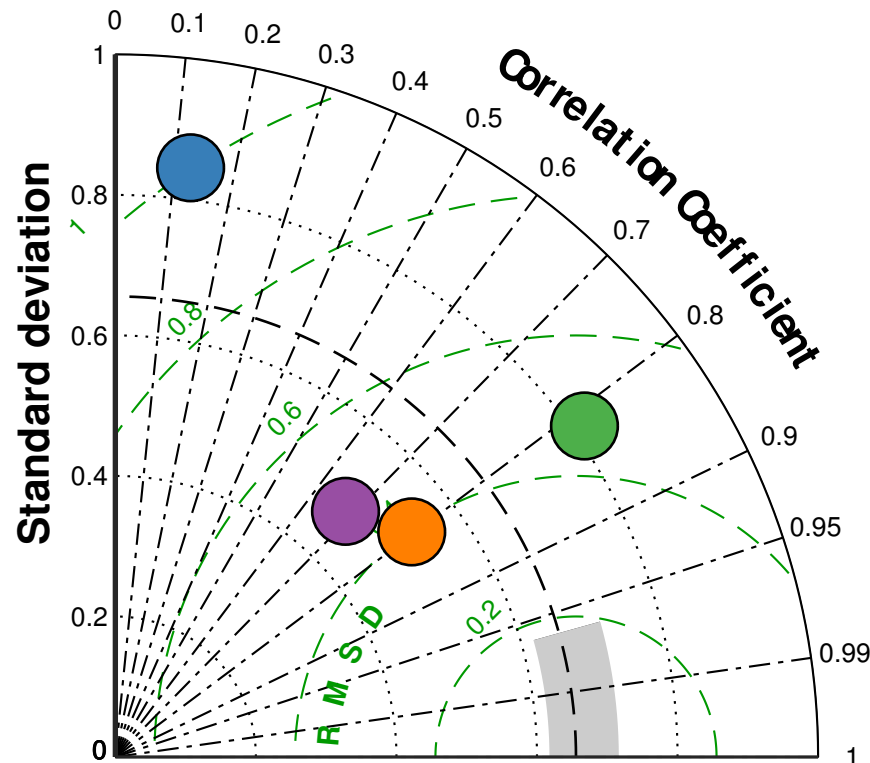
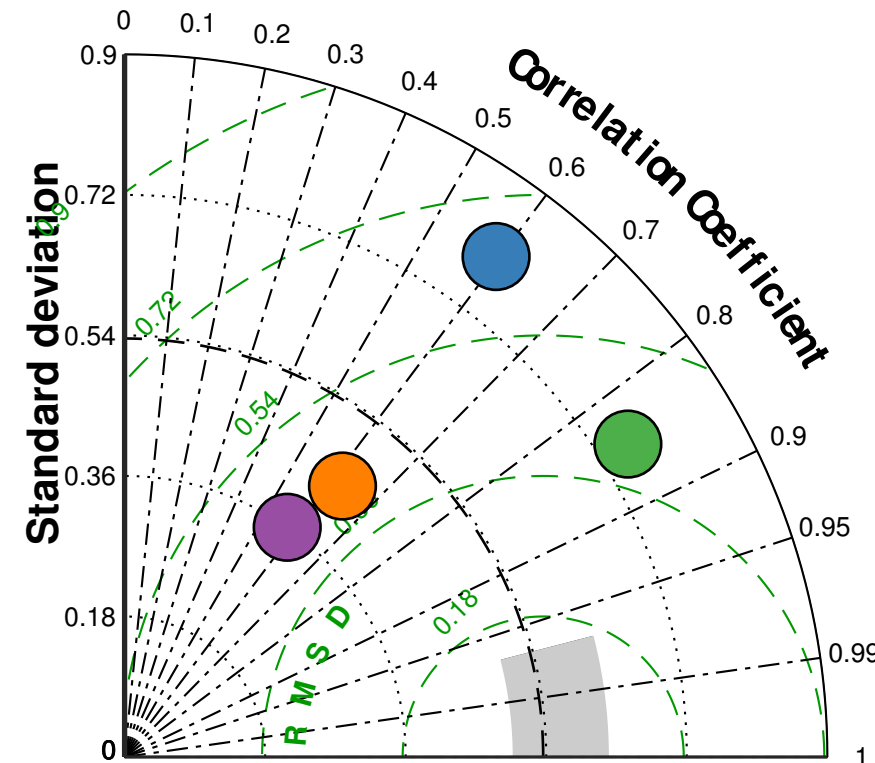


Fig_7.

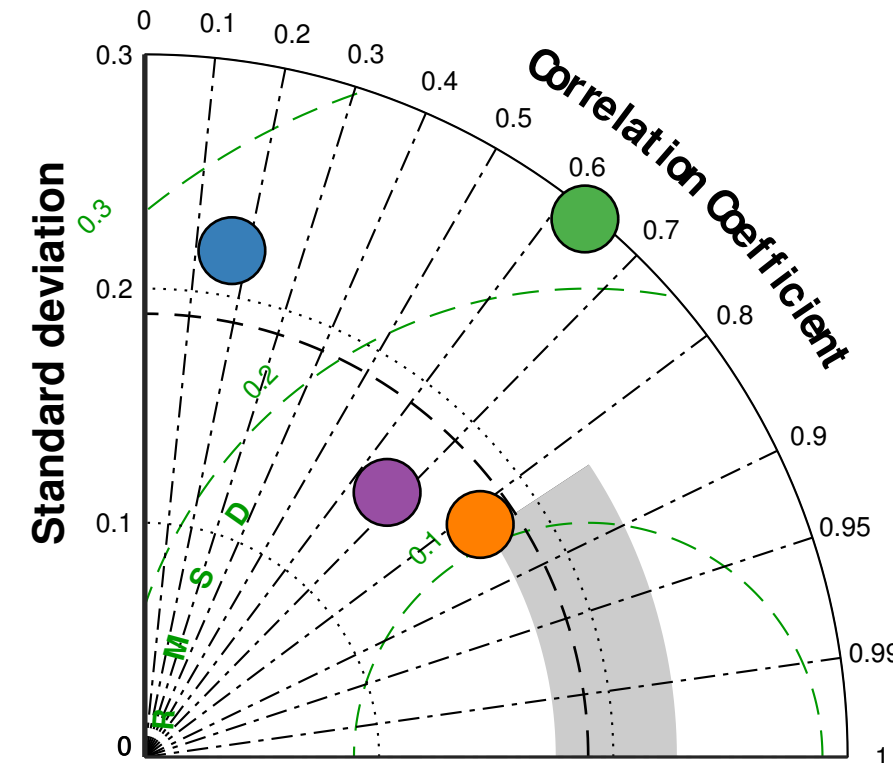
Surface temperature



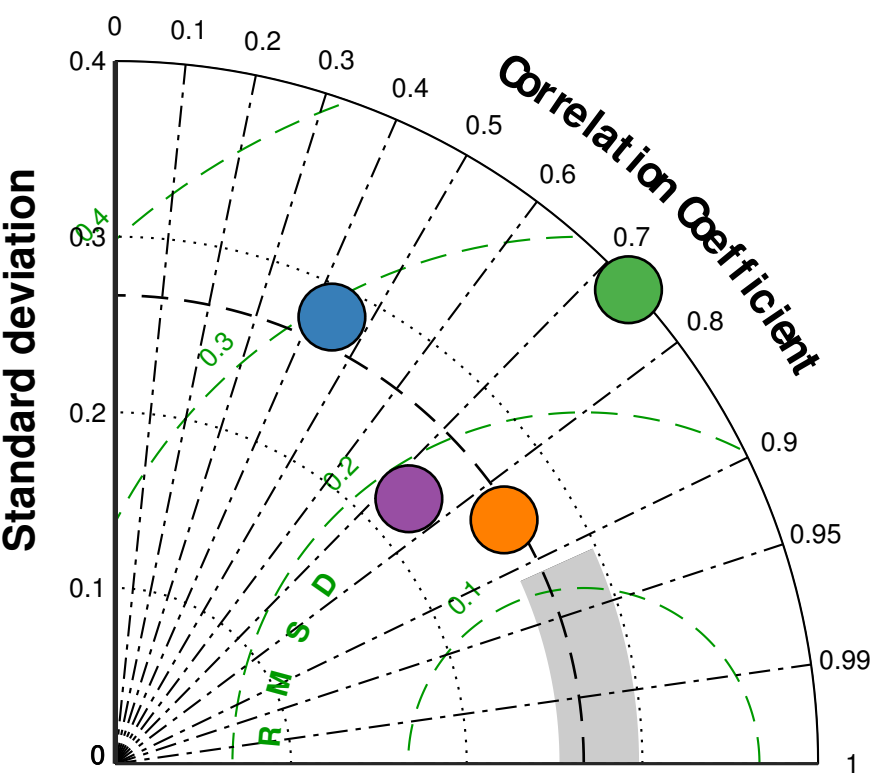
Maximum Monthly Temperature



Precipitation



Precipitation-Evapotranspiration



Maximum Monthly Precipitation

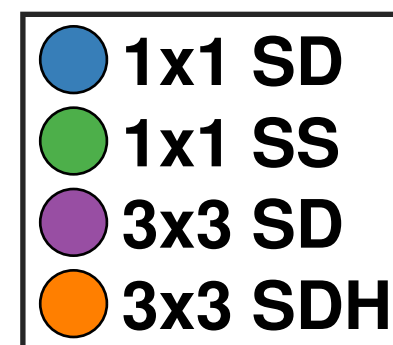
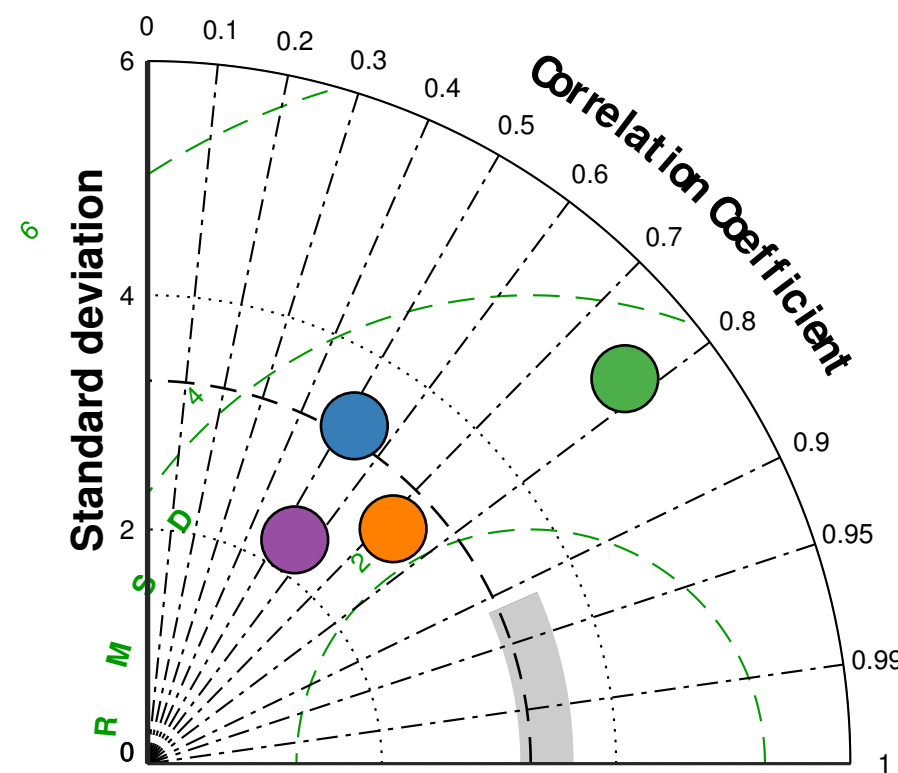


Fig_8.

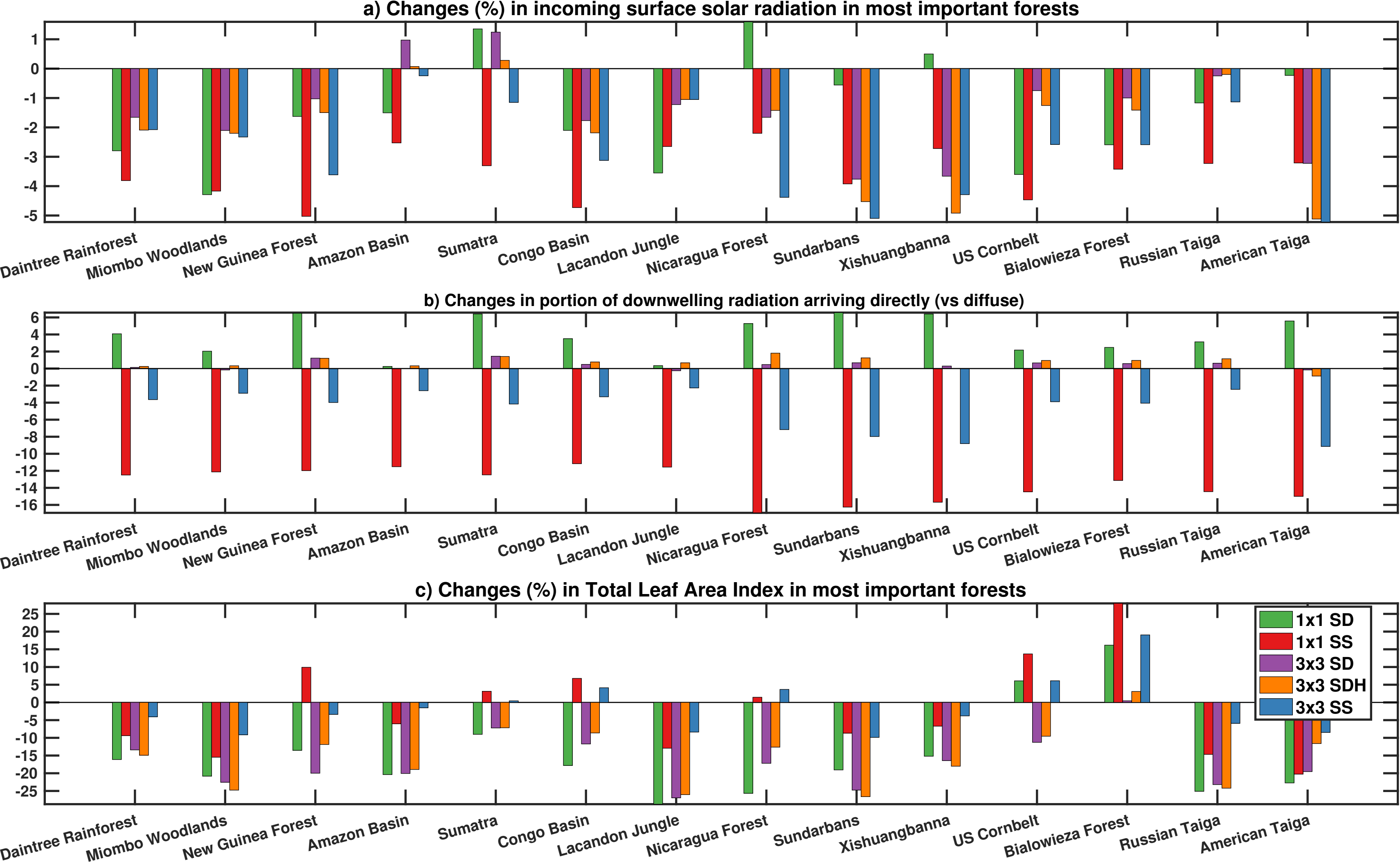
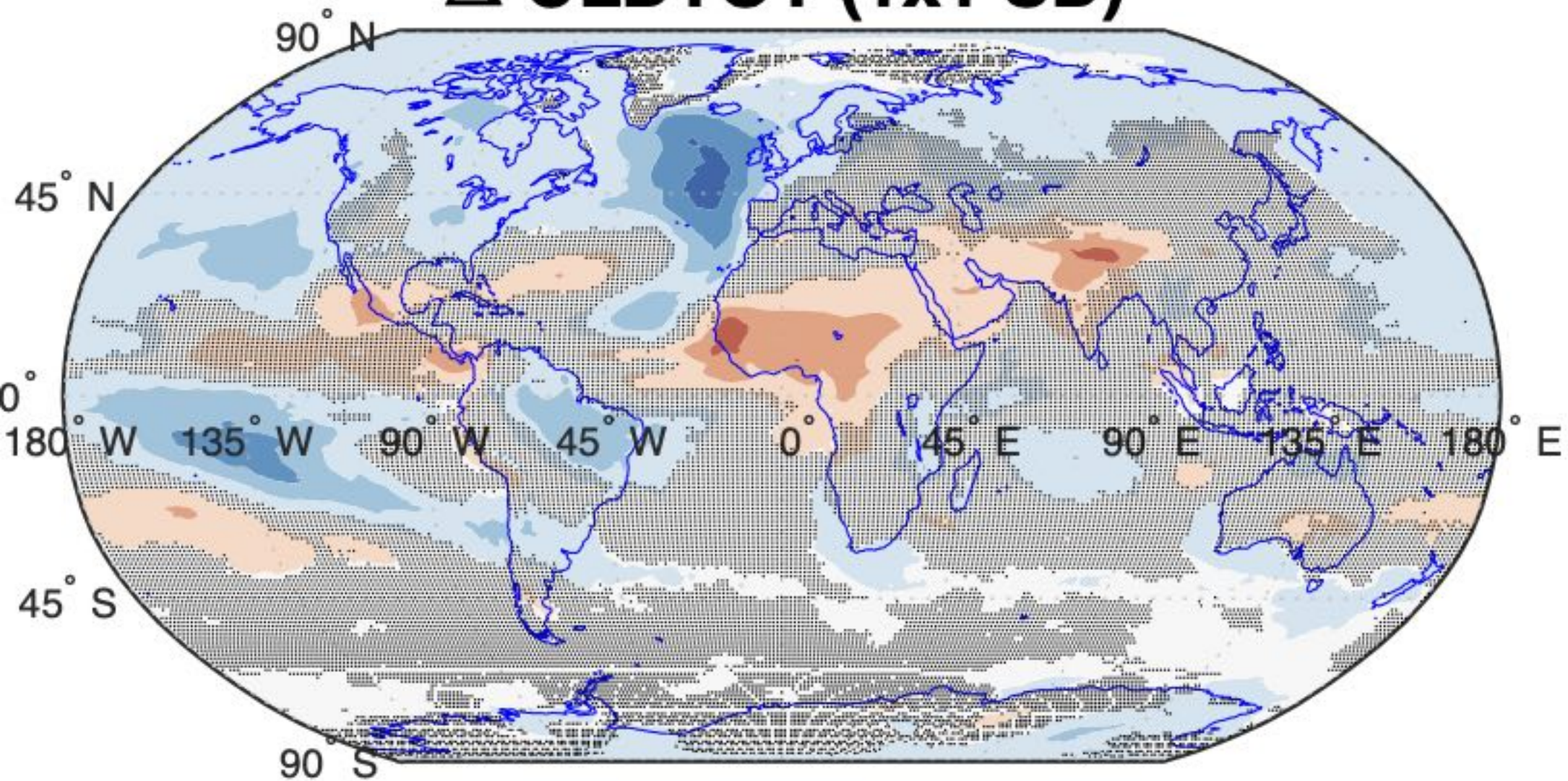
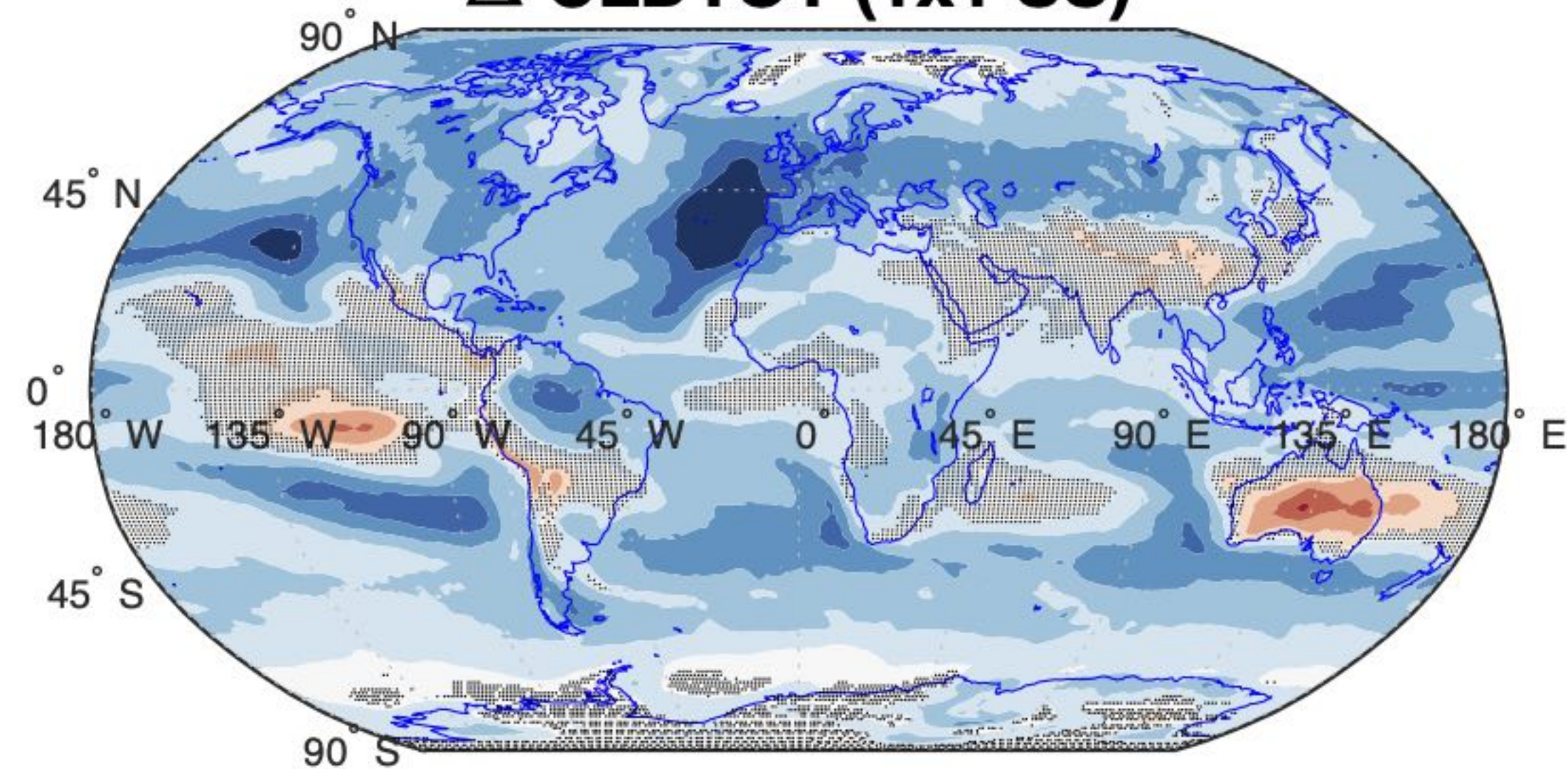


Fig_9.

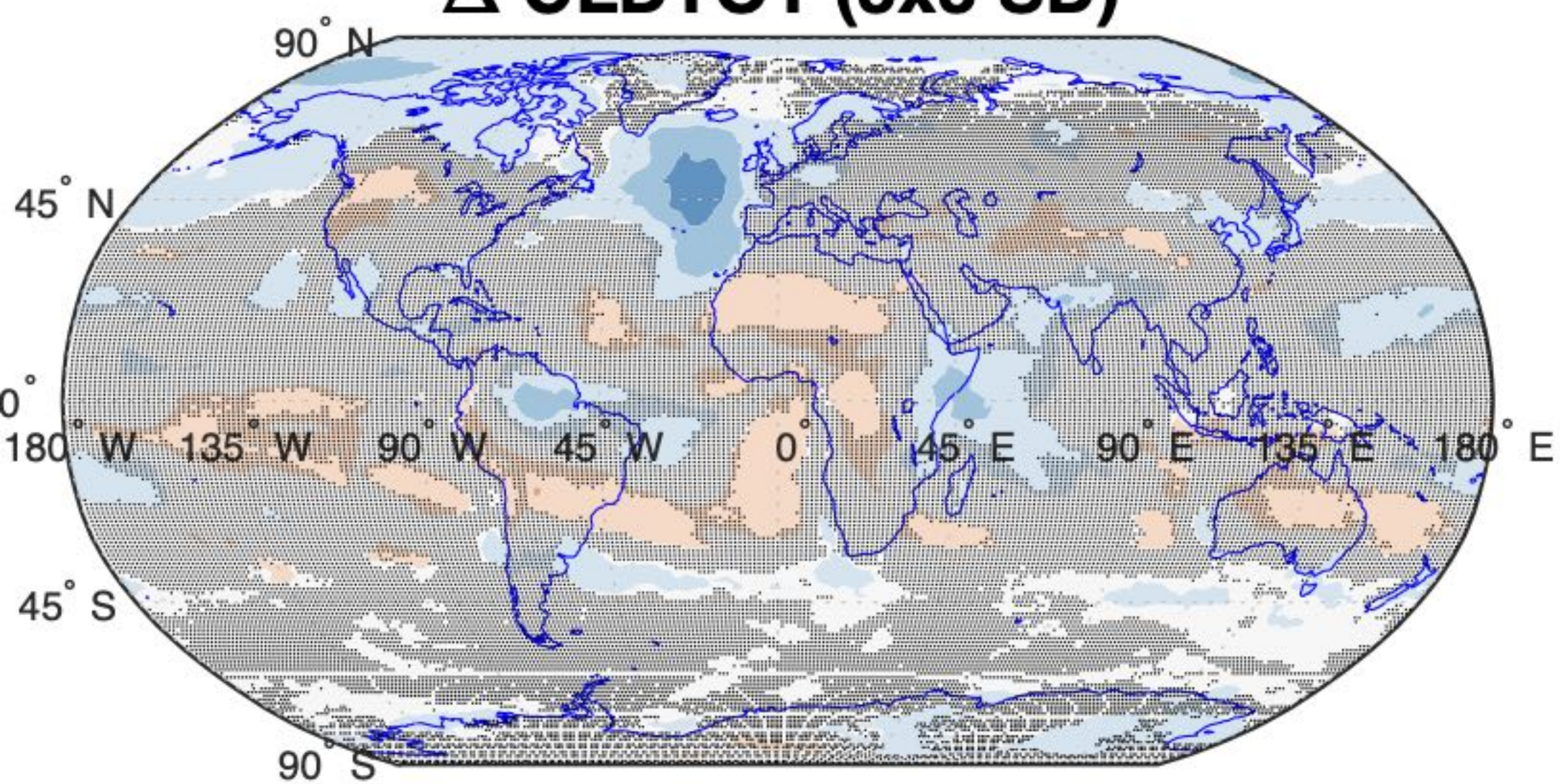
Δ CLDTOT (1x1 SD)



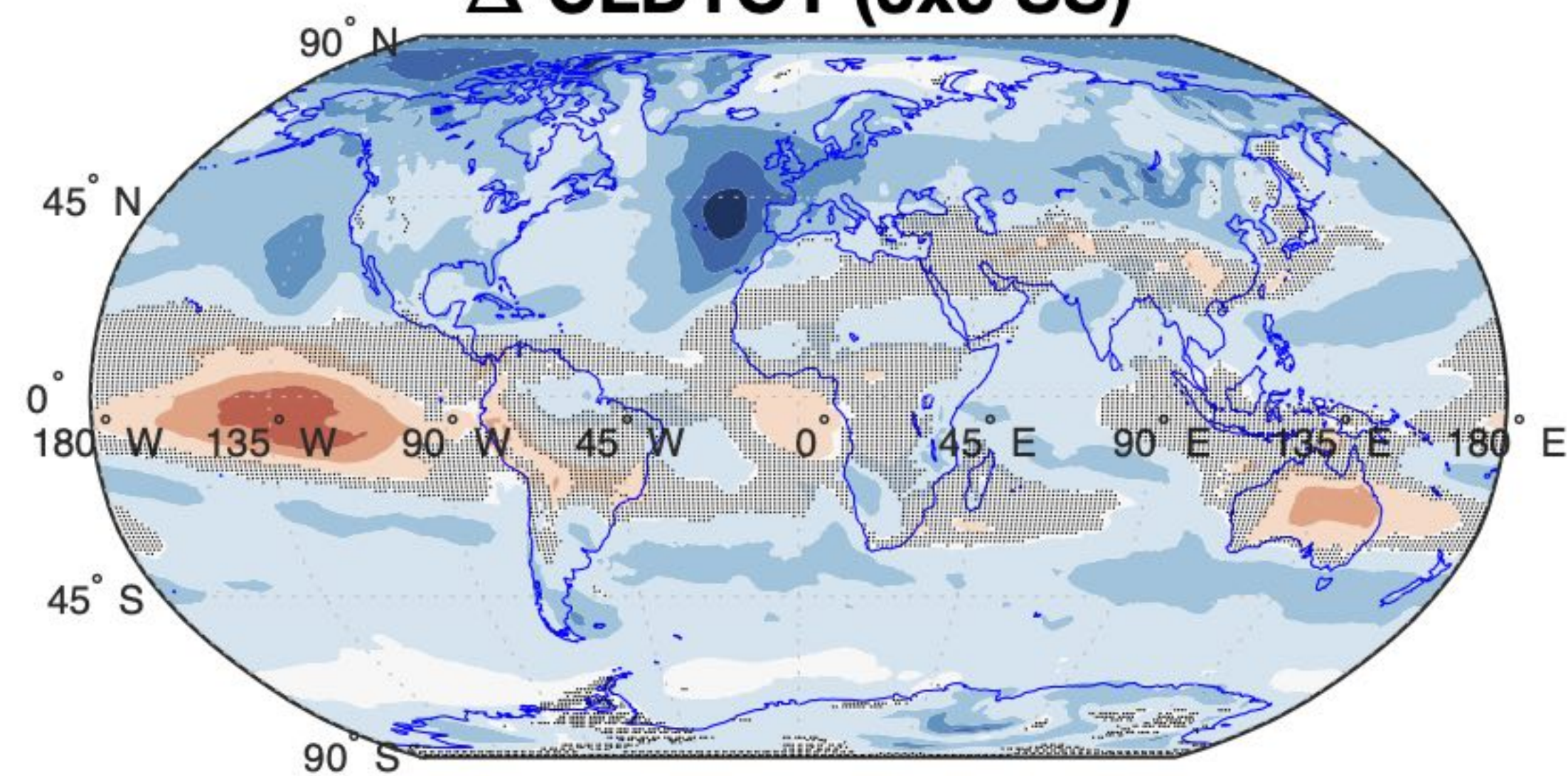
Δ CLDTOT (1x1 SS)



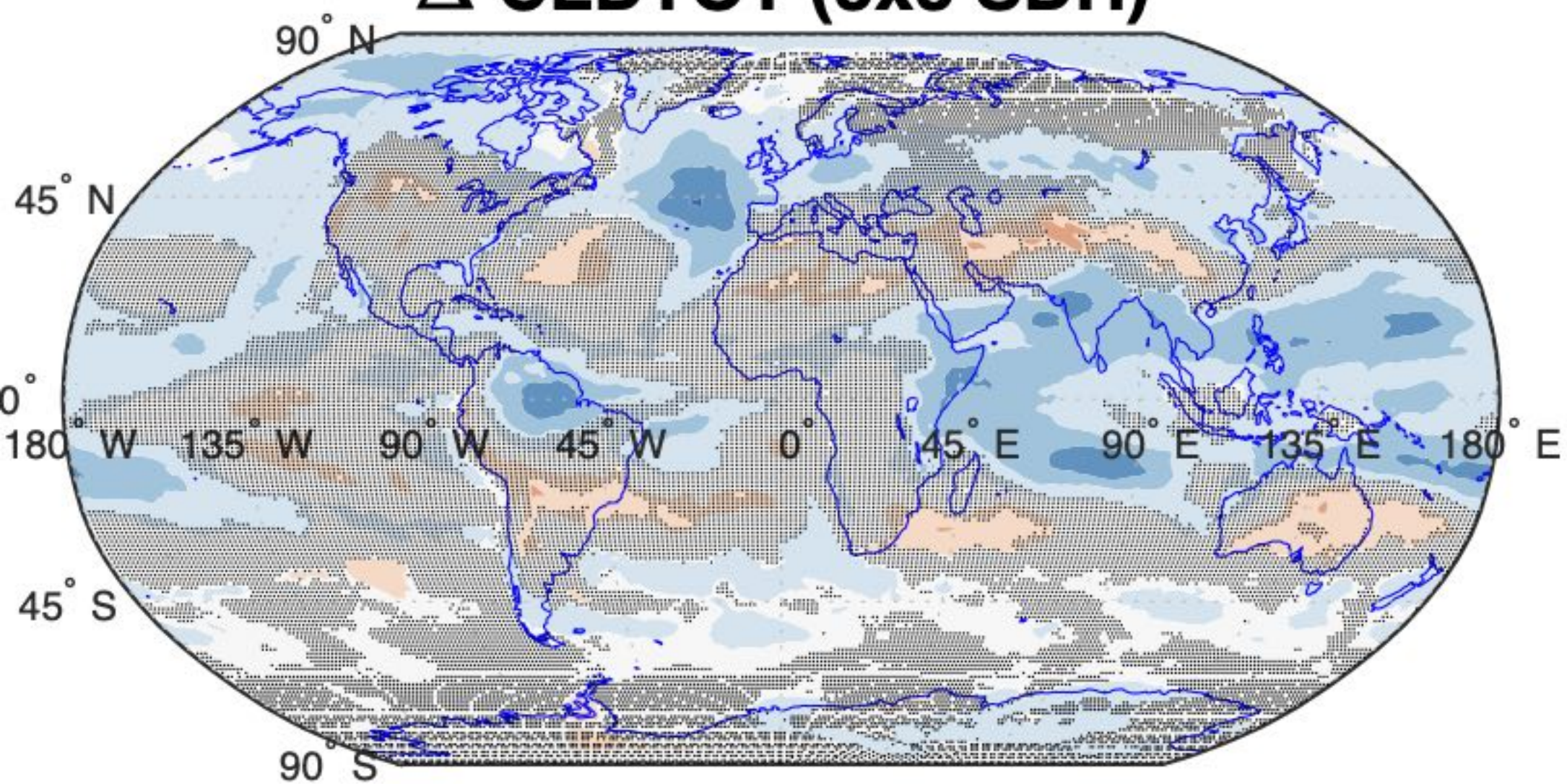
Δ CLDTOT (3x3 SD)



Δ CLDTOT (3x3 SS)



Δ CLDTOT (3x3 SDH)



-0.11 -0.09 -0.07 -0.05 -0.03 -0.01 0.01 0.03 0.05 0.07 0.09 0.11



Fig_10.

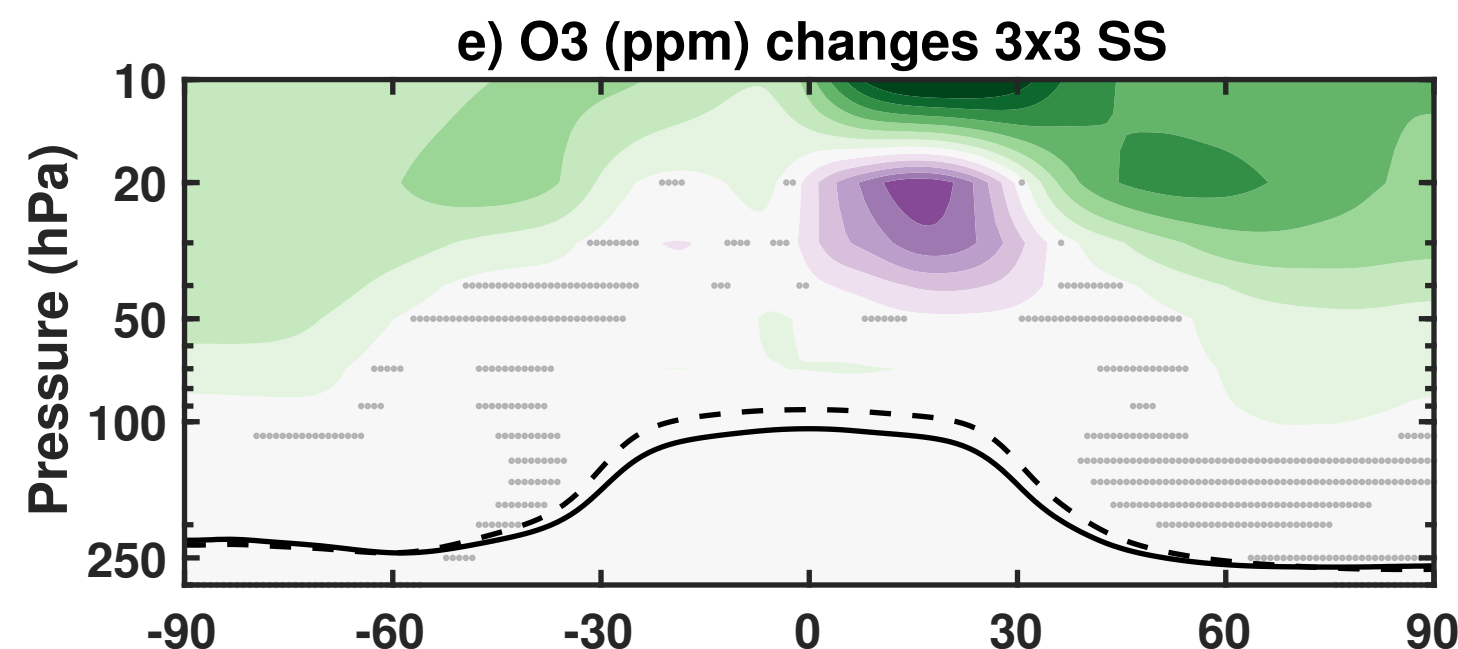
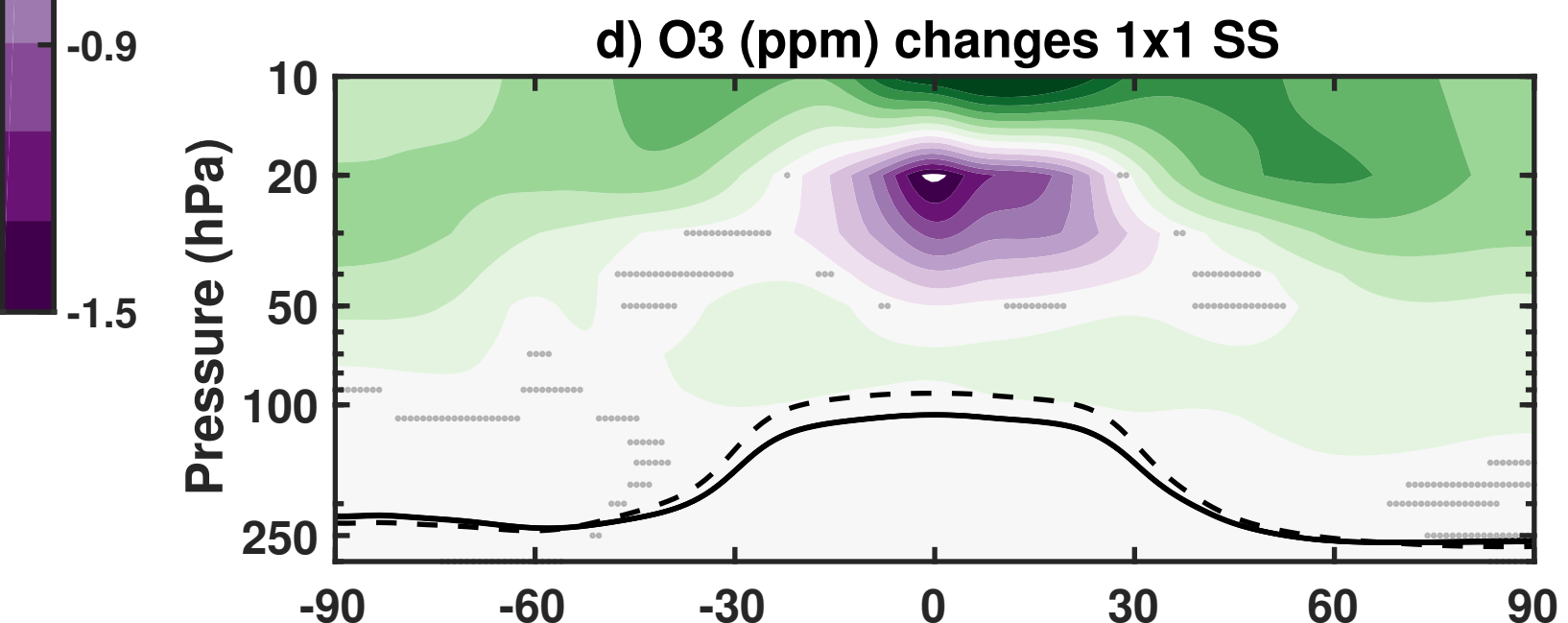
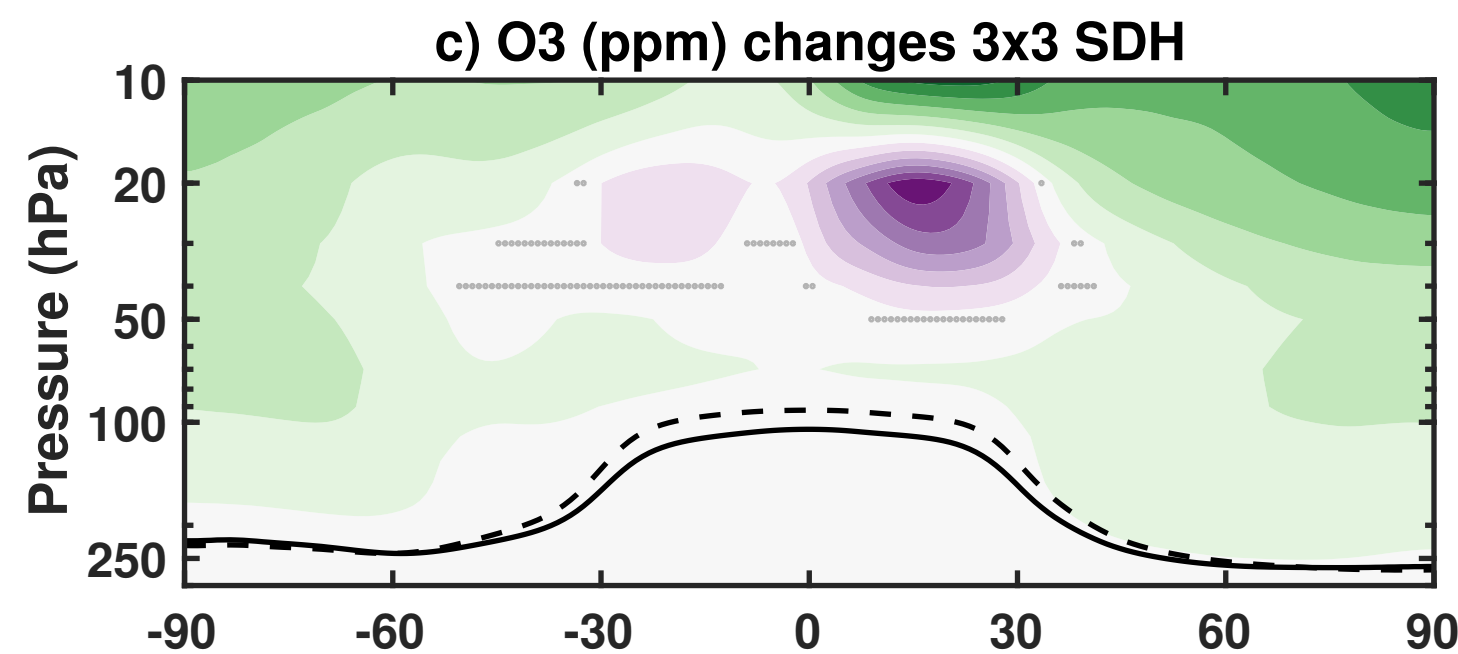
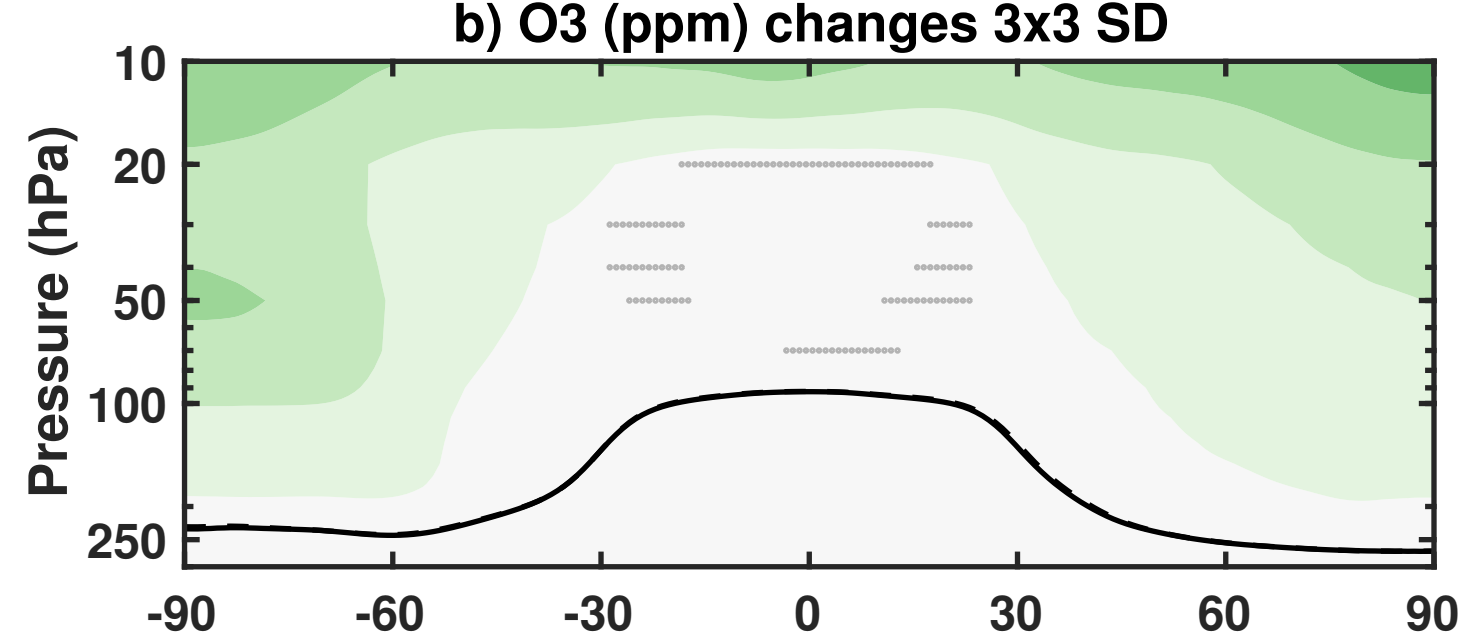
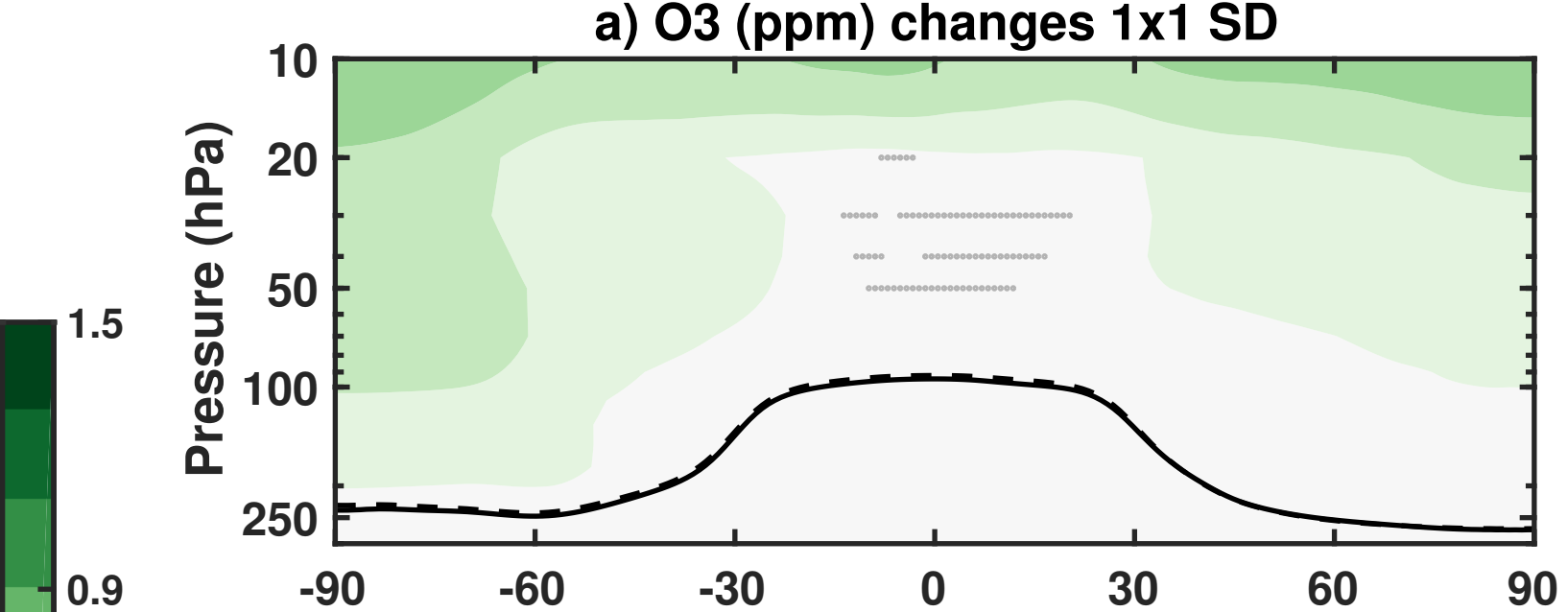


Fig_11.

